MICHIGAN STATE UNIVERSITY

CYCLOTRON LABORATORY

THEORY OF RELATIVISTIC HEAVY ION COLLISIONS

JOSEPH J. MOLITORIS, DETLEV HAHN and HORST STÖCKER

JUNE 1985

MSUCL-530

MSUCL-530
June 1985

Theory of Relativistic Heavy Ion Collisions

Joseph J. Molitoris, Detlev Hahn,* and Horst Stöcker**

Department of Physics and Astronomy and
National Superconducting Cyclotron Laboratory
Michigan State University, East Lansing, Michigan 48824

Abstract

The current status of heavy ion physics from medium energies to the quark gluon plasma is discussed in the light of several theoretical approaches. Relativistic mean field theory is discussed. The nuclear equation of state at high density and temperature is investigated in a nuclear fluid dynamic model: nuclear matter is considered as a relativistic interacting Bose and Fermi gas of π and η mesons, photons, and nucleonic resonances. At the microscopic level, the approach to local kinetic equilibrium in relativistic heavy ion collisions is studied by following the time evolution of the Wigner function in configuration and momentum space using the Vlasov-Uehling-Uhlenbeck theory. This theoretical approach includes the nuclear mean field, two body collisions, particle production, relativistic kinematics, and the Pauli principle. A Newtonian Force Model, TDHF, the Vlasov equation, the IntraNuclear Cascade model, macroscopic Nuclear Fluid Dynamics, and a simple shock model are studied as reference cases. In the VUU theory, rapid equilibration of the participant region is observed within time spans on the order of 10 fm/c. Total stopping of the projectile occurs at small impact parameters: a sidesplash of nuclear matter is predicted due to the interplay of the nuclear compressional energy and collisions. These theoretical approaches are compared to the experimental data. The pion yields, single particle spectra, and kinetic energy flow angular distributions are found to be sensitive to the nuclear compressibility and the Pauli principle: preliminary evidence for a surprisingly stiff nuclear equation of state is presented. Nuclear fragmentation or complex particle production is studied in a quantum statistical model that includes the isotopes up to Ne and also by applying a six dimensional coalescence model to the VUU final state.

Erice School April 10-22, 1985

* NATO Fellow of the Deutscher Akademischer Austauschdienst (DAAD)

** Permanent address: Institut für Theoretische Physik,
Johann Wolfgang Goethe Universität, D-6000 Frankfurt am Main, Germany

Introduction and Motivation

Little is definitely known about the properties of hadronic matter at finite temperatures and densities other than the ground state density $\rho_0 = 0.15\ fm^{-3}$. Hadronic matter may have a rich structure in the hitherto unexplored domain of high excitation energies and high compression (see figure I.1). There are conjectures about a nuclear liquid-vapor phase transition at temperatures $T < 20$ MeV and $\rho < \rho_0$, abnormal nuclear matter (density isomers and pion condensates) at high densities $\rho \approx 3 - 5\ \rho_0$, pionization of nuclear matter for high temperatures $T > 50$ MeV, and the possibility of the deconfinement phase transition from hadronic matter into the quark-gluon plasma at high densities $\rho \approx 5 - 10\ \rho_0$ and/or high temperatures $T \approx 150 - 250$ MeV. These possiblities have recently received much attention, spurring much experimental and theoretical work along with plans for relativistic heavy ion facilities around the world. Extreme energy densities, temperatures and baryon number densities have prevailed in the first fractions of a second during the birth of the universe (in the big bang) and during the death of stars (in supernova explosions and neutron star formation). However, until recently, there was no opportunity to study these extreme conditions in the laboratory. This has changed in the last decade.

Experimental information on this unexplored domain is now being sought by analyzing high energy collisions of heavy nuclei (see figure I.2). If the nuclei can stop each other, high energy densities can be obtained for $t \approx 10^{-22}$ seconds. Collisions of massive nuclei could not be studied experimentally in the past. Only recently have ions with mass $A > 40$ been

accelerated at the Bevalac to bombarding energies between 100 MeV/nucleon to 2 GeV/nucleon.

In this paper we want to give a survey of recent experimental and theoretical developments in the field of high energy heavy ion reactions. First we discuss the statistical concepts necessary to study the properties of infinite hadronic systems at high density and finite temperatures, in particular the nuclear matter equation of state and the conjectured phase transitions. We then give an overview of various theoretical approaches developed to describe the dynamical evolution of the highly excited strongly interacting system in an ephemeral heavy ion collision. Finally, we discuss the recent 4π experiments on fragment formation, pion production and collective flow. The implications of these experiments for the nuclear equation of state are pointed out.

I. Infinite Nuclear Matter in Global Equilibrium - The Nuclear Equation of State

1. Statistical and Thermodynamical Concepts

Systems composed of 'infinite nuclear matter' exist(ed) only in astrophysical events remote in space and time - e.g. in the big bang, supernova explosions, and in the interior of neutron stars. High density matter is formed in nuclear collisions only for brief moments, and global equilibrium can not be reached at high bombarding energies. However, statistical concepts have been successfully applied to nuclear collisions, e.g. in the Nuclear Fluid Dynamical model, which assumes that local (rather than global) equilibrium is closely approached even on these short time scales. But the assumption of statistical equilibrium in nuclear collisions must be checked via microscopic theories, which are able to describe the

evolution of the system from the nonequilibrium situation to the locally equilibrated state. These theories and the questions related to the equilibration are discussed in detail in the second part of this article.

What are the general statistical concepts appropriate to describe the near equilibrium situation? The nuclear matter properties can be characterized by two canonical variables: the density ρ and the temperature T. The discussion of the properties of a piece of hadronic matter at rest usually starts with the definition of the energy per baryon, $W(\rho,T)$, as a function of these two variables. This energy can be related to the center of mass energy in nuclear collisions. It is convenient to divide the total energy per baryon into a thermal and a compression part:

$$W(\rho,T)= E_T(\rho,T) + E_C(\rho) + W_o \qquad (1)$$

where

$$E_C(\rho)= W(\rho,T=0)-W(\rho_o,T=0)= W(\rho,T=0)-W_o \qquad (2)$$

is defined to be the compressional energy and E_T is the thermal excitation energy per baryon, which is zero if the temperature vanishes. $W_o \approx 923$ MeV is the rest energy of a nucleon at equilibrium density and T=0.

In order to understand the physical significance of $W(\rho,T)$ let us consider a piece of nuclear matter of volume V. It's energy content is given by $E_V = \int_V \rho\, W(\rho,T)\, dV$, where $e = \rho\, W$ is the energy density of the matter. In evaluating this quantity we have excluded the Coulomb energy and the long range part of the Yukawa energy, which lead to divergence if infinite systems are considered. Hence we have considered only the short range part of the nuclear interaction. This is the origin of the binding energy of 16 (rather than 8) MeV/nucleon: it comes from the volume term of the Bethe-Weizäscker formula (surface and Coulomb terms are neglected).

Once the functional form of W is given, standard thermodynamic relations can be used to calculate the pressure p, entropy S, and enthalpy H of the system at a given density and temperature. For example, the pressure is calculated from the internal energy as

$$p = -\left.\frac{\partial E}{\partial V}\right|_S = \rho^2 \left.\frac{\partial E}{\partial \rho}\right|_S \qquad (3)$$

and can also be separated into two parts P_C and P_T. Similarly one obtains the entropy of the system from the thermal energy alone: because of Nernst's theorem (1906), the T = 0 part of the equation of state does not contribute to the entropy. The entropy of any body vanishes at the absolute zero of temperature.

2. A Model Lagrangian for a Relativistic Mean Field Theory

The total energy per baryon can also be expressed in kinetic and potential terms. This becomes particularly obvious in the mean field approach. The relativistic mean field theory developed by Walecka [Wal 74, Ser 85], Boguta [Bog 77, Bog 83], and others is of special interest, since one can show that these approaches are strictly relativistically covariant, thermodynamically consistent, and renormalizable as field theories. This relativistic mean field model consists of nucleons obeying the time-dependent Dirac equation, a classical spin zero attractive meson field (sigma) obeying the Klein Gordon equation, a spin one repulsive meson field (omega) obeying the Proca equation and a meson-baryon interaction between them. The resulting coupled field equations are solved simultaneously in a mean field approximation.

The Hartree approximation which yields an effective Lagrangian. Masses and coupling constants for the mesons are phenomenological and are

adjusted to fit static nuclear matter properties. The model Lagrangian density is

$$\mathcal{L} = -\bar{\psi}(\gamma_\mu \partial/\partial x_\mu + m_N)\psi - \frac{1}{2}(\partial\sigma/\partial x_\mu)^2 - U(\sigma) - \frac{1}{4} F_{\mu\nu}F_{\mu\nu} - \frac{1}{2} m_v^2 \omega_\mu \omega_\mu + i g_v \bar{\psi}\gamma_\mu \psi \omega_\mu - g_s \bar{\psi}\psi\sigma, \quad (4)$$

where

$$F_{\mu\nu} = (\partial/\partial x_\mu)\omega_\nu - (\partial/\partial x_\nu)\omega_\mu . \quad (5)$$

The potential function is taken to be a quartic polynomial in the field σ [Bog 77, Bog 83]:

$$U(\sigma) = \frac{1}{2} m_s^2 \sigma^2 + \frac{1}{3} b\sigma^3 + \frac{1}{4} c\sigma^4 . \quad (6)$$

The addition of nonlinear terms to the Lagrangian allows for a more realistic fit to other nuclear properties, such as the compressibility and effective nucleon mass [Sar 85].

3. Cold Nuclear Matter

For translationally and rotationally invariant infinite nuclear matter the field equations in the mean field approximation $\sigma \to \sigma_0$ and $\omega_\mu \to i\delta_{\mu 0}\omega_0$ are

$$m_s^2\sigma_0 + b\sigma_0^2 + c\sigma_0^3 = -g_s\rho_s , \quad m_v^2\omega_0 = g_v\rho_v , \quad \omega_i = 0, \quad (7)$$

where

$$\rho_v = \frac{2}{3\pi^2} k_F^3$$

is the vector density, referred to here as the baryon number density. The scalar density is given by

$$\rho_s = \frac{4}{(2\pi)^3} \int^{k_F} d^3k \, \frac{m^*}{\sqrt{(k^2+m^{*2})}} ,$$

and the effective mass of the nucleon is

$$m^* = m_N + g_0\sigma_0 . \quad (8)$$

Above, we have written down the expressions for zero temperature matter; finite temperatures in this approach are discussed elsewhere [Bog 82, The 83]. The energy density e, pressure p and compressibility constant K at T = 0 are

$$e = \frac{1}{2}\,(g_v/m_v)^2\rho_v^2 + \frac{4}{(2\pi)^3}\int^{k_F} d^3k\sqrt{(k^2+m^{*2})} + U(\sigma), \tag{9}$$

$$p = \rho_v^2(d/d\rho_v)(e/\rho_v), \tag{10}$$

$$K = \rho_v^2(d^2/d\rho_v^2)(e/\rho_v), \tag{11}$$

respectively. The energy of a particle moving through matter with momentum k is

$$E = g_v\omega_o + \sqrt{(k^2 + m^{*2})} \tag{12}$$

$$= \sqrt{(k^2 + m_N^2)} + U_{eff},$$

where U_{eff} is the effective nuclear potential

$$U_{eff} = E - \sqrt{[(E-g_v\omega_o)^2 + m_N^2 - m^{*2}]}\ . \tag{13}$$

This model has been applied to dynamical calculations [Cus 85]. But let us here discuss the equation of state resulting from these relativistic mean field theories for infinite nuclear matter, neglecting the space and time derivatives in the equations of motion and assuming thermal equilibrium. In [Bog 83] the compression energy $E_C(\rho)$ of nuclear matter has been calculated in the relativistic field theory with additional nonlinear terms in the Lagrangian and in non-relativistic many-body calculations using the variational method. The results of both approaches agree for $\rho < 1.2\ \rho_o$ for any reasonable set of parameters for the incompressibility coefficient K and effective nucleon mass m^* at saturation density ρ_o. However, at higher densities $\rho > 1.2\ \rho_o$ the nuclear equation of state is so sensitive to K and m^* at ρ_o that differences of several hundred percent arise even if K and m^* are only varied within their present experimental 10-20% uncertainties.

These results demonstrate the obvious fact that even a precise determination of the nuclear properties at ground state densities does not enable us to predict the high density behavior of nuclear matter. A theoretical determination of these properties is also very difficult in view of the fact that many body forces may play an essential role.

Unfortunately, a field theoretical treatment beyond the mean field approximation is not yet developed. To describe the collision dynamics in a time dependent theory, semi-classical approaches must be used which include the nuclear potential, but also the effects of two body collisions (see Chapter II). For such approaches, phenomenological equations of state have been developed. In the following we present the equation of state in such a phenomenological theory and study further simplifying assumptions. The compression energy $E_C(\rho)$ incorporates phenomenologically the nuclear binding energy, the Fermi energy of the nucleons, hard core effects and the exchange part of the nuclear forces. It is often loosely referred to as the "nuclear equation of state (EOS)." Two commonly used functional forms for $E_C(\rho)$ originate from the extended liquid drop model of Scheid and Greiner [Sch 68]:

$$E_C(\rho) = K_l(\rho-\rho_o)^2/(18\rho\rho_o) \qquad (14a)$$

$$E_C(\rho) = K_q(\rho-\rho_o)^2/(18\rho_o^2) \qquad (14b)$$

the linear and the quadratic EOS, respectively.

4. Finite temperatures

The temperature of the system is the second thermodynamic variable of importance for the equation of state. The total energy of the system at finite temperature is described by the interaction energy plus the kinetic energy of the particles in the system. The latter is given by interacting

relativistic Fermi-Dirac and Bose-Einstein distributions, hence the total energy per baryon is given by [Hei 79, Hah 85a]

$$W = U + \sum_{i=1}^{\sigma_b} \left\{ \frac{\rho_i^{\circ} m_i c^2}{\rho} + \frac{4\pi\lambda_i}{\rho(2\pi\hbar c)^3} \int_{m_i c^2}^{\infty} \frac{\varepsilon^2\sqrt{(\varepsilon^2 - m_i^2 c^4)}}{\exp[\varepsilon/T]-1}\, d\varepsilon \right\}$$
$$+ \sum_{i=\sigma_b+1}^{\sigma} \frac{4\pi g_i}{\rho(2\pi\hbar c)^3} \int_{m_i c^2}^{\infty} \frac{\varepsilon^2\sqrt{(\varepsilon^2 - m_i^2 c^4)}}{\exp[(\varepsilon+U-\mu))/T]+1} d\varepsilon \qquad (15)$$

where the first sum runs over the Bose-degrees of freedom (the pion and heavier mesons) while the second sum is over all the excited states of the nucleon (the Δ (1232) resonance being the most important resonance in the GeV/nucleon energy region). Here it is assumed that all nucleonic resonances feel the same interaction energy per particle U, which depends only on the total baryon density ρ [Hei 79, Hah 85a]. This potential energy must be included into the Fermi-Dirac distribution function in a self-consistent way. It is also assumed that all the particles are in chemical and thermal equilibrium and that the chemical potential μ is the same for all baryons. Both the chemical potential and the interaction potential for the bosons are taken to be equal to zero. ρ_i° is the contribution of the Bose ground-state to the density of the boson-phases. The connection between the baryon density and the chemical potential reads

$$\rho = \sum_{i=\sigma_b+1}^{\sigma} \frac{4\pi g_i}{(2\pi\hbar c)^3} \int_{m_i c^2}^{\infty} \frac{\varepsilon\sqrt{(\varepsilon^2 - m_i^2 c^4)}}{\exp[(\varepsilon+U-\mu)/T]+1} d\varepsilon \,. \qquad (16)$$

The number of mesons can be calculated via

$$N_i = \frac{g_i}{\exp(m_i c^2/T)-1} + \frac{4\pi g_i V}{(2\pi\hbar c)^3} \int_{m_i c^2}^{\infty} \frac{\varepsilon\sqrt{(\varepsilon^2 - m_i^2 c^4)}}{\exp[\varepsilon/T]-1} d\varepsilon \qquad (17)$$

For our calculations, we also need the connection between U and the compression energy E_C. For $T \to 0$ eq. (16) becomes

$$(\mu - U)^2 = m^2 c^4 + (\rho C/g)^{2/3} \qquad (18)$$

with $C = 6\pi^2(hc)^3$. In the same limit, we get for eq. (15)

$$W(T=0) = 0.75X + U + \frac{m^2c^4}{8}\left\{\frac{3X}{X1^2} - \frac{3m^2c^4}{X1^3}\ln[(X+X1)/mc^2]\right. \qquad (19)$$

with $g = 4$, $mc^2 = 939$ MeV, $X1=(\rho C/g)^{1/3}$, $X=\sqrt{(m^2c^4 + X1^2)}$ assuming that for T=0 only the nucleonic ground state is populated (which should be true for small densities unless the nucleon-Δ interaction is much stronger than the nucleon-nucleon interaction [Bog 82]). Expanding (18) and (19) for small densities, we obtain the well known $\rho^{2/3}$ dependence for the energy

$$\mu - U \approx mc^2 + 1/2\ X1^2/mc^2 + \ldots \qquad (20)$$

$$W \approx U + mc^2 + 0.3\ (\rho/\rho_o)^{2/3}h^2/m\ (6\pi^2\rho_o/g)^{2/3} + \ldots \qquad (21)$$

The difference between the exact expression (19) and the approximation (21) is about 1 MeV for $\rho/\rho_o=3$. By comparing (1) and (19) we finally get the relation between U and E_C:

$$U(\rho) = E_C + W_o - 0.75\ X - \frac{m^2c^4}{8}\left\{\frac{3X}{X1^2} - \frac{3m^2c^4}{X1^3}\ln[(X+X1)/mc^2]\right\} \qquad (22)$$

For the pressure, we have [Hei 79, Hah 85a]

$$p = -T\sum_{i=1}^{\sigma_b}\frac{4\pi g_i}{(2\pi hc)^3}\int_{m_ic^2}^{\infty}\varepsilon\sqrt{(\varepsilon^2-m_i^2c^4)}\ \ln(1-\exp[-\varepsilon/T])d\varepsilon$$
$$+ T\sum_{i=\sigma_b+1}^{\sigma}\frac{4\pi g_i}{(2\pi hc)^3}\int_{m_ic^2}^{\infty}\varepsilon\sqrt{(\varepsilon^2-m_i^2c^4)}\ \ln(1+\exp[(\mu-U-\varepsilon)/T])d\varepsilon$$
$$+ \rho^2\frac{\partial U}{\partial\rho} \qquad (23)$$

and the entropy per baryon is

$$S/N_B = P/(\rho T) - \frac{\rho}{T}\frac{\partial U}{\partial\rho} - 1/N_B\sum_{i=1}^{\sigma_b} g_i\ln(1-\exp[-m_ic^2/T])$$
$$+ (W-\mu)/T = -\left.\frac{\partial\Omega}{\partial T}\right|_{\mu,V}. \qquad (24)$$

5. Pionization in Hot Systems - Formation of the Hadron Plasma

These equations have been used in simplified models of heavy ion reactions [Hah 85a] to extract the temperature from pion multiplicities. The dependence of the number of pions per nucleon on the temperature as calculated with the above approach, which includes all firmly established resonances, the pion, the η meson, and the photon is shown in figure I.3. Observe that the pion yield increases rapidly with temperature from zero to about one per nucleon at $T \approx 100$ MeV, and then flattens out - nuclear matter is gradually transformed into a hadron plasma. This becomes obvious in figure I.4, which shows the distribution of pions over the various pion producing channels [Hah 85a]. At low energy, temperatures of the order of 50 MeV or less, most of the pions reside in the Bose condensed zero momentum state. At higher temperatures, the pion yield is due to nuclear resonances. The $\Delta(1232)$ resonance is of particular importance in the Bevalac energy regime, $E_{lab} \approx 1$ GeV/nucleon, while the more massive resonances become important at temperatures above $T \approx 100$ MeV. Fig. I.3 can be used to extract the temperatures in the moment of pion emission from the observed pion yields [Hah 85a] - see figure I.5. One finds that the temperature rises smoothly with the bombarding energy, reaches $T \approx 100$ MeV at the top Bevalac energies and can be extrapolated to temperatures exceeding the critical temperature for deconfinement, $T \approx 200$ MeV, at energies in the range of relativistic heavy ion facilities presently under construction at CERN and Brookhaven, $E_{lab} > 10$ GeV/nucleon. This equation of state is too complicated to be of practical importance for many three dimensional model calculations. Therefore we will now discuss simpler approximations widely used to determine the energy and density dependence of the thermal energy.

The simplest ansatz for the thermal energy is the classical ideal gas relation $E_T = 3/2\ T$. This is actually the asymptotic value for the full

non-interacting non-relativistic Fermi gas: it neglects the influence of the interactions on the thermal energy, but it contains the Fermi degeneracy energy. This means $E_T = 3/2\ T$ is the full kinetic energy; the degeneracy energy should be subtracted from the compressional energy if this approximation is used [San 85]. However, the classical approximation is only reasonable, if the temperatures are considerably larger than the chemical potential or the Fermi energy at a given density. On the other hand, for temperatures below the Fermi energy, the Fermi gas expansion has been used:

$$E_T(\rho,T) = \frac{\beta}{2}\,\rho^{-2/3}\,T^2 = \frac{S^2}{2\beta}\,\rho^{2/3} = E_T(\rho,S) \qquad (25)$$

where

$$T = \left.\frac{\partial W}{\partial S}\right|_{\rho} = \frac{S}{\beta}\,\rho^{2/3}, \quad \beta = \left(\frac{g\pi}{6}\right)^{2/3}\frac{mc^2}{(\hbar c)}\ ,$$

S being the nucleon's specific entropy.

At high temperatures, the production of resonances can be treated explicitly using the statistical approach described above. However, a nice physical insight to the formation of resonances is obtained from the simpler classical gas ansatz for a mixture of resonances [Cha 73, Hof 76, Stö 81a]. As practically nothing is known about the N-N^* and N^* - N^* interactions, assume that the N^* interaction only depends on the total baryon density. Therefore the compression energy $E_C(\rho)$ is unchanged (assuming that the subtraction of the Fermi degeneracy energy discussed above can be neglected). The first interesting quantity is the thermal excitation energy of the isobars. The thermal energy of a free gas of resonances with mass $m_i c^2$ is

$$E_{T_i} = \frac{3}{2}\,T\ . \qquad (26)$$

The resonances can be viewed as excited nucleons (resonance pair production is not important at the above temperatures). A Boltzmann distribution for the excitation probability of the i-th resonance can be assumed at temperatures much above the Fermi energy. Baryon number conservation then yields the partitions [Stö 81a]

$$\lambda_i = \frac{\tau_i e^{E_i/T}}{\sum \tau_k e^{-E_k/T}} \tag{27}$$

where

$$\tau_i = \frac{g_i \; m_i^{3/2}}{g_n \; m_n^{3/2}} = \frac{(2 \text{ Spin}(i)+1)\cdot(2 \text{ Isospin}(i)+1) \; m_i^{3/2}}{4 \qquad\qquad m_n^{3/2}} \tag{28}$$

is the statistical weight factor of the i-th resonance, and $E_i=(m_i-m_0)c^2$ is the energy necessary for the resonance excitation.

The density of the i-th phase is then given by

$$\rho_i = \lambda_i \, \rho \tag{29}$$

and the total energy density $e=\rho W$ is given as the sum over the energy densities of all phases

$$e = \sum_i e_i = \sum_i \rho_i W_i \; . \tag{30}$$

As all baryons are assumed to interact only via $E_c(\rho)$, the energy per resonance i is

$$W_i = m_i c^2 + E_C + E_{T_i} \tag{31}$$

which corresponds to a mean energy per nucleon

$$W(\rho,T) = m_o c^2 + E_C + \sum_i \lambda_i (E_{T_i} + E_i) \tag{32}$$

where the mean thermal energy per baryon is

$$E_T = \sum_i \lambda_i E_{T_i} \tag{33}$$

and

$$\Delta Mc^2 = \sum_i \lambda_i E_i \tag{34}$$

is the mean additional rest mass due to the occupation of the resonances with $m_i > m_0$. A free pion gas can be included via a polynomial fit [Mek 78ab] to give the pionic energy per baryon

$$E_\pi = 1.85 \cdot \rho_0 \, (T/m_\pi)^{9/2} \, m_\pi \tag{35}$$

That this is of little importance at higher temperatures has been seen above in the evaluation of the relativistic integrals, because most of the pions stem from the decay of the Δ resonance. The direct production of pions due to pion bremsstrahlung has also been studied, but we will not discuss this here [Vas 80ab,84].

The pressure is evaluated from equation (3). Taking nucleons only, we immediately obtain

$$p = p_C + p_T = \rho^2 \frac{dE_C}{d\rho} + \rho^2 \left. \frac{\partial E_T(\rho,S)}{\partial \rho} \right|_S . \tag{36}$$

For the EOS (14a) the compression pressure is:

$$p_C = \frac{K_0}{18\rho_0} (\rho^2 - \rho_0^2) . \tag{37}$$

If the temperatures are small compared to the Fermi energy, the thermal pressure of the Fermi gas is given by

$$p_T = 1/3 \;\; \beta^{-1} S^2 \rho^{5/3} = \frac{1}{3} \beta \; \rho^{1/3} T^2 \tag{38}$$

which leads to the relation

$$p_T = \frac{2}{3} \rho \, E_T . \tag{39}$$

This equation is valid not only for the low temperature Fermi gas limit but in fact holds in the nonrelativistic case for any temperature and for a classical ideal gas.

It is sometimes advantageous to use a modified form for the pressure, if resonances are included:

$$p_T = \alpha(\rho, E_T) \; \rho \; E_T . \tag{40}$$

The cooling influence of the resonance is absorbed in the density and temperature dependence of α. Calculations can then be carried out with the usual form of the EOS (36) supplemented with the temperature dependent α. Since a significant portion of the "thermal" energy goes into the excitation of hadronic resonances at higher bombarding energies, the relative reduction of the temperature is greatest there. This also reduces p_T, since part of the thermal energy now goes into the additional rest energy Δm of the resonances. Note that the coefficient $\alpha(\rho,E_T)$ is almost independent of the density and depends strongly on E_T .

6. The Liquid- Vapour Transition

At intermediate bombarding energies, $E_{lab} \approx$ 100 MeV/nucleon, the temperatures are not high enough (T < 20 MeV) to cause substantial hadronization. However, another interesting phenomenon has been predicted to occur in the late stages of the collisions when the density has dropped below normal nuclear matter density [Dan 79]: the pressure diagram $P(\rho,T=const)$ shown in Fig. I.6 [Stö 83] exhibits the maximum-minimum structure typical for matter with long range attractions and short range repulsions (i.e. a van der Waals gas). This can be interpreted as a liquid-vapour phase transition in low density nuclear matter. The nuclear EOS exhibits a critical point at $\rho_c \approx 0.4\rho_0$ and $T_c \approx$ 18 MeV. It turns out that these values are not too sensitive to the details of the assumed interaction [Kap 84, Cse 85]. The liquid and the vapour phase can coexist in a well determined density regime once the temperature is less than the critical T_c (the shaded area in figure I.6). Moderate T values are also achieved in the late expansion stage at higher energies due to the adiabatic cooling. The condition for thermodynamic stability of the two phase system is:

$$T_{liquid} = T_{gas},\ P_{liquid} = P_{gas},\ \mu_{liquid} = \mu_{gas}. \qquad (41)$$

At the critical point, $P_c(\rho_c, T_c)$, the isothermal has a saddle point, while for $T > T_c$ the isothermal pressure is monotonous. Then the liquid-vapour phase separation does no longer exist, and this phase is therefore called the fluid phase.

The occurence of a liquid-vapour transition in heavy ion collisions should manifest itself by substantial changes of the mass distributions of light and medium heavy fragments. The study of finite size effects and time scales and a detailed description of the correlations in the nuclear system in the late break-up stage of the reaction is important. For a detailed discussion we refer the reader to the excellent review article of Csernai and Kapusta [Cse 85].

7. Abnormal Matter

The possible existence of density isomers in nuclear matter has been suggested repeatedly by many authors [Fee 46, Bod 71, Mig 72, Lee 74]. Lee and Wick observed that the nonlinear scalar meson self-interaction model - the chiral sigma model - can lead to an abnormal state at high density, $\rho/\rho_0 \approx 3\text{-}5$. They found that chiral symmetry is restored in this state - the nucleons become massless. The binding energy can be enormous, leading to secondary minima in the compressional energy which are several hundred of MeV/nucleon deep. Another mechanism proposed to create secondary minima in $E_c(\rho)$ is the collective excitation of zero frequency spin-isospin modes in nuclear matter called pion condensation (since these modes carry the quantum number of the pion [Mig 72]). These conjectures have spurred considerable activity. However many of these proposals did not attempt to describe the nuclear EOS at other densities or (as in the case of the linear sigma model)

the description of the known properties of nuclear matter was incorrect. Since the existence of isomeric superdense matter is speculative, it is desirable to study this question in models which describe normal nuclear matter in a self consistent way. A recent calculation [Bog 82] fulfills this requirement and still predicts abnormal superdense states. The model used is the relativistic mean field theory discussed above, which is well able to describe normal nuclear matter. The abnormal state comes in by introducing the Δ resonance into the theory. The abnormal state occurence depends now on the strength of the scalar interactions of the Δ. If the coupling constant for this interaction is only one third larger than the corresponding coupling of the nucleon, secondary minima occur in E_C and the abnormal state is predominantly populated by the resonance rather than the nucleon. A similar mechanism has been discussed at high temperatures, leading to abundant resonance formation above a critical temperature [Hei 79, Gar 79]. Since the scalar coupling of the Δ is unknown, the possible existence of these baryonic resonance isomers can not be ruled out. Only by doing a careful analysis of high density experiments can this question be settled.

8. Deconfinement and Chiral Transition - Creation of Quark Matter

A transition from the deconfined quark-gluon plasma phase to confined color singlet states has (probably) occured during the rapid expansion of the early universe. Temperatures were very high but the net baryon charge was small. Therefore one can assume zero baryon chemical potentials in calculating the thermodynamic properties of strongly interacting matter in the early universe. It is sought to re-establish these conditions and thus study quark deconfinement in the laboratory via

nuclear collisions at ultrarelativistic energies $E_{c.m.} > 20$ GeV/nucleon [QM 79, QM 80, QM 82, QM 83, QM 84, Cle 85]. The energy densities attainable in both the central rapidity region (the nucleus-nucleus center of momentum frame) as well as in the fragmentation regions have been estimated to be 1-2 GeV/fm^3. This range of values coincides with the energy densities at which the deconfinement transition is predicted by SU(N) Yang Mills theory (pure gluon matter) on the lattice [Cle 85]. The Monte Carlo data indicate a first order phase transition at temperatures $T \approx 190$ MeV and zero baryon density [Eng 82].

Unfortunately, to date there is only very limited information available about the high density (high chemical potential) region. Lattice QCD calculations of the thermodynamic properties of a plasma including light quarks are hampered by severe theoretical difficulties. The introduction of fermions on the lattice is at this time only feasible in the quenched approximation: quarks have to aquire a large mass $m_q >> T_c$, so that the hopping parameter $(1/m_q)$ expansion converges [Cle 85]. Detailed nonperturbative calculations for the situation expected to occur in violent nuclear collisions, a plasma of light quarks and antiquarks plus gluons, can therefore not be studied. Furthermore, inclusion of fermions requires that the charge and baryon number assume integer values for color singlet states. These problems have been studied but so far without success.

The behaviour of the confined phase (hadron matter) can be described by the effective relativistic field theory of strongly interacting matter discussed above. This approach has been applied successfully to describe known properties of nuclei and nuclear matter. Though developed for normal nuclear systems, this theory may turn out very useful for a phenomenological approach to the phase transition region [The 83]: a sharp

rise is observed for zero chemical potential in the normalized energy density e/T^4. This rise occurs at a critical temperature T_c = 190 MeV and is a phase transition with quite similar thermodynamic appearance as the one observed for SU(2) and SU(3) Yang Mills theory on the lattice. The order of the phase transition depends on the strength of the coupling constants [The 83]. Furthermore, chiral symmetry is restored in this theory just above the critical temperature. The theory does not incorporate deconfinement, though.

Hence, a different approach is necessary if one wants to study deconfinement and the quark-gluon plasma phase at least qualitatively. One can approach the transition region from high temperatures, making use of a perturbative theory of QCD to estimate the thermodynamic properties of a plasma of light quarks and gluons at finite chemical potential μ and temperature T. We would like to emphazise that sizable nonperturbative corrections can be done, but the results should still be taken only as what they are intended to be, namely a qualitative handle on the unsolved nonperturbative treatment [Sto 84, Cle 85].

The energy density e, entropy density s, and baryon number ρ of the deconfined quark gluon phase are obtained from the thermodynamical potential via

$$e = -\mu \frac{\partial \Omega}{\partial \mu} - T \frac{\partial \Omega}{\partial T} + \Omega \tag{42}$$

$$s = - \frac{\partial \Omega}{\partial T} \tag{43}$$

$$\rho = - \frac{1}{3} \frac{\partial \Omega}{\partial \mu} \tag{44}$$

The pressure p and energy density e of the plasma tend towards $\pm B_{vac}$, respectively, for $\mu \to 0$. The running coupling constant exhibits, however, a pole at chemical potentials on the order of 100 MeV, so the curves can not

be continued below this value of μ. It is interesting to note that this chemical potential corresponds to zero baryon number density. Hence, the unphysical pole in the coupling constant can be avoided by plotting the thermodynamic variables as a function of the baryon number density ρ.

To do this let us use for simplicity the MIT bag model which describes hadrons and also the quark-gluon plasma as a volume in space from which the true vacuum has been expelled - it is filled with color carrying objects (quarks and gluons) which can not exist in the true vacuum. The bag is a color singlet state, for which a finite energy can be calculated. One can show that this simple bag model fits the mass spectrum of the light hadrons quite convincingly, if the following conditions are fulfilled. (a) The bag (the volume in which the quarks move), has a constant positive energy density, $B = \Lambda_{VAC}$, which therefore increases infinitely with the bag volume. This bag energy accounts for the quark confining potential, which does not allow the separation of single quarks from each other. (b) The zero point motion has to be included for quarks which move within the small volume of a hadron. (c) The energy of the quarks is included by solving the Dirac equation for a bound quark state inside the bag. (d) Low-order terms in the quark-gluon coupling constant are additionally included to take into account the mutual interactions more realistically.

For the extended quark gluon plasma the zero point motion can be neglected, as the bag here is supposed to be much larger than a hadron bag. For the kinetic energy of the quarks, the Fermi-gas expression for ultra-relativistic particles yields for zero temperature

$$E_{F_Q} = \frac{3}{4} \left(\frac{6\pi^2}{g_Q}\right)^{1/3} \hbar c \, \rho_Q^{1/3} \, . \qquad (45)$$

From the quark Fermi energy, the Fermi pressure may easily be calculated as

$$P_F = \rho^2 \left.\frac{\partial E}{\partial \rho}\right|_\sigma$$

which yields

$$P_{F_Q} = \frac{1}{4} \left(\frac{6\pi^2}{g_Q}\right)^{1/3} \hbar c \; \rho_Q^{4/3} \; . \tag{46}$$

Thus, the Fermi energy and pressure of the quark gas are related via

$$P_{F_Q} = \frac{1}{3} \rho_Q \, E_Q \; . \tag{47}$$

The latter relation holds not only for T=0, but is actually valid for all temperatures, if massless particles are considered. The interaction of the quarks can be calculated from the running coupling and leads to an effective rise of the density-dependent Fermi energy [Stö 77ab]. The density-dependent ground state energy of the quark bag is then given by

$$E_{BAG} = \sum_Q \left(\frac{\Lambda_{VAC}}{\rho_Q} + \frac{3}{4} \left(\frac{6\pi^2}{g_Q}\right)^{1/3} hc(1+\alpha_c)\rho_Q^{1/3} \right) = \sum_Q \left(\frac{\Lambda_{VAC}}{\rho_Q} + E_{F_Q} \right). \tag{48}$$

Finite temperature phase equilibrium calculations were done with this simple model [Sub 85] showing a broad phase coexistence region of the quark gluon plasma with the hadron plasma. A latent heat of about one to two GeV/fm^3 is to be released from the transition from the deconfined phase to the confined phase: thus the transition is first order. This may prove a major handicap for the detection of the quark plasma if it is formed in ultra-relativistic nuclear collisions: any signal from the interior of the system has to travel through the broad region of the phase coexistence and might be lost by the time it arrives at the surface of the system. This is particularly important for strongly interacting probes like antimatter [Hei 84, Sub 85] and strange matter [Raf 82, Koc 83], which will be subject to the complicated hadronic reaction dynamics which has to be tacked on top of the hard problems connected to the confinement problem.

II. Many Body Theory of Nuclear Collisions

1. Hierarchy of Theories

A comprehensive theory of nuclear collisions at high energies should describe relativistic quantum mechanical wave packets interacting via the correct many body interaction. Such a relativistic quantum mechanical treatment has not yet been attempted: even the formulation of the interaction itself poses formidable problems. A natural suggestion for a simpler treatment - and one that has been very successfully employed in the cascade calculations [Yar 79,81; Cug 80,81,82] - is to use measured free N-N cross sections as the primary physical input for a model. This is legitimate if only binary N-N interactions occur and the scattered nucleons always reach their asymptotic states before encountering another nucleon; in other words, if the system is dilute. Thus, the cascade models and all other models that assume point N-N scattering, require diluteness.

If one does not want to assume this diluteness, then the simultaneous interaction of many nucleons has to be allowed. In this case, scattering can no longer be described in terms of asymptotic states and cross sections, but an explicit interaction potential is required. The models that use this approach generally describe the nucleon motion in terms of classical trajectories and forces and are therefore often called classical dynamics models [Bod 77,80,81; Wil 77,78; Cal 79; Mol 84a,85c]. In the relativistic realm there are huge problems even with the formulation of the theory - the meson fields, which have to be included in a relativistic theory, do not obey classical equations even approximately, although it is possible to replace the Dirac equations by relativistic Newton equations. The only possibility to obtain a solvable model seems to

be to ignore second quantization and treat the meson fields classically. The closest treatment of the many-body aspect thus occurs in a model which solves the non-relativistic equations of motion [Mol 85c]. We will start the discussion of dynamical models with this approach.

2. Newtonian Force Model - the Classical Limit

Consider the classical Γ space description of an A body system with fixed degrees of freedom: we have in mind the colliding system of $A = A_P + A_T$ nucleons. Recall that the Γ space is a 6A dimensional phase space and the state of the system is represented by one point in this space. Let $\rho(\vec{r}_1,\ldots,\vec{r}_A,\vec{p}_1,\ldots,\vec{p}_A,t)d\Gamma$ be the probability to find the system at the point $(\vec{r}_1,\ldots,\vec{r}_A,\vec{p}_1,\ldots,\vec{p}_A)$ in Γ space at time t: ρ is the A-body distribution function. The classical Liouville equation then follows from considering ρ as a probability fluid:

$$\frac{\partial\rho}{\partial t} + \sum_{i=1}^{A} \left(\frac{\partial}{\partial \vec{r}_i} \cdot (\rho\, \dot{\vec{r}}_i) + \frac{\partial}{\partial \vec{p}_i} \cdot (\rho\, \dot{\vec{p}}_i) \right) = 0 \qquad (1)$$

$$= \frac{\partial\rho}{\partial t} + \sum_{i=1}^{A} \left(\dot{\vec{r}}_i \cdot \frac{\partial\rho}{\partial \vec{r}_i} + \dot{\vec{p}}_i \cdot \frac{\partial\rho}{\partial \vec{p}_i} \right) .$$

Hamilton's equations imply that:

$$\frac{\partial\rho}{\partial t} = \{H,\rho\} \qquad (2)$$

This is the classical Liouville equation which describes a microcanonical ensemble. For equilibrium, we have the condition $\{H,\rho\} = 0$ and hence $\rho = C\delta(E - H(\vec{r}_1,\ldots,\vec{r}_A,\vec{p}_1,\ldots,\vec{p}_A))$.

Applying the Newtonian Force Model to nuclear physics means solving Newton's or Hamilton's equations of motion for the A interacting nucleons. This is a theory for the full non-equilibrium classical situation. This approach has some similarities with the molecular dynamics

approach to the theory of liquids [Ald 57]. The NFM is more fundamental than a kinetic equation approach since it solves the Liouville equation.

Of course, there are no quantum effects in this model. However, one does have information about the A-body classical distribution function, once one has chosen some classical potential. Over the years, nuclear physicists have been driven to more and more complicated nucleon-nucleon interactions culminating e.g. in the Paris potential [Cot 73] in order to accommodate to the spin, isospin, etc. degrees of freedom.

A simple ansatz for a classical central potential that acts between each nucleon and all other A-1 nucleons consists of repulsive and attractive Yukawa terms [Mol 84a]:

$$V = (V_R\, e^{-k_R \cdot r} - V_A\, e^{-k_A \cdot r})/r. \qquad (3)$$

One may of course use some other convenient parameterization, such as a Morse potential [Mol 85c]. The parameters in the potential are chosen in a compromise between reproducing the n-p differential scattering cross section at $\theta_{CM} \approx 90^{\circ}$ (which has the largest influence on the transverse momentum transfer) and giving reasonable binding energies and stable nuclei in a completely classical calculation. Recall that the cross section classically is calculated from:

$$\frac{d\sigma}{d\Omega} = \frac{b}{\sin(\theta)}\left|\frac{db}{d\theta}\right| . \qquad (4)$$

It is not adequate to compare this quantity directly with the experimental differential cross section, because of the purely quantum mechanical diffraction and exchange effects. A meaningful quantity to fit is the viscosity moment of the scattering cross section:

$$\sigma_v = 2\pi \int \sigma(\theta)\sin^2(\theta)d(\cos(\theta)) \qquad (5)$$

which is related to the viscosity and thermal conductivity in a Boltzmann equation approach [Bod 77].

In the NFM approach [Mol 84a], nuclei are described as an ensemble of protons and neutrons initially distributed at random throughout a sphere with the nuclear radius $R = 1.2\ A^{1/3}$. Some cutoff on the interparticle positions, say 1.2 fm, must be imposed so that nucleons do not evaporate with large amounts of energy due to the repulsive potential. There is, of course, always some evaporation since it is a difficult problem to put the particles into stable orbits. The nucleons are also given random Fermi momenta. For a numerical simulation of a collision process, the nuclei are Galilei boosted with the respective center of mass momenta at given impact parameter. The Newtonian equations of motion are then integrated using a fourth order Adams-Moulton predictor-corrector method; energy conservation to better than a few percent is demanded. Newton's equations of motion are solved for the $A = A_P + A_T$ interacting nucleons:

$$\vec{F}_i = \frac{d\vec{p}_i}{dt} = - \frac{\partial U}{\partial \vec{r}_i} \qquad (6)$$

where $U(r_i) = \sum_{j \neq i=1}^{A} V(r_{ij})$.

We show in Fig. II.1 how a Nb + Nb collision at 400 MeV/nucleon evolves in this approach. Note the strong bounce-off or side-splash of nuclear matter [Mol 84a]. Calculations for many other systems have been done by other authors [Bod 77, Wil 77, Bod 80, Bod 81, Wil 78, Cal 79, Mol 85c].

The main problem with the NFM approach is that classical potentials can provide only a poor approximation to N-N scattering and nuclear binding properties. For example, we find that in order to simulate

nuclear saturation, the two body potential must have a small long range repulsive tail [Mol 85c], as had been suggested earlier [Wil 78]; a more convenient form for the potential is then a Morse form instead of (3) and an exponential for the long range repulsion [Mol 85c]. Additional complications occur in the relativistic generalization [Kun 81]. However, the NFM is the model, which comes closest to the solution of the many-body aspect and enables a study of finite range effects of the repulsive core [Mol 84a]. Also it is of fundamental importance to nuclear physics that such a classical approach can, with partial success, describe heavy ion interactions in the intermediate energy range. It would be most important to study also retardation effects in an appropriate generalization, which for v << c reduces to the NFM.

3. From the N-body density matrix to Time Dependent Hartree Fock

To solve the quantum non-relativistic A body nuclear physics problem, one has to solve the time dependent Schrödinger equation [Sch 25]:

$$i\hbar \frac{\partial \Psi}{\partial t} = H\Psi \qquad (7)$$

where

$$\Psi = \Psi(1,2,\ldots,A,t) \qquad (8)$$

is the time dependent many-body wave function, A is the total number of nucleons, and H is the many body Hamiltonian. This is in general an impossible task just as the complete relativistic problem is.

Recall that an approach to the static many body problem for atomic electrons is Hartree's theory of the self-consistent field [Har 27]. There one starts with a set of single particle wave functions, generates with this set a single particle potential by averaging the many body interaction, solves the single particle problem and gets a new set of single particle

wave functions. These steps are iterated until consistency between the wave functions and the potential is achieved.

Static Hartree-Fock theory includes an additional exchange term [Foc 30]. Here, the many body wave function is approximated as a Slater determinant of single particle wave functions, the hamiltonian containing the Hartree field and a non-local single particle potential. Again one proceeds iteratively to achieve consistency between the averaged interaction and the wave functions. The HF method constructs a Fermi sea of particles with a sharp Fermi surface, since in calculating the HF determinant one selects the A lowest single particle wave functions in energy. Thus one may regard the HF state as the particle hole vacuum $|\ >$ [Row 70].

Static Hartree Fock theory has had much success in the shell models for electrons and later nucleons. In heavy ion nuclear physics, however, one has a time dependent problem of A colliding nucleons. The complete nuclear wave function Ψ contains lots of information - perhaps more than we will ever need or be able to use. Therefore, some approximations to get a tractable Time Dependent Hartree Fock theory are justified.

Nucleons are bound together solely by their mutual interaction: there is no external central field as in the case of atomic electrons. The HF method is an approximation for reducing the problem of many interacting particles to one of non-interacting particles in a potential and neglects residual interactions. TDHF is used to describe excited states and to take into account the long range or field part of the residual interaction.

Recall that TDHF can be derived in the formalism of second quantization [Koo 75]. Let

$$|abc\ldots\rangle = 1/\sqrt{A!}\,{}_{(ab\ldots)}\Sigma\psi_a\psi_b\ldots\mathrm{sgn}(abc\ldots) \qquad (9)$$

be the Slater determinant, where the subscripts label space, spin, and isospin. We define the particle creation and destruction operators $a_i^\dagger$ and a_i, respectively. Antisymmetry and the Pauli principle yield the anti-commutation relations [Row 70]:

$$\{a_i^\dagger, a_j^\dagger\} = 0 \text{ and } \{a_i^\dagger, a_j\} = \delta_{ij}. \tag{10}$$

The state Ψ of the nucleus is then a linear combination of such Slater determinants.

The many body Hamiltonian is

$$H = T + V$$

$$= \sum_{ij} T_{ij} a_i^\dagger a_j + \frac{1}{2} \sum_{ijkl} U_{ijkl}\, a_i^\dagger a_j^\dagger a_l a_k \tag{11}$$

where the kinetic energy is a single particle operator and U is the two body interaction. The one body density matrix is

$$\rho_{ji} = \langle \Psi | a_i^\dagger a_j | \Psi \rangle \ . \tag{12}$$

The von Neumann equation

$$i\hbar\, d\rho/dt = \langle \Psi | [a_i^\dagger a_j, H] | \Psi \rangle \tag{13}$$

follows from the Schrödinger equation and the assumption that H is hermitean After inserting the many body Hamiltonian and some algebra, this time dependent density equation will <u>not</u> reduce to a purely one body equation. The two body force couples ρ to the two body density matrix $\rho^{(2)}$, leading to the so called BBGKY hierarchy. The TDHF approximation is based on the assumption that the matrix elements of $\rho^{(2)}$ factor:

$$\rho^{(2)}_{ijkl} = \rho_{jk}\rho_{il} - \rho_{jl}\rho_{ik} \ . \tag{14}$$

This terminates the BBGKY hierarchy and yields the TDHF equation

$$i\hbar\, d\rho/dt = [h, \rho] \tag{15}$$

where h is the HF hamiltonian:

$$h = \sum_{ij} \left(T_{ij} + \sum_{kl} (V_{ikjl} - V_{iklj})\rho_{lk}\right) \ . \tag{16}$$

It is not difficult to show that particle number and the energy are conserved in TDHF [Koo 75]. Furthermore, each of the single particle orbitals satisfies the time dependent Schrodinger equation with the HF hamiltonian h.

TDHF has been applied with some success at energies up to 10 MeV/nucleon. Fusion, compound nucleus formation, dissipation, strongly damped collisions, shock wave propagation, and fragmentation are all found in TDHF [Bon 76]. Beyond this range, TDHF and mean field theory in general is not sufficient because of the lack of two body collisions and the assumption of a long mean free path for the nucleons. The mainly potential scattering of TDHF implies only a single particle viscosity so that the nuclei are rather transparent for $E_{CM} > E_F = 38$ MeV. This transparency is illustrated in Fig. II.2 for C (85 MeV/nucleon) + C [Stö 80a,81b].

To go beyond TDHF, consider that some perturbing two body interaction causes particles to scatter from their unperturbed orbitals. In first order perturbation theory, the perturbed wave function is:

$$|\Psi\rangle = |\Psi_0\rangle + 1/i\hbar \sum_{klk'l'} \int dt\, e^{i\omega t} V_{k'l'kl} a^\dagger_{k'}, a^\dagger_{l}, a_l a_k |\Psi_0\rangle$$

$$= |\Psi_0\rangle - \sum_{klk'l'} \frac{e^{i\omega t}-1}{\hbar\omega} V_{k'l'kl} a^\dagger_{k'}, a^\dagger_{l}, a_l a_k |\Psi\rangle . \qquad (17)$$

The density matrix then evolves according to the von Neumann equation:

$$d\rho_{ii}/dt = \frac{1}{i\hbar} \langle\Psi| a^\dagger_i [a_i, V] + [a^\dagger_i, V] a_i |\Psi\rangle . \qquad (18)$$

Proceeding is now complicated by the fact that one has to evaluate octupole Fock space operators. Let us therefore consider a one body perturbing interaction as an illustrative example [Ber 84a]. Then the first order perturbed wave function is:

$$|\Psi\rangle = |\Psi_0\rangle - \sum_{kk'} \frac{e^{i\omega t}-1}{\hbar\omega} V_{k'k}\, a^\dagger_{k'}, a_k |\Psi_0\rangle . \qquad (19)$$

In the one body case, it is easily shown using the anti-commutation rules that

$$[a_i,V] = \sum_j V_{ji}a_j \quad \text{and} \quad [a_i^\dagger,V] = -\sum_j V_{ij}a_j^\dagger. \tag{20}$$

With the additional assumption that the one body density matrix is diagonal

$$\rho_{ji} = n_i\,\delta_{ij} \tag{21}$$

we have for the occupation number n_i the equation

$$dn_i/dt = 1/i\hbar \sum_j V_{ij}\langle\Psi|a_i^\dagger a_j - a_j^\dagger a_i|\Psi\rangle. \tag{22}$$

Substituting the bra and the ket first order perturbed wave functions, one gets terms of first, second, and third order in V. The first order terms are already in the mean field and the third order terms may be neglected with respect to the second order ones. A typical second order term is

$$\begin{aligned}\langle\Psi_o|a_i^\dagger a_j a_{l'}^\dagger a_l|\Psi_o\rangle &= \langle\Psi_o|a_i^\dagger(\delta_{jl'}-a_{l'}^\dagger a_j)a_l|\Psi_o\rangle \\ &= \rho_{li}\delta_{jl'} - \rho_{ljl'i} \\ &= \rho_{li}\delta_{jl'} - \rho_{jl'}\rho_{li} + \rho_{ji}\rho_{ll'} \\ &= n_i(1-n_j)\delta_{li}\delta_{jl'} + n_i n_l \delta_{ij}\delta_{ll'}\,. \end{aligned} \tag{23}$$

Combining the above equations, one finds

$$\begin{aligned} dn_i/dt &= 1/\hbar^2 \sum_j [2V_{ij}\sin(\omega_{ji}t)/\omega_{ji}][n_j(1-n_i)-n_i(1-n_j)] \\ &= 2\pi/\hbar \sum_j V_{ij}^2 \delta(E_j - E_i)[n_j(1-n_i)-n_i(1-n_j)]. \end{aligned} \tag{24}$$

where we have extended the time limit to infinity and made use of one definition of the delta function. This is a standard Boltzmann equation with the golden rule applied for the interactions. The extension to the δ function requires that the time t of the transition be sufficiently large but also less than the collision time, so that double and higher order collisions (formally higher order in V) can't take place. In the two body case, one expects by analogy the corresponding equation:

$$dn_i/dt = 2\pi/\hbar \sum_{ji'j'} V^2_{ijj'i'}\delta(E_{i'}+E_{j'}-E_i-E_j)$$
$$[n_{i'}n_{j'}(1-n_i)(1-n_j)-n_in_j(1-n_{i'})(1-n_{j'})]. \qquad (25)$$

This then provides some plausible justification for Uehling and Uhlenbeck's original ansatz for a collision term [Ueh 33].

4. The Vlasov-Uehling-Uhlenbeck Equation

One way to include two body collisions is thus to couple to the TDHF equation a master equation involving the occupation probabilities of the single particle states n_i [Rem 84]. We now replace the summation over the discrete single particle levels by continuous integrals over momenta:

$$\sum_{ji'j'} \rightarrow \int d^3p_2 d^3p_1' d^3p_2'/(2\pi\hbar)^3 \qquad (26)$$

Furthermore, the continuous analog of the occupation probability is the Wigner function

$$f(\vec{p},\vec{r}) = \int d^3s\, e^{i\vec{p}\cdot\vec{s}/\hbar}\rho_{r+s/2,r-s/2}$$
$$= \int d^3q\, e^{-i\vec{q}\cdot\vec{r}/\hbar}\rho_{p+q/2,p-q/2} \qquad (27)$$

which has the properties that

$$\rho(\vec{r}) = \int d^3p\, f(\vec{p},\vec{r})/(2\pi\hbar)^3 \text{ and } \rho(\vec{p}) = \int d^3r\, f(\vec{p},\vec{r})/(2\pi)^3. \qquad (28)$$

One can also eliminate the matrix element $\langle \vec{p}_1\vec{p}_2|V|\vec{p}_1'\vec{p}_2'\rangle$ with the Born approximation:

$$\langle p_1p_2|V|p_1'p_2'\rangle^2 = (2\pi\hbar^2/\mu)^2 d\sigma/d\Omega\ . \qquad (29)$$

Then one obtains from eq. (25) the Uehling-Uhlenbeck collision term

$$\left(\frac{df}{dt}\right)_{coll} = -\int \frac{d^3p_2 d^3p_1' d^3p_2'}{(2\pi)^6}\, \sigma v_{12} \times$$
$$[ff_2(1-f_1')(1-f_2')- f_1'f_2'(1-f)(1-f_2)]\delta^3(\vec{p}+\vec{p}_2-\vec{p}_1'-\vec{p}_2') \qquad (30)$$

where we have replaced f_1 by f. Finally, we may also write the total derivative as:

$$\frac{df}{dt} = \frac{\partial f}{\partial t} + \vec{v}\cdot\frac{\partial f}{\partial \vec{r}} + \frac{d\vec{p}}{dt}\cdot\frac{\partial f}{\partial \vec{p}} \quad . \tag{31}$$

This last equation set equal to zero is the Vlasov equation. Finally combining these, we get the Vlasov-Uehling-Uhlenbeck equation [Ueh 33]:

$$\frac{\partial}{\partial t} f + \vec{v}\cdot\frac{\partial}{\partial \vec{r}} f - \nabla U \cdot\frac{\partial}{\partial \vec{p}} f = -\int \frac{d^3p_2 d^3p_1' d^3p_2'}{(2\pi)^6} \sigma v_{12} \times$$
$$[ff_2(1-f_1')(1-f_2') - f_1'f_2'(1-f)(1-f_2)]\delta^3(\vec{p}+\vec{p}_2-\vec{p}_1'-\vec{p}_2') \tag{32}$$

The main input is now a potential and the free nucleon-nucleon differential cross section. The Fermi-Dirac distribution, which is a solution of the Vlasov equation, is also the equilibrium solution of the collision term.

For the interaction U, we use a local Skyrme interaction. Let us briefly review the Skyrme model [Sky 59]. Skyrme's interaction can be written as a potential:

$$V = \sum_{ij} V_{ij}^{(2)} + \sum_{ijk} V_{ijk}^{(3)} \tag{33}$$

with two and three body parts. In configuration space, the two body part is [Vau 72, Bei 75]:

$$V^{(2)}(\vec{r}-\vec{r}') = t_0(1 + x_0P_\sigma)\delta(\vec{r}-\vec{r}') + 1/2\ t_1(\vec{k}'^2\delta(\vec{r}-\vec{r}') + \delta(\vec{r}-\vec{r}')\vec{k}^2) +$$
$$t_2\vec{k}'\cdot\delta(\vec{r}-\vec{r}')\vec{k} + iW_0\vec{k}'\cdot\delta(\vec{r}-\vec{r}')\vec{\sigma}\hat{}\vec{k} \tag{34}$$

where

$$\vec{k} = (\partial/\partial\vec{r} - \partial/\partial\vec{r}')/2i \quad \text{and} \quad \vec{k}' = \vec{k}^\dagger \tag{35}$$

are the relative momentum operators and

$$P_\sigma = 1/2\ (1 + \vec{\sigma}_1\cdot\vec{\sigma}_2) \tag{36}$$

is the spin exchange operator.

The three body part is

$$V^{(3)}(\vec{r}_1,\vec{r}_2,\vec{r}_3) = t_3\delta(\vec{r}_1-\vec{r}_2)\delta(\vec{r}_2-\vec{r}_3). \tag{37}$$

Hartree-Fock calculations are usually done with this Skyrme interaction. The expectation value of the total energy is:

$$E = \langle\Psi|T + V|\Psi\rangle$$
$$= \int H(\vec{r})\, d^3r \qquad (38)$$

where H is the Hartree Fock functional energy density. For the Skyrme interaction, this energy density is an algebraic function of only three quantities: the nucleon density, kinetic energy density, and spin density:

$$\rho(\vec{r}) = \sum_{i=1}^{A} |\psi_i(\vec{r})|^2 \;,\; \tau(\vec{r}) = \Sigma\, |\nabla\psi_i(\vec{r})|^2 \;,\; \vec{J}(\vec{r}) = -i\, \Sigma\, \psi_i^*(\vec{r})\cdot(\vec{\nabla}\psi_i(\vec{r})\hat{\sigma}). \qquad (39)$$

For the case of a symmetric nucleus, N = Z, and a neglecting the Coulomb field, the densities for neutrons and protons are equal:

$$\rho_n = \rho_p = 1/2\ \rho \;,\; \tau_n = \tau_p = 1/2\ \tau \;,\; \vec{J}_n = \vec{J}_p = 1/2\ \vec{J}. \qquad (40)$$

Then the energy density simplifies to

$$H(r) = \hbar^2\tau/2m + \frac{3}{8}t_0\rho^2 + \frac{1}{16}\, t_3\rho^3 + \frac{1}{16}\,(3t_1 + 5\, t_2)\rho\tau +$$
$$\frac{1}{64}\,(9t_1 - 5t_2)(\vec{\nabla}\rho)^2 - \frac{3}{4}\, W_0\rho\vec{\nabla}\cdot\vec{J}\ . \qquad (41)$$

In nuclear matter $\vec{\nabla}\rho = 0 = \vec{\nabla}\cdot\vec{J}$, $\rho = \frac{2}{3}\, k_F^3/\pi^2$, and $\tau = 3/5\ k_F^2\rho$. Then the binding energy per particle reads

$$E/A = H/\rho = \frac{3}{5}\, E_F + \frac{3}{8}\, t_0\rho + \frac{1}{16}\, t_3\rho^2 + \frac{3}{80}(3t_1+5t_2)\rho k_F^2 \qquad (42)$$

and the potential is

$$U(\vec{r}) = \frac{3}{4}\, t_0\rho + \frac{3}{16}\, t_3\rho^2 + \frac{3}{40}(3t_1 + 5\, t_2)\rho k_F^2. \qquad (43)$$

Note that the potential and the energy density are related by $U = \left(\frac{\partial H}{\partial \rho}\right)_{\tau,\vec{J}}$.

For colliding relativistic nuclei in the non-ultra-relativistic case, we can to first order neglect the problems of the relativistic field and calculate the potential locally. In the spirit of the Skyrme interaction in nuclear matter, we take the potential in a density expansion $U = a\rho + b\rho^2$ so that the binding energy is $E/A = \frac{3}{5}\, E_F + \frac{1}{2}\, a\rho + \frac{1}{3}\, b\, \rho^2$. The long range Coulomb and Yukawa interaction are neglected here as well as the

nuclear surface. We now measure ρ in units of $\rho_o = 0.17/fm^3$. Then we impose the three conditions E/A = - 16 MeV, $\frac{3}{5} E_F$ = 23 MeV, and K = 380 MeV. The saturation condition $\frac{\partial(E/A)}{\partial k_F} = 0$ is equivalent to the zero pressure condition $p = \rho^2 \frac{\partial(E/A)}{\partial \rho} = 0$ and the compressibility $K = k_F^2 \frac{\partial^2(E/A)}{\partial k_F^2}$ may also be written as $K = 9 \rho \frac{\partial p}{\partial \rho}$. These three conditions fix the parameters a = -124 and b = 70.5. Similarly, if we take the expansion $U = a\rho + b\rho^{7/6}$ and impose K = 200 MeV, we find a = -356. and b = 303.

In Fig. II.3, we plot these two local Skyrme interactions and compare to the equation of state extracted recently from pion multiplicity data [Sto 82]. Note that the cascade and chemical model analysis, which derive a nuclear EOS from the differences of the calculated pion multiplicities and the observed pion yields, tend to agree with our stiff EOS.

5. Application of the VUU theory - Study of the Non-Equilibrium and Quantum Effects

The VUU equation is difficult to solve since it is a highly non-linear differentio-integral equation in six dimensional phase space. Since this equation comes close to the classical limit, one may solve it in terms of quasi-particles, whose mean positions are solutions of Newton's equations [Kru 85ab, Ber 84ab, Mol 84b, Mol 85ac]:

$$\vec{p}/m = d\vec{r}/dt \quad \text{and} \quad d\vec{p}/dt = -\partial U/\partial \vec{r} \; . \tag{44}$$

We actually go beyond the VUU equation by including not only a mean field and Pauli Blocking of the final state, but also relativistic kinematics and particle production. We call this the VUU theory.

The stability of the ground state nuclei in this VUU theory is an important issue to address in testing the method [Mol 85b,85c]. In Fig. II.4, we show that the ground state nuclei are quite stable up to times of the order of 80 fm/c. Smaller time steps can be used to obtain greater stability.

To solve the VUU equation, fifteen collision simulations are followed in parallel and the ensemble averaged phase space density in a sphere of radius 2 fm around each particle is computed [Kru 85a, Mol 85c]. The ensemble averaging results in statistical fluctuations at the 10% level and thus reasonably smooth single particle distribution functions, which are used to determine the mean field and the Pauli blocking probability. About a hundred such parallel ensembles are followed to simulate an actual reaction.

A constant time-step integration routine is used to insure synchronization of the ensembles. The acceleration of the test particles due to the field gradient is calculated prior to each transport step and is assumed to be constant within a synchronization time step. The local gradient of the field is computed via a finite difference method between two hemispheres centered around the test particle. This method is analogous to Lagrange's method in fluid dynamics, in contrast to the space-fixed Eulerian mesh.

Protons, neutrons, deltas and pions of different isospin are included separately with their experimental scattering cross sections. The question of double counting of the mean field and the collision term is a basic restriction for the VUU approach. We take the following operational point of view: the phenomenological Skyrme potential incorporates the real part of the potential, i.e. the attractive one meson exchange (the linear

term in U) and repulsive mean field interactions, while the two body scattering accounts for the residual interactions. It should be pointed out that energy and momentum conservation is fulfilled in the present approach for individual two body scatterings and for the ensemble average on the mean but not within each separate ensemble, because of the coupling between different ensembles (energy conservation problems have been studied for a similar approach by Koehler [Koe 80] using the relaxation time ansatz).

The free particle cross sections have to be corrected for "in medium" effects, the most important one being the Pauli blocking of collisions. Two particles may undergo s-wave scattering if they approach each other with a minimum distance of less than $\sqrt{(\sigma(\sqrt{s})/\pi)}$ and if the final states are not Pauli blocked. The Pauli blocking factor for each nucleon is given by $(1-f)$, and the scattering probability is then reduced by the Uehling-Uhlenbeck factor $(1-f_1)(1-f_2)$. The Pauli blocker has been tested on ground states of nuclei and forbids there about 97% of all collisions. It is very important at intermediate bombarding energies, too: even at 137 MeV/nucleon, 80% of the attempted collisions are blocked due to lack of available final state configurations (Fig. II.5). Many of these attempted collisions are between nucleons of the same nucleus.

What is the effect of the collision term in the VUU theory? The system Ar + Ca has been studied in the mean field approximation without two body collisions [Kru 85b], thus mimicking TDHF by solving the Vlasov equation - as far as we know this is the first time that a solution of the Vlasov equation in three dimensions has been done for nuclear collisions. The lack of two body collisions results in strongly forward peaked angular distributions, in qualitative agreement with 3D TDHF calculations [Stö 80a, 81b] in this energy regime. Figure II.6a shows the initial state in

momentum space for Ar (137 MeV/N) + Ca; note that at this energy the Fermi spheres of target and projectile nuclei are well separated. The Ar projectile moves in the positive z-direction, while the Ca target moves in the negative z-direction in this center of mass frame. Fig. II.6b,c show the final state of this reaction as obtained in the present theory without and with the Uehling-Uhlenbeck collision term. Note that the momentum space distribution is practically unchanged in the mean field calculation--equilibration of the momenta is not observed--while the inclusion of the Uehling-Uhlenbeck collision term results in strong equilibration--the isotropy in Fig. II.6c is indicative of substantial thermalization. A convenient way to compare momentum distributions is to use the ratio of transverse to longitudinal momenta

$$R = 2/\pi \, \Sigma \, p_{\perp} / \Sigma \, p_{||} \, , \tag{45}$$

where $p_{\perp}$ and $p_{||}$ are the momenta perpendicular to and parallel to the beam. Comparing the ratio of final to initial R values, we find 1.08 for the mean field only case and 2.05 for the mean field + collisions approach. At lower energies, the comparison is not as dramatic; the initial R values are already high since the nuclei overlap more in momentum space--furthermore, most of the collisions are Pauli blocked. But the collision term always leads to increased isotropy. In configuration space, one finds the well known transparency when the Vlasov equation is solved and stopping when the collision term is included: a substantial degrading of the initial momentum occurs once the collision term is included [Kru 85b, Aic 85a].

Figure II.2a,b shows for the lighter system C (85 MeV/nucleon) + C at b = 1 fm the time evolution in configuration space in the three dimensional TDHF [Stö 80a,81b] and Vlasov equation calculations [Aic 85a]. There is a very similar behavior in both the quantum mechanical and

classical mean field theories: both calculations exhibit transparency and nearly identical small longitudinal and transverse momentum transfers. The lack of two body collisions results in strongly forward peaked angular distributions, in sharp contrast with the data in this energy regime. Both theories predict that for central collisions of C + C the nuclei slip through each other and survive the reaction rather intact.

Just like for the Ar + Ca system [Kru 85b], the inclusion of the Uehling-Uhlenbeck collision integral changes this drastically (Fig. II.2c): each individual reaction can now be separated into two clearly distinct components. First, we observe the slipped-through projectile- and target-like fragments, which now retain about 40% of the nucleons and less than 20% of the initial longitudinal c.m. momentum. As we see in Fig. II.7, these slipped-through residues contain mostly particles which have not scattered at all.

The second component consists of the 60% of the nucleons which have undergone at least one nucleon-nucleon scattering and form a non-equilibrated mid-rapidity system with an almost isotropic emission pattern. At even higher energies, Ar (800 MeV/N) + Pb (see below), complete stopping of the projectile in the target has been predicted [Mol 84b, 85c]. What then is the reason for the incomplete deceleration of the nuclei in the present study? At these low energies a rather large fraction of the attempted nucleon-nucleon collisions are forbidden by the Pauli blocking of the exit channels and the nucleon's mean free path is effectively longer as a result of the Pauli principle. Furthermore, the C + C system is rather small, hence the chances for a nucleon-nucleon collision to occur is smaller than in a bigger system.

At less central impact parameters, negative angle scattering is observed in both pure mean field approaches, and again the classical and the quantum approach agree remarkably well [Aic 85a]. The collision term results in less inward scattering. The midrapidity source is much less apparent; two slightly decelerated and excited residues survive the collision. The effect of the collision term is less dramatic at these larger impact parameters due to the smaller geometrical overlap of the nuclei, which reduces the number of nucleon- nucleon collisions.

In Fig. II.7 we show the reaction C (85 MeV/N) + C at b = 1 fm in more detail [Aic 85a]. The initial and the final density profiles in configuration and momentum space are displayed. We distinguish between particles which did not undergo any collision ($N_c = 0$) and scattered particles with $N_c > 0$. The mid-rapidity region consists almost exclusively of scattered particles. The high momentum components of the initial momentum space distribution get most effectively depleted by collisions because for them the Pauli blocking is least effective. A collective deceleration of the projectile-like fragments is caused by the mean field. Those particles which have undergone collisions exhibit a nearly isotropic distribution in momentum space.

A generalized 6-dimensional coalescence model has been used to find the nucleons bound in clusters for the Ar + Ca system and prevent them from contributing to the proton cross sections [Kru 85b]. This has not been done for C + C [Aic 85a,85b,85c]. This coalescence is important at medium energies, where a large fraction of the emitted protons are found to be bound in fragments. In this scheme, a nucleon is part of a cluster, if it is within a configuration space distance r_0 from some other member of the cluster and within a momentum space distance p_0 from the center-of-momentum

of the cluster. The sequential evaporation of protons from residual fragments is not included. The generalized coalescence prescription has been used to calculate inclusive proton spectra from the primordial nucleon distribution with r_0=2.2 fm and p_0=200 MeV/c. It is interesting to point out that the phase space volume spanned by these values is very close to h^3, the volume occupied by a fourfold degenerate Fermion. Our approach gets further support from the agreement of the predicted fragment yields as a function of fragment mass to the experimental data for masses 1 - 14 [Jac 83].

Fig. II.8 shows the comparison between calculated and measured proton spectra for 42 and 92 MeV/nucleon Ar + Ca. The calculated absolute cross sections and the slopes of the spectra agree reasonably well with the data. In contrast, a simple cascade simulation, though appropriate for high energies, cannot reproduce the medium energy data [Kru 85b]. [Aic 85c] has compared un-coalesced proton spectra directly with experimental data by simply scaling them; we feel that the coalescence step is essential. Furthermore, coalescence is the easiest way to begin to study fragmentation and the liquid gas phase transition.

The dependence of the nuclear stopping power on the target mass has also been studied [Aic 85a]. Central collisions of C (85 MeV/nucleon) projectiles with 6 different targets from C to Au have been analyzed. The number of projectile nucleons undergoing at least one collision increases from about 60% for the C target to about 97% for the Au target. An almost complete stopping of the projectile in the target occurs for the heavier targets. The number of projectile nucleons being emitted without having undergone a collision up to a time t = 160 fm/c is shown in Fig. II.9 as a function of the target diameter D_t for 100 parallel runs. We observe an

exponential fall-off with D_t. This can be reproduced by assuming that the mean free path of the nucleons in heavy ion collisions in this energy region is $\lambda \approx 2.6$ fm, which is larger than the mean free path estimated from classical kinetic theory, $\lambda_c = (\sigma \rho)^{-1/2} = 1.4$ fm. This difference is mainly due to the effects of the Pauli-principle. Other effects are the density increase in the collision (which decreases λ) and the finite deceleration due to the mean field (which also decreases λ).

This result is similar to those obtained with the VUU method for Ar + Pb at 92, 400 and 800 MeV/nucleon bombarding energy [Mol 84b]. Let us examine the evolution of the single particle distribution function as calculated from the VUU approach for Ar (770 MeV/nucleon) + Pb collisions. In Fig. II.10 and 11 we display projections of the distribution function into configuration and momentum space for this system. It is remarkable how closely these figures resemble Fig. II.12 and 13, calculated with the Nuclear Fluid Dynamic model [Gra 84]. In the VUU approach, the collision term is essential at both intermediate and high energies, as one expects intuitively. At low impact parameter the Ar projectile is completely consumed by the Pb target as well in configuration as in momentum space (see fig. II.10, II.11). The t=0 configuration space plots show the correct nucleon-nucleon center of momentum frame Lorentz length contraction by a factor $1/\gamma = .85$. In configuration space, for t=10 fm/c, the squashed elliptical to octupole shape is an indication of the high density formed in these collisions. For example, at 1 fm impact parameter, the density within a sphere of radius 2 fm centered at the origin reaches $2.7\ \rho_o$ at 5 fm/c ; then, the density falls very rapidly - by 17 fm/c it is below the ground state value. The directed sidewards flow of nucleons is easily seen in configuration space at b = 3 and 5 fm by the excess of nucleons in the

quadrant with $x < 0$ and $z < 0$ (as opposed to $x < 0$ and $z > 0$) as early as t=20 fm/c. Spectator fragments are also observed, namely at 5 fm. The projectile is seen to not just shear off the target; it rather experiences a substantial transverse momentum transfer away from the region of high density - the bounce-off effect predicted earlier on the basis of nuclear fluid dynamics [Stö 80b, Buc 83a,84a]. Thus, simple geometric models can only be a very rough approximation to the more complicated reaction dynamics illustrated here.

The momentum space evolution of the single particle distribution function displayed in Fig. II.11 shows rapid equilibration at low impact parameters: the projectile sphere in momentum space is rapidly depopulated by two body collisions at b = 1 and 3 fm. At t = 5 fm/c substantial filling of the nucleon-nucleon center of momentum region is observable, indicating the formation of a participant zone. At t = 10 fm/c, there are practically no nucleons left in the originally densely populated projectile momentum sphere; almost all of the projectile nucleons have been scattered out of their initial momentum states. At b = 1 fm, this scattering has been with about equal probability into the positive and negative p_x direction. At b = 3 fm, a preference for the positive p_x direction can clearly be observed - this is due to the expansion of the compressed participant matter away from the high density repulsive interaction into the vacuum. At t = 40 fm/c the number of hard nucleon - nucleon collisions has become negligible, the final state in momentum space is closely approached. Secondary, tertiary, and higher collisions of the participants have resulted in a further decrease of the number of fast particles and in a more diffuse momentum distribution in the projectile hemisphere, with a very pronounced sidewards flow visible at b = 3 fm.

At the intermediate impact parameter, b = 5 fm, the situation is even more complicated: since projectile and target exhibit only about half overlap, there are a substantial number of projectile nucleons which do not experience collisions with the target nucleons. Hence the depopulation of the projectile momentum sphere is incomplete, part of the projectile is stopped and forms the participant zone together with the struck nucleons from the target, while the projectile spectators move ahead with nearly their initial longitudinal momentum. The behavior of the participant nucleons is almost the same as at the lower impact parameters - equilibration is achieved rapidly (t ≈ 10 fm/c) and sidewards flow is observed. The projectile nucleons which have not undergone collisions, and thus the projectile like fragments formed from them, exhibit a finite transverse momentum transfer into the same direction as the directed participant side splash. This bounce-off of the participants is a result of the repulsive interactions felt by the spectators in the vicinity of the compression zone. The simultaneous occurrence of this bounce off and the sidesplash has recently been observed experimentally in symmetric [Gus 84] and asymmetric [Ren 84] systems with high statistical confidence.

The equilibration at low impact parameter goes hand in hand with nuclear stopping; without the collision term, the nuclei are transparent. As a reference case, we have also solved the Vlasov equation by turning off the collision term; then the final momentum distribution looks very much like the initial one, as we saw above at lower energies.

An easily accessible experimental quantity is the longitudinal momentum (p_z) distribution in the laboratory frame. The multiplicity dependence of this quantity should give information on the nuclear stopping. Initially the Ar nuclei form a bump at beam momentum p_z= 1430 MeV/c, whereas

energy reaction could be regarded as a cascade process. Collisions occur between the incident particles and those particles which are directly struck in the nucleus. This model was first investigated in two dimensions in 1948 by Goldberger [Gol 48], who performed his calculations by hand for the case of high energy neutrons interacting with heavy nuclei. The first three dimensional calculations were done in 1958 [Met 58] for incident protons and neutrons using the MANIAC computer; also a second stage to the cascade calculation was added during which the excited residual nucleus evaporates particles, as had also been suggested by Serber.

Many others have contributed to the development of the intranuclear cascade model. The two most commonly used versions of the cascade code in the theory of high energy heavy ion reactions are due to Yariv and Fraenkel [Yar 79,81] and Cugnon et. al. [Cug 80,81,82]. These codes simulate a heavy ion reaction at high bombarding energies on a microscopic level by treating nuclear collisions as a superposition of independent two-body nucleon-nucleon collisions. Nucleons move on straight line trajectories (since there is no field) until they collide, with a probability given by the free nucleon-nucleon scattering cross section. The creation of deltas, pions, and other particles and the interaction of all these particles occur according to experimental cross sections. Relativistic kinematics is included. Target and projectile nucleons are initialized in configuration and momentum space with random Fermi momenta and then Lorentz boosted to an appropriate frame, where the collision simulation proceeds. Momentum and energy are conserved in the particle-particle interactions and the evolution of the system is computed up to a time where the majority of interactions has ceased. Collisions are Pauli blocked according to the simple criterion that the collisions are forbidden if the total center of

mass energy is less than the Fermi energy in ground state nuclear matter [Cug 80,81,82] or if the outgoing particle would scatter into momentum space regions originally occupied by projectile or target [Yar 79,81].

Both the Yariv-Fraenkel and the Cugnon cascade satisfy the above criteria. They differ in two respects: (1) the particles in the Yariv-Fraenkel simulation sit in a potential well of constant depth V_0; (2) in the original Yariv-Fraenkel approach the incoming particles (projectile nucleons) are cascading independently through a medium (the target) - in the updated version, this scheme has been improved by including the so-called cascade-cascade interactions.

In the Cugnon cascade, one has the problem that the nucleons are not bound; hence one may get spurious effects due to nuclear instability, see Fig. II.4 [Mol 85b]. It is possible to bind the nucleons by letting each nucleon move only with the beam velocity until it interacts with another nucleon, at which point it 'remembers' it's Fermi momentum [Gyu 82]. However, this bound Cugnon cascade is not very satisfying either, since in real nuclei, nucleons can travel in all directions.

7. Nuclear Fluid Dynamics

Conservation Laws and the Transition to Local Equilibrium

Just as in the classical case, one can derive from the VUU equation a general transport equation. Let us re-write the VUU equation in the simple form:

$$\left(\frac{df}{dt}\right)_{coll} = \frac{\partial f}{\partial t} + \vec{v}\cdot\frac{\partial f}{\partial \vec{r}} + \vec{F}\cdot\frac{\partial f}{\partial \vec{p}} \quad . \tag{46}$$

Assume for simplicity that the external force $\vec{F} = d\vec{p}/dt$ is momentum independent. Then an integration of this equation over p produces:

$$\frac{\partial \rho}{\partial t} + \vec{\nabla}\cdot(\rho\vec{u}) = \int d^3p \left(\frac{df}{dt}\right)_{coll} \tag{47}$$

The term containing the external force vanishes by partial integration. The collision term on the right hand side of eq. (47) describes the net gain rate of particles at position $\vec{r}$ and with momentum $\vec{p}$. Since the collisions take place at one point and only redistribute particles in momentum space while conserving their number, the integral over all momenta must vanish. Thus we get the first equation of nuclear fluid dynamics, the continuity equation:

$$\frac{\partial \rho}{\partial t} + \vec{\nabla}\cdot(\rho\vec{u}) = 0 \ . \tag{48}$$

To get an equation for the momentum density, we integrate the VUU equation with a weight of $\vec{v}$:

$$\frac{\partial}{\partial t}(\rho\vec{u}) + \vec{\nabla}\cdot\int d^3p \vec{v}\vec{v}f + \sum_j F_j \int \vec{v}\frac{\partial f}{\partial p_j} d^3p = 0 \ . \tag{49}$$

Again the collision term yields a vanishing contribution, because momentum is conserved in the collisions locally. In the second term on the left, one may separate an average and a fluctuating part:

$$\int d^3p \vec{v}\vec{v}f = \int d^3p \vec{u}\vec{u}f + \int d^3p(\vec{v}-\vec{u})(\vec{v}-\vec{u})f + \int d^3p\vec{u}(\vec{v}-\vec{u})f + \int d^3p(\vec{v}-\vec{u})\vec{u}f \tag{50}$$

The last two terms vanish because the average of $\vec{v} - \vec{u}$ is zero. The fluctuating part defines the kinetic stress tensor:

$$\underline{P}(\vec{r},t) = \int d^3p(\vec{v}-\vec{u})\hat{}(\vec{v}-\vec{u})f(\vec{r},\vec{p},t) \ . \tag{51}$$

Note that the stress tensor is identically zero only if all the particles have exactly the mean velocity $\vec{u}$. The external force contribution can be rewritten using

$$p_i \frac{\partial f}{\partial p_j} = \frac{\partial}{\partial p_j}(p_i f) - \delta_{ij} f \tag{52}$$

and then the first term on the right hand side vanishes in partial integration. The momentum conservation equation is then:

$$\frac{\partial}{\partial t}(\rho\vec{u}) + \vec{\nabla}\cdot(\rho\vec{u}\vec{u}) = - \vec{\nabla}\cdot\underline{P} + \frac{\rho}{m}\vec{F} \ . \tag{53}$$

Define the energy density as:

$$\rho E = \frac{m}{2} \int d^3p \; v^2 f(\vec{r},\vec{p},t) \; . \tag{54}$$

Then, through the introduction of the average velocity, ρE may be split up into a flow kinetic energy and a thermal contribution:

$$\rho E = \frac{m}{2} \rho u^2 + \frac{m}{2} \int (\vec{v}-\vec{u})^2 f(\vec{r},\vec{p},t) d^3p \; . \tag{55}$$

Integrating the VUU equation with a weight of $mv^2/2$ gives

$$\frac{\partial}{\partial t}(\rho E) + \nabla \cdot \int d^3p \; \frac{m}{2} \; v^2 \vec{v} f + \vec{F} \cdot \int d^3p \; \frac{m}{2} \; v^2 \; \frac{\partial f}{\partial \vec{p}} = 0 \tag{56}$$

where again the collision term gives no contribution because it conserves the kinetic energy of the particles. The second term is split up into a number of parts:

$$\begin{aligned} \int d^3p \; \frac{m}{2} \; \vec{v} v^2 f &= \int d^3p \; \frac{m}{2} \; (\vec{v}-\vec{u})^2 (\vec{v}-\vec{u}) f + \int d^3p \; f \; \frac{m}{2} u^2 \vec{u} + \\ &\quad m \int d^3p \vec{u} \cdot (\vec{v}-\vec{u})(\vec{v}-\vec{u}) f + \int d^3p \; \frac{m}{2} \; (\vec{v}-\vec{u})^2 \vec{u} f \\ &= \vec{q} + \rho E \vec{u} + \vec{u} \cdot \underline{P} \end{aligned} \tag{57}$$

wherein the first term $\vec{q}$ describes the transport of thermal energy by thermal motion (thermoconductivity). The second and third term are combined to give the transport of total energy by collective flow and the last term describes the work done against the stresses. Finally the external force contribution can be re-written by partial integration:

$$\vec{F} \cdot \int d^3p \; \frac{1}{2} \; v^2 \; \frac{\partial f}{\partial \vec{p}} = - \vec{F} \cdot \int d^3p \vec{v} f = -\rho \vec{u} \cdot \vec{F} \tag{58}$$

and the equation for energy conservation reads:

$$\frac{\partial}{\partial t}(\rho E) + \vec{\nabla} \cdot (\rho E \vec{u}) = -\vec{\nabla} \cdot (\vec{u} \cdot \underline{P} + \vec{q}) + \rho \vec{u} \cdot \vec{F} \; . \tag{59}$$

These then are the general fluid dynamics equations (48, 53, and 59). One obtains the usual Nuclear Fluid Dynamical equations by using $P_{ij} = p\delta_{ij}$ and $q_i = 0$. Also, a potential $\vec{F} = -\nabla U$ is introduced.

For the applicability of the fluid dynamical concepts it has to be ensured that fast equilibration and thermalization of the incident momentum

and energy occurs in high energy heavy ion collisions. We saw some support for this conjecture in the results of the VUU theory. A simple argument is, that this is the case, if the mean free path λ is small compared to the typical dimension, L, of the system

$$\lambda/L << 1. \tag{60}$$

The mean free path λ is given by

$$\lambda = \frac{1}{\sigma \cdot \rho}$$

where σ is the total nucleon-nucleon scattering cross section and ρ is the actual nuclear density. For normal nuclear matter density ρ_0 and a free N-N scattering cross section $\sigma_{NN} \sim 30$ mb at high energies ($E_{Lab} > 200$ MeV/nucleon), the mean free path is $\lambda \approx 2$ fm, which is not too small against the nuclear dimensions $L \approx 10$ fm for heavy nuclei [Sch 68, Sch 74].

The large longitudinal momentum decay length calculated from the free N-N scattering cross section was interpreted as a complete transparency for the two nuclei at high energies and as the death for compression (shock) waves at energies above 1 GeV/nucleon [Sob 75]. However, in the "formation flight" of ensembles of nucleons, collective scattering phenomena cannot be neglected, namely compression effects and the enlargement of the cross section due to precritical scattering close to phase transitions [Gyu 77,Ruc 76], so that the scattering cross section and the density can be modified drastically leading to a decrease of the mean free path:

$$\lambda \approx 1.4 \frac{\sigma_{NN}}{\sigma_{coll}} \cdot \frac{\rho_0}{\rho} \text{ fm} \quad . \tag{61}$$

The precritical scattering of nucleons in the vicinity of a phase transition point is analogical to critical opalescence, which is characterized by the great enhancement of the scattering cross section of light near a liquid-gas phase transition, the critical scattering of

neutrons in ferromagnets near the Curie point [Sta 71], or the critical scattering appearing in two colliding plasma beams. Thus the vicinity of a phase transition, e.g. the onset of pion condensation or gluon condensation is expected to be marked by the occurrence of critical nucleon-nucleon scattering, a large enhancement (a factor of 2-4 for pion condensation) of the density-dependent N-N cross section [Gyu 77, Ruc 76].

This would mean that even at bombarding energies above one GeV/nucleon nuclei do not become transparent to each other: on the contrary, very violent collisions can be expected. One should keep in mind, however, that nucleus-nucleus collisions are a quantum mechanical process. Hence--in the sense of quantum mechanical fluctuations--under the same initial conditions processes with violent randomization (e.g. the occurrence of pronounced shock waves) may occur as well as processes with less pronounced interaction. It is a formidable experimental task to separate the former from the latter. Recent experiments show that up to lab-energies of 4 GeV/nucleon a considerable part (~30%) of the total cross section is due to violent events with very high multiplicities and large momentum transfer.

What about the relationship between quantum mechanics and fluid dynamics? Immediately after the discovery of quantum mechanics, the formal analogy to fluid dynamics was pointed out [Mad 26]. One uses the Schrödinger equation

$$-\frac{\hbar^2}{2m}\nabla^2\psi + V(r)\psi = i\hbar\frac{\partial\psi}{\partial t} \tag{62}$$

and the separation of a phase S in the wave function

$$\psi(r,t) = \phi(r,t)\cdot e^{imS(r,t)/\hbar} \tag{63}$$

to get

$$\frac{\partial}{\partial t}\phi^2 + \vec{\nabla}\cdot(\phi^2\vec{\nabla}S) = 0\ . \tag{64}$$

This is the well known continuity equation describing the conservation of probability density in quantum mechanics. The probability density is

$$\rho(r,t) = \phi^2(r,t) \tag{65}$$

from which it can be shown that

$$\frac{\partial}{\partial t}(m\rho\vec{u}) + \vec{\nabla}\cdot(m\rho\vec{u}\vec{u}) = -\rho\vec{\nabla}U - \rho\vec{\nabla}\left(-\frac{\hbar^2}{2m}\frac{\sqrt{\rho}\nabla^2\sqrt{\rho}}{\rho}\right). \tag{66}$$

This is identical with the conservation equation of the momentum with an external force due to a potential U as in equation (53). Only the last term on the right-hand side is different. It depends solely on the density and may be interpreted as an inner pressure caused by quantum mechanical effects. It disappears in the classical limit of $\hbar \to 0$.

Equations (64) and (66) have been obtained for the probability density of <u>one</u> single particle. The extension to a quantum mechanical <u>many</u> body system, behaving like interpenetrating fluids with interaction, is obvious. It is important to note that (in contrast to kinetic theory) each single quantum mechanical particle is a continuum itself. Therefore the problem of granulation of the microscopic density does not occur. However, the main problem is a reasonable definition for the many particle densities and velocities. An important question is whether all quantities entering the equations of motion may be described as functions of these macroscopic variables (and a temperature) or not.

It is also possible to derive continuity equations for many particle systems. However, the procedure is very lengthy. For reasons of simplicity, we will therefore restrict ourselves to a derivation of the hydrodynamic equations by analogy to the TDHF equations. This is less

general, but the principal argument [Won 77, Mar 77] is the same as the one used above. The TDHF equations are well known:

$$i\hbar \frac{\partial}{\partial t} \psi_\alpha = - \frac{\hbar^2}{2m} \nabla^2 \psi_\alpha(r,t) + \psi_\alpha(r,t) \int d^3r' V(r-r') \sum_\beta \psi^*_\beta(r',t)\psi_\beta(r',t)$$
$$- \sum_\beta \psi_\beta(r,t) \int d^3r' V(r-r') \psi^*_\beta(r',t)\psi_\alpha(r',t) \qquad (67)$$

where ψ_α is the single particle wave function and $V(r-r')$ is the two particle interaction. We define a many particle density:

$$\rho(r,t) = \sum_\alpha \psi^*_\alpha(r,t)\psi_\alpha(r,t) = \sum_\alpha \phi^2_\alpha(r,t) \qquad (68)$$

with a separation of the one particle wave function:

$$\psi_\alpha(r,t) = \phi_\alpha(r,t) \cdot \exp[imS_\alpha(r,t)/\hbar] \; . \qquad (69)$$

In complete analogy to the previous section, we obtain again a continuity equation with the mean collective velocity. However, the velocity field $\vec{u}$ is no longer curl-free.

The derivation of the momentum equation is completely analogous and can be written

$$\frac{\partial}{\partial t} \vec{j}(r,t) + \vec{\nabla} \cdot \sum_\alpha (\phi^2_\alpha \vec{\nabla} S_\alpha \vec{\nabla} S_\alpha) = - \frac{1}{m} \sum_\alpha \phi^2_\alpha \vec{\nabla} \left\{ \frac{\phi_\alpha (- \frac{\hbar^2}{2m} \nabla^2) \phi_\alpha}{\phi^2_\alpha} \right\}$$
$$- \frac{\rho}{m} \vec{\nabla} \int d^3r' \; V(r-r')\rho(r') \qquad (70)$$
$$+ \frac{1}{m} \int d^3r' \; \vec{\nabla} V(r-r') \left| \sum_\alpha \psi^*_\alpha(r)\psi_\alpha(r') \right|^2 \; .$$

This form is not yet comparable to a fluid dynamical description. For the transition to hydrodynamics all one-particle quantities have to be expressed by ρ, $\vec{j}$ and by a temperature field T with $\underline{P}$ being (in analogy to (51)) the stress tensor

$$\underline{P} = m \sum_\alpha \phi^2_\alpha (\vec{\nabla} S_\alpha - u)(\vec{\nabla} S_\alpha - u). \qquad (71)$$

Now the hydrodynamic equations of motion can be written as continuity equations for the baryon density ρ, momentum density $\vec{M} = \rho\vec{u}$, and

energy density $e = \rho E$ with the gradients of the pressure p, the potentials U, and the stress tensor $\underline{P}$ as source terms:

$$\partial_t \rho + \partial_i(\rho u_i) = 0, \tag{72}$$

$$\partial_t(\rho u_i)+\partial_j(\rho u_j u_i)=-\frac{1}{m}\partial_i p+\frac{1}{m}\partial_j\left[\eta(\partial_i u_j+\partial_j u_i-\frac{2}{3}\delta_{ij}\partial_k u_k)+\zeta\delta_{ij}\partial_k u_k\right]-\frac{\rho}{m}\partial_i U,$$

$$\partial_t(\rho E_T)+\partial_j(\rho E_T u_j)=\kappa\partial_j^2 T+\partial_i u_j\left[-p_T\delta_{ij}+\eta(\partial_i u_j+\partial_j u_i-\frac{2}{3}\delta_{ij}\partial_k u_k)+\zeta\delta_{ij}\partial_k u_k\right].$$

The indices i, j and k are running over the space coordinates and the Einstein summation convention is used. κ is the heat conductivity, η is the shear viscosity, and ζ is the bulk viscosity. The coupled nonlinear equations for the density fields $\rho(\vec{r},t)$, momentum density fields $\rho(\vec{r},t)\vec{v}(\vec{r},t)$, and energy density fields $\rho(\vec{r},t)E(\vec{r},t)$ must be solved simultaneously.

How do these equations change, if relativistic effects become important? The range of validity of the non-relativistic formalism is not sharply defined, but at bombarding energies $E_{lab} > 500$ MeV/nucleon, the classical relative velocity of projectile and target exceeds the speed of light and at best qualitative results may be obtained.

There are two ways in which a system may become relativistic: (a) macroscopically relativistic when the flow velocity becomes large or (b) microscopically relativistic when the excitation energy is non-negligible in comparison to the rest energy. Case (a) is reflected by the equations of motion and case (b) by the equation of state. As in the nonrelativistic case, the fluid dynamic equations reflect the conservation of baryon number, momentum and energy, and may be brought into the continuity equation form:

$$\begin{aligned}
\partial_t \rho_L + \partial_k(\rho_L u_k) &= 0 \\
\partial_t M_i + \partial_k(M_i u_k) &= -\partial_i P \\
\partial_t e_L + \partial_k(e_L u_k) &= -\partial_k(P u_k) \ ,
\end{aligned} \tag{73}$$

where long range potentials and dissipative terms have been dropped.

The quantities ρ_L, M and e_L are the densities for baryon number, momentum and energy as specified in a fixed ("lab") reference frame. These are related to the "proper" or "co-moving" densities in the local rest frame by

$$\begin{aligned} \rho_L &= \gamma\rho \\ M_i &= \gamma^2(e + p)v_i \\ e_L &= \gamma^2(e + p) - p \end{aligned} \tag{74}$$

where $\gamma = (1-v^2)^{-1/2}$ is the usual Lorentz factor, ρ = the proper baryon number density, p the pressure, and $e = \rho(m_0c^2 + E_C(\rho) + E_T(\rho,T))$ the proper internal energy density including the rest energy. The proper densities ρ, e and the velocity $\vec{v}$, which are the physically interesting quantities, must be obtained from the lab densities ρ_L, M, e_L by inverting the nonlinear equations with $p=p(\rho,e)$ from the equation of state. This nontrivial technical problem is a complication over the nonrelativistic case, where the velocity can be calculated directly from ρ and $\rho\vec{u}$.

We show in Figs. II.12 and 13 the relativistic nuclear fluid dynamical model calculations [Gra 84] for the reaction Ar (770 MeV/nucleon) + Pb at b = 0 and 4 fm, studied above in the VUU nonequilibrium theory. Note the surprising similarities of the fluid dynamical results with the VUU calculation. Similar results are, however, only obtained when heavy projectile and targets are studied, because only in this case the VUU approach does predict thermal equilibrium. For light systems like C + C the fluid dynamical model does not apply - there is simply not enough target material in the way of the projectile to result in nuclear stopping.

8. One dimensional shocks

It is often advantageous to gain more insight into the physical processes by solving more simplified, schematic models, which can be solved (at least to some extent) analytically. In this case another set of equations is applied in the more schematic treatment of the fluid-dynamical description of high energy heavy ion collisions, namely the shock equations. Shock waves have to be clearly distinguished from sound waves. In contrast to sound waves, shock waves are connected with a strong, density dependent mass flow velocity v_f. The shock front itself propagates with the shock velocity $v_s > v_f$ and also depends strongly on the compression amplitude [Bau 75]. Shock waves are non-linear phenomena--for large amplitudes $\rho >> \rho_o$ both v_s and v_f tend to the velocity of light, while for small perturbations $\rho \approx \rho_o$ they approach the linear limit of sound waves. Shock waves imply a large entropy production: the matter flow through the shock front is highly irreversible, it is not only connected with strong compression, but also with large thermal excitation [Hof 76, Stö 77b,78].

The shock calculations have to be viewed as an idealization, assuming a zero width of the shock front together with a discontinuous jump of the state variables (e.g. ρ, T, e, p). However, comparison of the nuclear shock wave calculations with the result of the full Navier Stokes calculations [Stö 79a] shows that the resulting compression rates and temperatures are very similar, although in the Navier Stokes calculations the compression front is smeared out over 1-2 fm due to the viscosity. Such a width seems to be realistic, as the width of a shock front is approximately given by 2-3 times the mean free path, which can be less than half a fermi in high energy nuclear collisions. For a large nuclear transparency, the shock front width may be of the order of the nuclear

radius. However, no indication for transparency has been found in the high energy experiments up to now.

The relativistic Rankine-Hugoniot equations can be derived from the continuity of

$$\text{particle flux density} \qquad [j^0] = [\rho\, u_x] = 0$$

$$\text{energy flux density} \qquad [T_{ox}] = [g\, u_o u_x] = 0$$

$$\text{and momentum flux density} \quad [T_{xx}] = [g\, u_x^2 + p] = 0 \qquad (75)$$

where [] denotes the jump of the respective variable across the shock front and x gives the direction normal to the shock front as seen from the shock front's rest frame. Eliminating the velocities u_x from the continuity equations yields the relativistic shock equation

$$\frac{g_o^2}{\rho_o^2} - \frac{g^2}{\rho^2} + (p-p_o)\left(\frac{g_o}{\rho_o^2} + \frac{g}{\rho^2}\right) = 0 \qquad (76)$$

which gives a unique connection between the free enthalpy g, pressure p, and density ρ within the respective rest frame of the matter (nought stands for the undisturbed matter in front of the shock wave, quantities without subscript refer to matter in the compressed state). When we insert $g=\rho W+p$, $g_o=\rho_o W_o$, and $p_o=0$ the equation

$$W^2 - W_o^2 + p\left(\frac{W}{\rho} - \frac{W_o}{\rho_o}\right) = 0 \qquad (77)$$

is obtained. This is the Rankine- Hugoniot equation, which determines the temperature T as a function of ρ, i.e. $T(\rho)$. If W is equated with the center of mass kinetic energy one can solve eq. (77) for the density $\rho(E_{lab})$ and therefore for the bombarding energy dependence of any other thermodynamic quantity. Here $W(\rho,T)$ is the energy per baryon, which characterizes the nuclear equation of state. Neglecting pions and resonances and regarding the pure nucleon fluid only, the relation $p_T=\alpha\rho\, E_T$ can be used to obtain a quadratic equation in E_T, which can be solved in terms of the nucleon density ρ analytically. E_T is the temperature-dependent part of $W(\rho,T)$.

The shock velocities v_s and v_f are given by the continuity of the energy and momentum flux density. From the relative velocities of the matter with respect to the shock front, the relative matter flow velocity v_f is obtained by covariant summation:

$$\frac{v_s}{c} = \sqrt{\left\{ \frac{pw\rho}{(w\rho - w_0\rho_0)(w_0\rho_0 + p)} \right\}}$$

$$\frac{v_f}{c} = \left\{ \frac{p(\rho w - \rho_0 w_0)}{\rho w(p + \rho_0 w_0)} \right\} \qquad (78)$$

A simple model can be constructed to calculate the shock compression and temperature in the central collision of two heavy nuclei as a function of the bombarding energy [Bau 75, Stö 78, Hah 85a]. This model assumes the compressed fluid to be at rest in the center-of-momentum system. Three-dimensional fluid dynamical calculations show that this requirement is fulfilled fairly well for nonperipheral collisions of heavy nuclei near the collision axis: a sort of stationary compression stage develops. Practically all of the incident kinetic energy is transformed into internal energy (compression and excitation). As v_f denotes the flow velocity of the shocked matter, which is at rest in the c.m. frame, relative to the target matter, the laboratory bombarding energy is

$$E_{LAB} = \left[\left(1 - \left(\frac{v_p}{c}\right)^2\right)^{-1/2} - 1 \right] W_0 \qquad (79)$$

where $v_p = \frac{2v_f}{1+(v_{f/c})^2}$ is the projectile velocity.

Though this model will, due to its lack of kinetic energy of the compressed matter and its neglection of the outflow of matter perpendicular to the collision axis (as compared to three dimensional calculations), give too large values for compression and temperatures as function of the bombarding energy, it is sufficiently good to give a rather quantitative overview about the expected compression and the thermal excitation. The

influence of the beam energy and the nuclear equation of state and the importance of resonance and pion production in the collision dynamics can be studied almost analytically.

III. Confrontation of the Theory with Experimental Data

1. Expansion, Fragment Formation and the Entropy Puzzle

In the preceding chapter the Nuclear Fluid Dynamical model, which was historically the first approach to be applied to high energy nuclear collisions, has been introduced. NFD refers directly to thermodynamical concepts and, therefore, the underlying physics of high compression and excitation can be discussed in a macroscopic language. Spatial and temporal distributions of the density, velocity, and temperature can be directly obtained with this approach. The dependence of the thermodynamic variables on the impact parameter, bombarding energy, and projectile-target combination can be studied. The fluid dynamical model is the only one of the approaches discussed above, for which the nuclear equation of state serves as immediate input - the VUU theory includes the compression energy, but since it is a microscopic and nonequilibrium theory, the thermodynamic variables are not immediately accessible. We use the fluid dynamical model in the following as a reference case to compare to the data and also to the microscopic theories.

The fluid dynamical development of a heavy ion collision typically proceeds in the following way (Fig. II.12,13): when the two nuclei collide at high energy the overlap zones are stopped and a strong nonlinear shock wave is formed. The nuclear matter in the shock-zone is compressed and heated: high density, pressure and temperature are created in this interaction region. At E_{lab}= 200 MeV/nucleon, for example, a maximum

compression of three times equilibrium density and a temperature of about 40 MeV can be reached. During the compression stage the entropy of the system rises up to a certain saturation value, which depends on the nuclear EOS, the bombarding energy, and the viscosity in the system.

More specifically, for a Nb+Nb collision at 400 MeV/nucleon and an impact parameter of 3 fm, entropy is created during the first 20 fm/c of the collision. During that time the colliding zones of the two nuclei are stopped and compressed. When the maximum density of the system starts to drop (after 20 fm/c) the entropy has reached its saturation value of about 2.6 per nucleon. This value of S/A is maintained during the rest of the reaction. The entropy even saturates when a large shear viscosity η is present in the Navier-Stokes equations. Then, the absolute value of the entropy rises from 2.66 (nonviscous) over 2.96 (η=20 MeV/fm^{2}c) to 3.17 (η=60 MeV/fm^{2}c), but still remains constant after 20 fm/c [Cse 80ab, Stö 84, Buc 84a].

After the compression phase the temperature drops during the hydrodynamic (quasi-adiabatic) expansion while the entropy S stays almost constant. The system expands due to it's large internal pressure and at densities $\rho \approx 0.5\text{-}0.7\ \rho_0$ the collisions between the particles cease: the hydrodynamic description looses its validity and the nuclear fluid breaks up into light fragments like π, p, n, d, and He. These fragments are the only messengers from the reaction which are observed experimentally. They carry information about the initial dense state of the system, modified by the following expansion and the freeze-out. The physics of their formation is a topic of great current interest because of their possible relation to the entropy and the nuclear liquid gas phase transition [Stö 83, Cse 85]. There are two important questions about these fragments. (1) What is the

"chemical" composition of the reaction products, i.e. how abundantly are the different nuclei and π's produced? (2) What is their distribution in momentum space, i.e. what are their spectra?

In practice, the hydrodynamic calculation is stopped when the average density is $\approx 0.5\rho_0$. Then the light fragment composition may be determined from a statistical model by assuming that the baryon number and energy per particle of the interacting nucleon fluid is conserved. The quantum statistical model [Gos 78, Sub 81, Stö 83, Hah 85b] used to calculate the fragment yields assumes that chemical equilibrium between the different fragments (p, n, d, t, ^{3}He and α's ...) is established at this late stage of the reaction. This assumption is supported by rate calculations for the appropriate densities and temperatures [Mek 78ab].

This quantum statistical model works as follows. Baryon number and charge conservation are enforced via

$$\bar{Z} = \sum_{i=1}^{N} n_i((Z_i,N_i)\cdot Z_i \qquad (1)$$

$$\bar{N} = \sum_{i=1}^{N} n_i(Z_i,N_i)\cdot N_i \qquad (2)$$

where n_i is the number of particles of species i with Z_i protons and N_i neutrons. The equilibrium is established in a volume V_{ext} (or at a density ρ) and at a temperature T. Every particle moves freely in the volume V left over from the external volume V_{ext} after subtracting the volume occupied by each particle

$$V = V_{ext} - \sum_i n_i V_i \qquad \rho = (\bar{N} + \bar{Z})/V_{ext} \qquad (3)$$

where V_i is the ith particle's volume. Thus, the point-like particles move freely in a reduced volume V. For fermions we have

$$\lambda_i^3 n_i/g_i V = (2/\sqrt{\pi})F_{FD}(v_i) \qquad i = p,n,^3He,t... \qquad (4)$$

where

$$\lambda_i = h/(2\pi m_i kT)^{1/2} \tag{5}$$

is the thermal wavelength of the ith particle with mass m_i, $g_i=2S_i+1$ the spin degeneracy factor. The chemical potential of the ith particle is μ_i,

$$v_i = \beta\mu_i = \mu_i/kT \tag{6}$$

and

$$F_{FD}(v) = \int_0^\infty dx \frac{x^{1/2}}{\exp(x-v) + 1} \tag{7}$$

The function $F_{FD}(v)$ is tabulated in the literature [Sub 81]. For bosons we have

$$n_i = g_i/(\exp(\alpha_i)-1)+(g_i V/\lambda_i^3)F_{BE}(\alpha_i) \qquad i = d, {}^4He... \tag{8}$$

where $\alpha_i=-\beta\mu_i$. The first term gives the number of condensed particles, and the last one can be evaluated via

$$F_{BE}(\alpha) = \sum_{n=1}^{\infty} \exp(-n\alpha)/n^{3/2}. \tag{9}$$

The constraint of chemical equilibrium implies that the chemical potential

$$\mu_i = Z_i\mu_p + N_i\mu_n + E_i \tag{10}$$

with

$$E_i = Z_i m_p c^2 + N_i m_n c^2 - m_i c^2 \tag{11}$$

is the binding energy of the cluster (Z_i,N_i).

The thermal momentum distribution of the fragments inside a fluid cell is described by relativistic Fermi or Bose distributions. To obtain the momentum distribution of all fragments in the laboratory frame the distributions are Lorentz transformed to this frame by the relativistic boost velocity β_j of the cell j arising from the collective flow [Cse 80ab, Buc 81ab, Cse 82]:

$$f_j^{lab}(\vec{P})d^3\vec{P} = \frac{w(\vec{p})}{W} f_j[\vec{p}(\vec{P})]d^3\vec{P}. \tag{12}$$

Here $\begin{pmatrix} W \\ \vec{p} \end{pmatrix}$ and $\begin{pmatrix} W \\ \vec{P} \end{pmatrix}$ are the four-momenta in the cell and lab systems, respectively. The double differential cross section of the emitted fragments is then

$$\frac{d^2\sigma}{dW d\Omega} = \sum_j \frac{4V_j\sigma_o}{(2\pi\hbar)^3} \frac{A_j(W^2-m^2)^{1/2}}{\exp[(A_j-\mu_j)/T]+1} N_{particle} \qquad (13)$$

where V_j is the volume of the corresponding fluid cell, σ_o is the geometrical cross section of the reaction, and

$$A_j = \gamma_j(W - \vec{\beta}_j\vec{P}_j) \; . \qquad (14)$$

$N_{particle}$ is the fraction of the corresponding particle species calculated in the chemical equilibrium model from above. The momentum vector $\vec{p}$ of the observed particle depends on the observation energy E and angles θ and ϕ:

$$\vec{p} = (W^2 - m^2)^{1/2} \begin{pmatrix} \sin\theta\cos\phi \\ \sin\theta\sin\phi \\ \cos\theta \end{pmatrix} \; , \qquad (15)$$

where W=m+E. This method is applied to calculate fragment spectra and angular distributions from the fluid dynamical model.

What about thermodynamic variables like entropy and temperature? A method that would allow the determination of the entropy from experiment would yield important insight into the state of the matter in the moment of highest compression and excitation during the collision. It has been suggested [Sie 79] to measure the entropy S via the observed proton-to-deuteron ratio R_{dp} since in chemical equilibrium we have

$$S = 3.95 - \ln R_{dp} \; [\text{for } \langle p\rangle_{equil} >> \langle d\rangle_{equil}] \qquad (16)$$

This formula has been used to extract entropy values from the inclusive fragment data [Nag 81]. The experimental values of S seem to be much larger than the calculated entropy values, in particular for $E_{LAB} \leq 400$ MeV/nucleon, even after the viscosity effects are considered. However, the proton to deuteron ratios calculated from the fluid dynamical model, R_{dp}<

0.35, agree well with the experimental data over the whole range of bombarding energies considered [Nag 81].

This paradox is resolved [Stö 84] as being due to the decay of the particle unstable excited nuclei,

$$A^* \rightarrow (A-1) + p, \qquad (17)$$

which become increasingly important at intermediate and low energies [Stö 84]. In fact, the resonance decay products dominate the chemical equilibrium contribution for $E_{LAB} < 400$ MeV/nucleon. Hence the relation between the entropy and the observables is not due to the simple formula (16). The entropy can be related to the d to p ratios in a quantum statistical model where the decay of particle instable states is explicitly included. The relation to the entropy is then determined from a full numerical calculation of the quantum statistical model with several hundreds of stable and unstable nuclides [Hah 85b]. Recent data from the GSI/LBL Plastic Ball collaboration have made clear that experimentally the d to p ratio depends strongly on the multiplicity of the event in which the particles are emitted: in peripheral collisions, which dominate the inclusive particle spectra, the ratio is much smaller than in central collisions with high multiplicity [Gus 85]. The quantum statistical model has been used to extract the entropy from the asymptotic (infinite miultiplicity) 'data' [Dos 85]. We want to emphazise that the data are in strong disagreement with the fireball calculations - they seem to indicate strong compression effects and point towards a stiff nuclear equation of state.

The temperatures T as calculated in the hydrodynamical model [Stö 81a] may be compared to the experimentally determined slope factors T_0 [Nag 81] of protons and pions emitted from violent nuclear collisions at

various bombarding energies (Fig. III.1). The data seem to rule out a pure nucleon Fermi gas at energies $E_{LAB} > 800$ MeV/nucleon. A mixture of noninteracting gases of the different hadrons with an exponentially increasing hadronic mass specrum seems to be in much better agreement with the data. However, one must keep in mind that the finally observed slope factors do not give a direct measure of the initial temperature: due to the expansion the temperature drops substantially [Sie 79, Stö 81a]. This energy loss is compensated by an increase in the collective flow velocity.

2. Pion Production

The nuclear fluid dynamical model can also be used to predict pion yields and to study their dependence on the nuclear equation of state [Stö 78, Dan 79, Hah 85a]. Stöcker, Scheid and Greiner first proposed to measure the stiffness of the nuclear EOS via the pion multiplicities. The first exclusive measurements of the pion multiplicities as a function of the participant multiplicity [San 80] have been used recently to extract the compressional energy via the proposed method [Hah 85a, Har 85] and via a substraction procedure, which used the cascade model (which does not employ any compressional energy) as input [Sto 82]. It turns out that the data can only be explained if a very stiff compression potential is assumed (see figure II.3). The assumption of immediate freeze-out in the high density stage in this procedure could overestimate the pion multiplicities [Stö 81c, 84]. However, cascade calculations indicate that the pion degree of freedom decouples from the baryonic 'heat bath' very early in the collision, namely in the high density stage [Cug 80, Sto 82].

We show in figure III.2 the pion multiplicities calculated with this model. The linear equation of state with K_1 = 1400 MeV and the

quadratic one with K_q = 800 MeV give the best fit to the observed pion yields over the whole BEVALAC bombarding energy range. With respect to the large values of K, one must keep in mind that they are fitted for densities far away from normal nuclear matter density. Including an isentropic expansion of the system before freeze-out [Stö 81c, 84] would lower the pion multiplicities, leading to lower compression constants.

Hard photon cross sections for the C + C system, calculated from the photon yield per baryon [Hah 85a] are shown in figure III.3. Also shown are recent data [Gro 85] which have been extracted assuming an isotropic differential cross section [Vas 80a]. The yields shown include, due to experimental uncertainties at the lowest energies, only photons with E > 30 MeV. One would expect that the experiment gives much less photons than the theory, as a result of the small electromagnetic coupling constant, which would imply a largely increased equilibration time for statistical equilibirium. In this respect, it is surprising that the photon yields are overestimated by only factors of 3.5 at the most in this simple model calculation.

To study thermodynamic variables and pion production on the microscopic level the VUU theory can be employed [Kru 85a, Mol 85c]. Pions of different isospin are produced in this model via the production of Δ-resonances in elementary nucleon-nucleon collisions: thus both production and absorption mechanisms are treated microscopically. The VUU approach has been tested by turning off the Pauli blocking and mean potential field. Then the parallel ensembles decouple and the test particles move on straight line trajectories until they scatter: the intranuclear cascade model is recovered. The pion yields calculated with the VUU method in this cascade mode agree quantitatively with results obtained with the conventional

cascade [Cug 80, Yar 81]. Both results differ substantially from the data. If the nuclear compression energy and the Pauli blockng are introduced in the VUU method, the pion multiplicities change dramatically, as shown in figure III.4 [Kru 85a]. Take the 360 MeV/nucleon case, for instance. The π^- yield is 1.05 in the cascade mode, but drops to 0.56 if the compression energy is included; the suggested large difference due to the nuclear matter EOS is observed. The pion yield drops further to 0.46 when the VUU Pauli blocking is applied. These results differ by factors of three from results published elsewhere [Ber 84b]; a revised version of that program [Aic 85b] now reproduces the results presented here.

The pion multiplicities as calculated with the full VUU theory are also shown in figure III.4 as a function of the bombarding energy. The VUU theory with stiff EOS plus phase space Pauli blocker compares well with the data whereas the cascade mode overestimates the data by factors > 2 at energies up to 1 GeV/nucleon. The required drop in the predicted pion yield is due to the transformation of kinetic energy into potential energy during the high density phase of the reaction as well as due to Pauli blocking. To check the sensitivity of the pion yields on the EOS the calculations have been repeated with the medium potential. At 772 MeV/nucleon we find n_{π^-} = 2.45 and 2.13 with the medium and the stiff EOS, respectively. At lower energies, statistical errors of 10% prevent an accurate assessment of the effect of the potential. At other energies, where the errors are < 3%, the calculation with the medium EOS overestimates the yields systematically by about 10%. The stiff equation of state which reproduces the pion yields best is shown in Fig. II.3 together with the medium EOS.

The time dependence of the total pion multiplicity as calculated from the VUU approach [Mol 85c] for Nb (1050 MeV/nucleon) + Nb collisions at

b = 3 fm is shown in figure III.5. The pion number rises rapidly to a maximum value at t = 10 fm/c and drops then to a stable final value at 20 fm/c. There is a small but significant effect due to re-absorption until the pions escape the hot interaction zone. We want to emphasize that in this theory - as in the previously discussed cascade calculations - the pion yield approaches it's asymptotic value at a time, which nearly coincides with the moment of highest compression and 'temperature', thus demonstrating once more that information on the high density stage can be attained.

The bombarding energy dependence of the total pion multiplicity at b = 3 fm for Nb + Nb collisions is shown in Fig. III.6. There is a strong energy dependence as there was for Ar + KCl. The decrease of the total pion yield with impact parameter happens in an almost linear fashion (the decrease is faster when the impact parameter becomes near peripheral), this provides some justification for the usual extrapolation of multiplicity selected pion data to zero impact parameter. There is also a large effect due to atomic number: for Nb + Nb at 400 MeV/nucleon and b = 3 fm, we have n_π equal to 2.9, wheras for Au + Au n_π is 5.7. For the system Au + Au, the pion multiplicity for b = 3 fm collisions is shown in figure III.7 for the different isospin channels in the final state. Note that the VUU theory predicts a distinct difference of the pion multiplicity with a charged pion ratio $\pi^- / \pi^+ \approx 2$.

The VUU approach has also been used to study pion production in asymmetric nucleus-nucleus collisions [Mol 84b]. How do asymmetric collisions compare with symmetric ones of the same atomic mass, when the same number of nucleons is involved? For the Ar (770 MeV/nucleon) + Pb case at b = 3 fm we obtain $n_\pi = 9.9$, which is less than the pion multiplicity for Nb + Nb at the same energy ($n_\pi = 12.0$) even though the united mass is

greater for the asymmetric system. Thus asymmetric systems appear to be less efficient in creating pions. The total pion multiplicities vary from 10.6 at b = 1 fm to 3.7 at b= 7 fm; again, an almost linear relation with b is found. About 25-30% more pions are created when the Pauli blocking is turned off; equivalently, with the Pauli principle turned on, many collisions that would otherwise produce pions are forbidden by Pauli blocking.

3. Macroscropic and Microscopic Analysis of Collective Flow

We would like to point out that little information about the details of the reaction mechanism can be extracted from comparison of the inclusive data to impact parameter averaged calculations. For example, in spite of it's obvious presence at small impact parameters, no signatures of the collective sidewards flow predicted by the fluid dynamical calculations for central impact parameters seems to be visible in the calculated inclusive cross sections [Ams 75 and 77ab, Buc 83b]: only by triggering for nearly central collisions (high multiplicity selected events) can the sensitivity of the experiments be improved. Furthermore, since the production probability for free protons is largest in hot regions [Sub 81] the effect of the collective flow is smeared out by the thermal motion of the particles, which makes e.g. the proton cross sections almost isotropic. This phenomenon has been observed at high energies [Sto 80] and seems in agreement with previous three dimensional nonviscous calculations [Stö 81a,82ab].

A better experimental testing ground for flow effects is provided by particles heavier than the proton. These particles are produced in colder regions of the system [Stö 81a,82ab]. Hence, they tend to bear the

imprint of the collective flow more strongly. Calculations have been compared with with recent measurements [Jac 83] for Ar + Au at 137 MeV/nucleon. For the inclusive double differential ^{3}He cross section and for tritons a reasonable agreement is found between the calculation and the data. Especially the tendency of the ^{3}He spectrum to decrease with decreasing energy and the opposite behavior of the triton spectrum is reproduced fairly well. This systematic behavior is due to the neutron rich Au-target, preferring neutron-rich fragment production at low energies.

The Ar + Au spectra at lower energies seem to indicate a transition to a different reaction mechanism - whereas the 92 MeV/nucleon data still show a reasonable agreement with the fluid dynamical calculations, there is a clear disagreement for E_{lab}= 42 MeV/nucleon. Especially at forward angles the data disagree with the fluid dynamical calculation, thus indicating that the stopping power of nuclear matter decreases drastically at these low energies.

First fingerprints for collective flow have been found in early high multiplicity selected particle track detector experiments [Bau 75], which exhibit sidewards maxima in the angular distribution of He nuclei emitted in very asymmetric reactions, e.g. C + Ag. Also the double differential cross sections of light fragments (p,d,t), emitted from high multiplicity selected reactions of Ne + U, exhibits sidewards maxima, in accord with the longstanding predictions of the nuclear fluid dynamical model [Sch 74, Stö 80ab], while the intranuclear cascade model predicts forward peaking [Stö 81c]. If we consider especially protons, cascade calculations [Stö 81c,82b] yield forward-peaked angular distributions, even if central collisons are selected, contrary to the experiment. Hydrodynamic calculations without thermal breakup yield sidewards peaks which are too

narrow [Stö 81c,82b]. The simplified two component and firestreak models give similar results as the three dimensional cascade calculations. On the other hand, the fluid dynamical model with final breakup included [Stö 81c,82b] gives a reasonable description of the observed forward suppression and also reproduces qualitatively the forward shift of the position of the sidewards maxima with projectile energy.

As the bombarding energy is increased, relativistic effects become increasingly important. Already at 400 MeV/nucleon the relativistic treatment has a substantial influence on the spectra [Stö 80b] of protons, deuterons and tritons emitted from central collisions of Ne + U. The relativistic calculations [Gra 84] give much improved agreement with the data [Stö 80b] compared to the nonrelativistic calculations. The forward emission of particles is still strongly suppressed exhibiting sidewards maxima. These maxima are predicted to be even more pronounced for the summed charges than for protons. In fact, such behavior has been found in experiments with α-particle detectors [Bau 75]. Also, the high multiplicity selected angular distributions of ^{2}H and ^{3}H show sharper sidewards peaking than the protons.

The qualitative features of ϕ-averaged distributions do not change dramatically with impact parameter, once violent collisions with $b \lesssim 4$ fm are selected. This means, unfortunately, that ϕ-averaged double differential cross sections are of limited value for obtaining information on details of the reaction dynamics and on the nuclear equation of state [Ber 78,Stö 80b].

With the cross sections discussed above we have investigated the "classic" observable of nuclear collisions. However, this observable describes more or less final state features of the reaction, i.e. the situation after the freeze-out of different clusters. Therefore a lot of

different models like the fireball or the cascade [Yar 79,Cug 80] reproduce at least some (i.e. inclusive) experimental results fairly well. We have seen above that in this context the fluid dynamical model plus chemical equilibrium is a powerful tool to describe the experimental data. But, the principal difference (e.g. stopping, compression, sidewards emission, bounce-off) between NFD and other models cannot be seen in the double differential inclusive spectra. Selection of high multiplicity events helps a little, but still more information is needed.

The first step in order to find messengers from the compression phase is to look for the quantitities which are integrated in the equations of motion. Such a quantity is the density, for example. But the density rises and falls off during the reaction. A density distribution is not observable in experiments. The various momentum components also have very different histories during the collisions. P_z starts with a high value and is decreased, whereas p_y and p_x are built up. On first glance it seems that only the direction of $\vec{p}$ could be interesting. In the experiment there is only a distinction between $p_{||}$ and $p_{\perp}$ possible, reducing the outcome of information. However, in each event there is a distinction between p_x and p_y if the reaction plane is chosen to be the xz-plane; more detailed information can be obtained by an event by event analysis where all the momenta of the fragments from a single nuclear collision are measured.

In an event by event analysis, the individual collisions are analyzed by diagonalizing the kinetic energy flow tensor [Gyu 82]

$$F_{ij} = \sum_{\nu} p_i(\nu)p_j(\nu)/2m(\nu) \qquad (18)$$

or the momentum flow tensor:

$$P_{ij}=\Sigma_{\nu}\,[p_i(\nu)p_j(\nu)/\mathrm{abs}(p(\nu))]/\Sigma_{\nu}\,\mathrm{abs}(p(\nu)) \qquad (19)$$

where the sum is over all charged particles in a given event and (i,j) represent the Cartesian components (x,y,z). By diagonalizing this tensor, the flow angle θ_F is obtained for each event.

We now turn to the microscopic NFM and VUU theories and compare their event by event predictions to NFD, INC, and experiment. In the Newtonian Force Model [Mol 84a], for Nb (400 MeV/nucleon) + Nb at b = 3 fm, the computations are stopped at t = 30 fm/c, after which the flow results remain constant. The evolution of a collision at b = 3 fm impact parameter was shown in figure II.1. The resulting sidewards flow can clearly be seen. Note that the average deflection angle of the center of mass of projectile and target nucleons, respectively, is approximately equal to the average calculated flow angle, which associates a simple meaning to the flow concept. The demonstrated strong correlation between configuration space and momentum space can be attributed to the repulsive short range component of the nucleon-nucleon potential.

The distribution of flow angles $dN/d\cos\theta_F$ is presented in Fig. III.8 for various impact parameter intervals. The qualitative behavior of the flow pattern in the NFM model is as follows: the flow angle θ_F rises smoothly from 0° at large impact parameters to 90° at b=0 fm. It is interesting to note that large changes in the peak flow angle are not seen in models which lack compressional energyl like the intranuclear cascade model. The contribution of zero impact parameter collisions to the observable cross sections is negligible. Thus a finite range of impact parameters is sampled to compute the distribution of the flow angle,

$dN/d\cos\theta_F$, which is to be compared to the experimental data of the GSI/LBL collaboration (Fig. III.9).

For the computation of the flow angle distribution the formation of fragments via the generalized coalescence model discussed above was taken into account. We have found that one obtains roughly the same flow distribution by doing the flow analysis with protons only (no clustering), with clustering (protons only), or by counting all particles obtained with the coalescence model.

Figure III.9 shows the experimental data [Gus 84] for the Nb (400 MeV/nucleon) + Nb case discussed above, together with the predictions of the intranuclear cascade and fluid dynamical calculations [Buc 84b]. The data exhibit nonzero average flow angles once high multiplicity, i.e. small impact parameter collisions, are selected. This is in contrast to the intranuclear cascade calculation (using the Yariv Frankel and Cugnon approaches), which yields zero flow angles even at the highest multiplicities (also see figure III.10 [Mol 85b]). The microscopic NFM model, on the other hand, predicts peaks in the angular distributions of the flow angles, which shift to larger angles with increasing multiplicity. This is in qualitative agreement with the experimental data. The physical difference between the INC model and the NFM approach can be traced back to the different treatments of the NN collision process. The INC applies a stochastic 4π scattering at the point of closest approach of straight line trajectories; this allows for substantial transparency. In contrast, the repulsive short range component in the NN potential used for the NFM approach is a hard core and thus effectively results in an excluded volume effect. The nuclei are not as transparent and easily compressible as in the

INC. This causes incident nucleons to be deflected away from zones of high density towards sidewards angles.

The VUU theory also predicts finite flow angles. We study the flow angle as a function of time: in Nb (1050 MeV/nucleon) + Nb, at b = 3 fm, the flow angle reaches a maximum at t = 14 fm/c (see figure III.11). The compression or density of nuclear matter reaches its maximum value earlier at 5 fm/c (figure III.12), it takes a finite amount of time for the equilibration of the momentum distribution to occur and for the final saturation value of the flow angle to be attained.

As a function of energy, the density reached in heavy ion collisions is very similar in Au + Au (see figure III.13), Nb + Nb, or Ar + KCl collisions [Mol 85c]. What is important for the maximum density is not the atomic number, but the EOS: higher densities are achieved with softer equation of states. Notice that the densities calculated with the VUU theory are much lower than those reached with the less realistic intranuclear cascade model [Cug 81]. The density is related to the flow angle for a given system via the EOS: a softer equation of state results in lower peak flow angles (Fig. III.14) and higher densities.

How does the peak flow angle vary as a function of the bombarding energy? At fixed impact parameter (b = 3 fm), the flow angle reaches a maximum value at 400 MeV/nucleon and then does not change further as the collision energy increases (Fig. III.15). There is however a very strong effect due to the atomic number (Fig. III.16) at fixed energy E = 400 MeV/nucleon. This is easily understood: even though the same densities are reached in these different symmetric systems, there are many more collisions for the higher atomic numbers. The collective flow in the VUU theory thus is determined by an interplay between the collision term and the EOS. We

find similar results for the peak flow angle in Au + Au at b = 3 fm as in Nb + Nb (Fig. III.17) except that the maximum flow angle is now twice as large (Fig. III.14). These results are entirely consistent with forthcoming experimental data from the GSI/LBL plastic ball group [Gus 85].

Asymmetric collisions present results somewhat different from the above. Here a new difficulty arises - namely the problem of analyzing an asymmetric collision. E.g. for the Ar (770 MeV/nucleon) + Pb experiment, the data [Ren 84] were interpreted on an event by event basis in a rather non-trivial way. First, only charged particles were used. Then the center of mass velocity for each event was computed from the momenta of all charged particles with transverse momenta per nucleon greater than the Fermi momentum and, finally only the forward hemisphere of this participant center of mass frame was considered. We compare in Fig. III.18 these data with the predictions of the Vlasov-Uehling-Uhlenbeck theory. Both in theory and experiment a broad bump is observed in the distribution of flow angles for near central collisions, while a rather sharp peak occurs at 15-30 degrees for the medium impact parameters, i.e. intermediate multiplicity events. This contrasts strongly with the results of intranuclear cascade calculations, which exhibit forward peaked angular distributions independent of impact parameter as well for asymmetric as for symmetric collisions.

We suggest a different approach to the data analysis for asymmetric collisions [Mol 84b]. One sees from figure II.11 that in order to detect the collective sidewards flow of nuclear matter one needs to look at the projectile hemisphere in momentum space for asymmetric systems. An asymmetry here is evidence of collective flow; this is easily recognized at the intermediate impact parameter b = 5 fm in figure II.11. As in the case

for symmetric systems, the flow of nucleons in momentum space is correlated with a flow in configuration space. Therefore, the flow analysis should be done in the nucleon-nucleon center of momentum system with the usual kinetic energy flow tensor, but restricted to the projectile momentum hemisphere; this will avoid the distortion of the event shape by the large number of target spectators at rather small momenta and thus give the best reflection of the flow of the participant nucleons. We see in figure III.18c that the flow distribution changes it's characteristics in particular for the high multiplicity events. It is skewed towards 90° for the small impact parameters, while the peak remains near 20° degrees for the intermediate impact parameters. This is similar to the results for symmetric systems; the peak of the flow angle distribution decreases with increasing impact parameter. However, the peak flow angle at b = 3 fm appears to be greater than even the one for Au + Au collisions!

In figure III.19 the standard kinetic energy flow distributions for the system Ar + Pb are compared for individual impact parameters to the new transverse momentum analysis of Danielewicz and Odyniec [Dan 85]. Here, the transverse momentum spectrum $p_x(y)$ was analyzed, where y is the rapidity

$$y=1/2 \ln (E+p_{||})/(E-p_{||}) \qquad (20)$$

E the total energy of the fragment, and $p_{||}$ the momentum in the beam z-direction. Note that in the simulations shown here the projectile has $p_{||} = p_z > 0$. This technique has also been used to predict the presence of collective flow for O (600 MeV/A) + O within a time dependent Dirac equation approach [Cus 85].

As is evident from figure II.11, the flow angle approaches it's asymptotic value rather rapidly; indeed at b= 3 fm, the final flow angle distribution is established in less than 20 fm/c. At b = 1 fm, the flow

angle distribution is skewed to 90°, i.e., the projectile momentum hemisphere exhibits sidewards peaking (see figure III.19); a significant number of particles are thrust to the side perpendicular to the beam axis. A broad peak around 55° is observed at b = 3 fm; the flow angle becomes well defined. For b = 5 fm, there is a clear peak at 20-30 degrees. Thus it is only at the intermediate impact parameters where the flow is evident by a sharp peak in such asymmetric systems. Part of the reason why the peak is not so pronounced at lower impact parameters is statistical: the projectile hemisphere contains substantially fewer fragments in the final state in an Ar + Pb collision than in a Nb + Nb collision.

In the transverse momentum plots (Fig. III.19), much the same behavior is seen. However, here the analysis is not restricted to the forward hemisphere in momentum space. Summation over p_x and division by the number of protons in each rapidity bin shows very little flow effects in the target rapidity region, which is dominated by target spectator matter. At b = 1 fm, p_x/N is about 50 MeV/c/nucleon at the projectile rapidity 0.60, whereas at target rapidity, $y_T = -.60$, p_x amounts to only 25 MeV/c/nucleon. The flow at b = 3 fm is particularly pronounced in this method of analysis: $p_x(y_P)$ is equal to 150 MeV/c/nucleon whereas $p_x(y_T)$ is only 40 MeV/c/nucleon. At b = 5 fm, we have much the same result as at b = 3 fm. Note that in the massive system studied here the transverse momentum transfer (bounce-off effect) is larger than in lighter systems at higher energies - 100 MeV/c/nucleon have been observed for the system Ar (1.8 GeV/N) + KCl (Fig. III.22).

The influence of the nuclear matter equation of state has been studied by varying the compressibility from K=380 MeV to K=200 MeV at b=1,3 and 5 fm. At the lower impact parameter, the broad distribution prevents

any statistically significant difference from being seen. At the intermediate impact parameter, one sees a small shifting of the flow angle to the smaller angles as the compressibility decreases, this is consistent with what we have found for symmetric systems (Fig. III.14), but less dramatic. Note that one sees a great difference if K=0 MeV, the cascade model is used; then the distributions are peaked at zero degrees for all impact parameters. An equation of state with compressional energy seems essential to qualitatively reproduce the data; but asymmetric systems are less sensitive to the details of the equation of state than symmetric ones. Furthermore, one can look for quantum effects by turning off the Pauli principle at b= 3 and 5 fm. No strong effects are seen, which is somewhat a surprise in view of the strong effect we see in the symmetric case [Mol 85c] and the fact that about 50% of the collisions are Pauli blocked even at this high energy. However, this may be understood since many of the blocked collisions are between nucleons in the same nucleus, not between nucleons in the compression zone.

Let us consider now the system Ar + Pb at a lower energy, 400 MeV/nucleon (see figure III.19). The kinetic energy distribution becomes more forward peaked at fixed impact parameter b = 5 fm. The transverse momentum transfer $p_x(y_p)$ decreases to 100 MeV/c/nucleon. Preliminary results from the streamer chamber group indicate an experimental maximum of 76 MeV/c/nucleon; this is somewhat smaller than our prediction with the stiff EOS. Thus it will be important to relate their experimental multiplicities with finite impact parameters. A similar system, Ar (92 MeV/N) + Au, shows what happens in an event by event analysis as the energy is decreased further: the flow distributions at b= 2, 3, and 4 fm impact parameter become very broad; the transverse momentum at beam and target

rapidities is zero to within 10 MeV/c/nucleon. At still lower energies, the transverse momentum spectra are inverted as the attractive part of the nuclear potential becomes dominant: the bounce-off caused by the short range repulsion at high density is converted into the negative angle deflection known from TDHF calculations in this energy region [Stö 80a and 81b] and from experimental data.

The transverse momentum for the symmetric systems Nb + Nb (figure III.20) and Au + Au (Fig. III.21) is a strong function of energy. At b = 3 fm the transverse momentum $p_x(y_p)$ rises from negative or zero values for E < 100 MeV/nucleon to 140 to 160 MeV/c/nucleon at 1050 MeV/nucleon for Nb and Au systems, respectively. The bounce-off increases dramatically with energy but only slightly with atomic number.

For light systems and high energies flow effects are not observed when the standard kinetic energy flow analysis is used. In fact, the experimental flow angular distributions for the reaction Ar(1800 MeV/nucleon, b<2.4fm) + KCl are peaked at zero degrees as the cascade model predicts. But also the Vlasov-Uehling-Uhlenbeck approach, which does predict finite flow angles for heavier systems at lower energies, does not yield any observable sidewards maxima in the flow angle distributions; even less so can a difference between hard and medium equations of state be seen when the standard kinetic energy flow tensor analysis is used. All flow angle distributions are peaked at zero degrees [Mol 85a]. However, one should not hastily conclude that flow effects do not occur for light systems.

Experimentally, one may determine the scattering plane by controlling the finite multiplicity distortions carefully [Dan 85]. Danielewicz and Odyniec detected collective flow effects in the streamer

chamber data for Ar(1800 MeV/nucleon)+ KCl using this technique (see Fig. III.22a). There is a transverse momentum accumulation at both the projectile and target rapidities y = ±0.86 in the center of momentum frame. The collective flow effects are weaker than in the hydrodynamic model, but much stronger than in the cascade (see figure III.22b). It is important to point out that the intranuclear cascade model fails to reproduce this data, even though it appeared to be consistent with it when the kinetic energy flow analysis had been applied [Mol 85a].

The transverse momentum analysis technique has been applied to the Vlasov-Uehling-Uhlenbeck results [Mol 85a] for the reaction Ar(1800 MeV/nucleon, b < 2.4 fm) + KCl. One finds that the peak in the transverse momentum spectrum $p_x(y)$ depends linearly on the nuclear equation of state: the cascade model predicts $p_x^{max} \approx 25$ MeV/c/nucleon (figure III.22b), the medium equation of state in the Vlasov-Uehling-Uhlenbeck approach predicts $p_x^{max} \approx 50$ MeV/c/nucleon (figure III.22d), and the stiff equation of state yields $p_x^{max} \approx 100$ MeV/c/nucleon (figure III.22c). Only the latter is in agreement with the data. At the lower energy 1.2 GeV/nucleon, one finds experimentally p_x/N (peak) = 70 MeV/c/nucleon; the VUU prediction is p_x/N = 80 MeV/c/nucleon. At still lower energies of 770 MeV/nucleon, we predict a value of 70 MeV/c/nucleon. The variation over the energy range 770 - 1800 MeV/nucleon is thus not large. We would like to stress that the stiff equation of state reproduces best the pion yields observed in the streamer chamber at this energy (1800 MeV/nucleon) and also at lower energies, down to 360 MeV/nucleon (figure III.3). This equation of state also agrees well with the one extracted phenomenologically from the pion data.

Conclusions

Much progress has been made both theoretically and experimentally over the past decade in the study of relativistic heavy ion physics. Over the next decade, even more difficult problems must be solved to extend both experimental apparatus and theoretical models to the ultra-relativistic domain. What has been achieved so far is encouraging. Tantalizing insight has been gained into the nuclear equation of state. The precise determination of this equation of state will require much more effort, but it is a prize worth seeking.

References:

Aic 85a J. Aichelin and H. Stöcker, MSUCL-522.

Aic 85b J. Aichelin, private communication.

Aic 85c J. Aichelin and G.F. Bertsch, Phys. Rev. C31, 1730, 1985.

Ald 57 B.J. Alder and T.E. Wainwright, J. Chem. Phys. 27, 1208, 1957.

Ams 75 A.A. Amsden, G.F. Bertsch, F.H. Harlow, and J.R. Nix, Phys. Rev. Lett. 35, 905, 1975.

Ams 77a A.A. Amsden, F.H. Harlow, and J.R. Nix, Phys. Rev. C15, 2059, 1977.

Ams 77b A.A. Amsden, J.N. Ginocchio, F.H. Harlow, J.R. Nix, M. Danos, E.C. Halbert, and R.K. Smith,Jr., Phys. Rev. Lett. 38, 1055, 1977.

Bau 75 H.G. Baumgardt, J.U. Schott, Y. Sakamoto, E. Schopper, H. Stöcker, J. Hofmann, W. Scheid and W. Greiner, Z. Phys. A273, 359, 1975.

Bei 75 M. Beiner, H. Flocard, N.V. Giai, P. Quentin, Nucl. Phys. A238, 29, 1975.

Ber 78 G. Bertsch and A.A. Amsden, Phys. Rev. C18, 1293, 1978.

Ber 84a G.F. Bertsch, Erice School in Nuclear Physics 1984.

Ber 84b G.F. Bertsch, H. Kruse, and S. das Gupta, Phys. Rev. C29, 673, 1984.

Bod 71 A.R. Bodmer, Phys. Rev. D4, 1601, 1971.

Bod 77 A.R. Bodmer and C.N. Panos, Phys. Rev. C15, 1342, 1977.

Bod 80 A.R. Bodmer, C.N. Panos, and A.D. MacKellar, Phys. Rev. C22, 1025, 1980.

Bod 81 A.R. Bodmer and C.N. Panos, Nucl. Phys. A356, 517, 1981.

Bog 77 J. Boguta and A.R. Bodmer, Nucl. Phys. A292, 413, 1977.

Bog 82 J. Boguta, Phys. Lett. 109B, 251, 1982.

Bog 83 J. Boguta and H. Stöcker, Phys. Lett. 120B, 289, 1983

Bon 76 P. Bonche, S. Koonin, and J.W. Negele, Phys. Rev. C13, 1226, 1976.

Buc 81a G. Buchwald, L.P. Csernai, J.A. Maruhn, W. Greiner, and H. Stöcker, Phys. Rev. C24, 135, 1981.

Buc 81b G. Buchwald, L.P. Csernai, G. Graebner, J.A. Maruhn, W. Greiner and H. Stöcker, Z. Phys. A303, 111, 1981.

Buc 83a G. Buchwald, G. Graebner, J. Theis, J. Maruhn, W. Greiner, H. Stöcker, K. Frankel, and M. Gyulassy, Phys. Rev. C28, 2349, 1983.

Buc 83b G. Buchwald, G. Graebner, J. Theis, J.A. Maruhn, W. Greiner, and H. Stöcker, Phys. Rev. C28, 1119, 1983.

Buc 84a G. Buchwald, Ph.D. thesis, Universität Frankfurt, 1984.

Buc 84b G. Buchwald, G. Gräbner, J. Theis, J. Maruhn, W. Greiner, and H. Stöcker, Phys. Rev. Lett. 52, 1594, 1984.

Cal 79 D.J.E. Callaway, L. Wilets and Y. Yariv, Nucl. Phys. A327, 250, 1979.

Cha 73 G.F. Chapline, M.H. Johnson, E. Teller, and M.S. Weiss, Phys. Rev. D8, 4302, 1973.

Cho 74 A. Chodos, R.L. Jaffe, K. Johnson, C.B. Thorn, and V. Weisskopf, Phys. Rev. D9, 3471, 1974.

Cle 85 J. Cleymans, R.V. Gavai and E. Suhonen, to be published in Phys. Rep.

Cot 73 W.N. Cottingham, M. Lacombe, B. Loiseau, J.M. Richard, R. Vinhmau, Phys. Rev. D8, 800, 1973.

Cse 80a L.P. Csernai, B. Lukacs and J. Zimanyi, Lett. al Nuovo Cimento, 27, 111, 1980.

Cse 80b L.P. Csernai and H.W. Barz, Z. Phys. A296, 173, 1980.

Cse 82 L.P. Csernai and H. Stöcker, Phys. Rev. C25, 3208, 1982.

Cse 85 L.P. Csernai and J.I. Kapusta, to be published in Phys.Rep.

Cug 80 J. Cugnon, Phys. Rev. C22, 1885, 1980.

Cug 81 J. Cugnon, T. Mizutani and J. Van der Meulen, Nucl. Phys. A352, 505, 1981.

Cug 82 J. Cugnon, D. Kinet and J. Vandermeulen, Nucl. Phys. A379, 553, 1982.

Cug 84 J. Cugnon, D. L'Hote, Phys. Lett. 149B, 35, 1984.

Cus 85 R.Y. Cusson, P.G. Reinhard, H. Stöcker, M.R. Strayer, and W. Greiner, MSUCL-497, Phys. Rev. Lett., in print.

Dan 79 P. Danielewicz, Nucl. Phys. A314, 465, 1979.

Dan 85 P. Danielewicz and G. Odyniec, Phys. Lett., in print.

Dos 85 K.G.R. Doss et al, LBL-preprint 18948

Eng 82 J. Engels, F. Karsch, H. Satz, I. Montvay, Nucl. Phys. B205, 545, 1982.

Fee 46 E. Feenberg and H. Primakoff, Phys. Rev. 70, 980, 1946.

Foc 30 V. Fock, Zeit. für Phys. 61, 126, 1930.

Gar 79 S.I.A. Garpman, N.K. Glendenning and Y.J. Karant, Nucl. Phys. A322, 382, 1979

Gol 48 M.L. Goldberger, Phys. Rev. 74, 1269, 1948.

Gos 78 J. Gosset, J. Kapusta, and G. Westfall, Phys. Rev. C18, 844, 1978.

Gra 84 G. Graebner, Ph.D. Thesis, Universität Frankfurt, 1984, unpublished.

Gro 85 E. Grosse, Proc. Int. Workshop on Gross Prop. of Nuclei, Hirshegg, 1985.

Gus 84 H.A. Gustafsson, H.H. Gutbrod, B. Kolb, H. Löhner, B. Ludewigt, A.M. Poskanzer, T. Renner, H. Riedesel, H.G. Ritter, A. Warwick, F. Weik, and H. Wieman, Phys. Rev. Lett. 52, 1590, 1984.

Gus 85 unpublished and private communication.

Gyu 77 M. Gyulassy and W. Greiner, Ann. Phys. 109, 485, 1977.

Gyu 82 M. Gyulassy, K.A. Frankel and H. Stöcker, Phys. Lett. 110B, 185, 1982.

Hah 85a D. Hahn and H. Stöcker, MSUCL-506, 1985.

Hah 85b D. Hahn and H. Stöcker, to be published.

Har 27 D. Hartree, Proc. Camb. Phil. Soc. 24, 111, 1927.

Har 85 J.W. Harris, R. Bock, R. Brockman, A. Sandoval, R. Stock, H. Ströbele, G. Odyniec, H.G. Pugh, L.S. Schröder, R.E. Renfordt, D. Schall, D. Bangert, W. Rauch and K.L. Wolf, Phys. Lett. 153B, 377, 1985.

Hei 79 U. Heinz, W. Greiner and W. Scheid, J.Phys. G5, 1383, 1979.

Hei 84 U. Heinz, J. Reinhardt, B. Müller, W. Greiner and W.T. Pinkston Zeit. f. Physik A316, 341, 1984

Hof 76 J. Hofmann, H. Stöcker, U. Heinz, W. Scheid, and W. Greiner, Phys.Rev. Lett. 36, 88, 1976.

Jac 83 B.V. Jacak, G.D. Westfall, C.K. Gelbke, L.H. Harwood, W.G. Lynch, D.K. Scott, H. Stöcker, M.B. Tsang, and T.J.M.Symons, Phys. Rev. Lett. 51, 1846, 1983.

Kap 79 J.I. Kapusta, Nucl. Phys. B148, 461, 1979.

Kap 84 J.I. Kapusta, Nucl.Phys. A418, 573c, 1984.

Koc 83 P. Koch, J. Rafelski and W. Greiner, Phys. Lett. 123B, 151, 1983.

Koe 80 H.S. Koehler, Nucl. Phys. A343, 315, 1980.

Koo 75 S. Koonin, PhD Thesis, MIT 1975.

Kru 85a H. Kruse, B.V. Jacak, and H. Stöcker, Phys. Rev. Lett. 54, 289 1985.

Kru 85b H. Kruse, B.V. Jacak, J.J. Molitoris, G.D. Westfall, and H. Stöcker, Phys. Rev. C31 1985.

Kun 81 J. Kunz, R. Babinet, L. Wilets and U. Mosel, Nucl. Phys. A367, 459, 1981.

Lee 74 T.D. Lee and G.C. Wick, Phys. Rev. D9, 2291, 1974

Mad 26 E. Madelung, Z. Phys. 40, 332, 1926.

Mar 77 J.A. Maruhn, Proc. Topical Conf. on Heavy Ion Collisions, Pikeville, TN 1977 p. 156.

Mek 78a A. Mekjian, Phys. Rev. C17, 1051, 1978.

Mek 78b A. Mekjian, Nukl.Phys. A312, 491, 1978.

Met 58 N. Metropolis, R. Bivins, M. Storm, A. Turkevich, J.M. Miller, and G. Friedlander, Phys. Rev. 110, 185, 1958.

Mig 72 A.B. Migdal, JETP 34, 1184

Mol 84a J.J. Molitoris, J.B. Hoffer, H. Kruse, and H. Stöcker, Phys. Rev. Lett. 53, 899, 1984.

Mol 84b J.J. Molitoris and H. Stöcker, MSUCL-514, to be published.

Mol 85a J.J. Molitoris and H. Stöcker, Phys. Rev. C, in print.

Mol 85b J.J. Molitoris, H. Stöcker, J. Cugnon and D. L'Hote, to be published.

Mol 85c J.J. Molitoris, MSU PhD thesis 1985 and to be published.

Nag 81 S. Nagamiya, M.-C. Lemaire, E. Moeller, S. Schnetzer, G. Shapiro, H. Steiner, and I. Tanihata, Phys. Rev. C24, 971, 1981.

QM 79 First Workshop on Ultra-Relativistic Nuclear Collisions, Lawrence Berkeley Laboratory report LBL 8957 (1979).

QM 80 Proceedings of an International Symposium in Bielefeld, August 1980 Statistical Mechanics of Quarks and Hadrons, edited by H. Satz North-Holland Publishing Company, Amsterdam 1980.

QM 82 Proceedings of the Bielefeld Workshop, May 1982 Quark Matter Formation and Heavy Ion Collisions, edited by M. Jacob and H. Satz, World Scientific Publishing Co, Singapore 1982.

QM 83 Proceedings of the Third International Conference on Ultra-Relativistic Nucleus-Nucleus Collisions, Brookhaven National Laboratory September 1983, Nucl. Phys. A418, 1984.

QM 84 Proceedings of the Fourth International Conference on Ultra-Relativistic Nucleus-Nucleus Collisions, Helsinki, June 1984 edited by J. Maalampi, Springer Verlag, Berlin, in press.

Raf 82 J. Rafelski and B. Müller, Phys. Rev. Lett. 48, 1066, 1982.

Rem 84 B. Remaud, F. Sebille, C. Gregoire and F. Scheuter, Nucl. Phys. A428, 101c, 1984.

Ren 84 R. E. Renfordt, D. Schall, R. Bock, R. Brockmann, J.W. Harris, A. Sandoval, R. Stock, H. Ströbele, D. Bangert, W. Rauch, G. Odyniec, H.G. Pugh, and L.S. Schroeder, Phys. Rev. Lett. 53, 763, 1984.

Row 70 D. Rowe, Nuclear Collective Motion, Methuen and Co., London, 1970.

Ruc 76 V. Ruck, M. Gyulassy and W. Greiner, Z. Phys. A277, 391, 1976.

San 80 A. Sandoval, R. Stock, H.E. Stelzer, R.E. Renfordt, J.W. Harris, J.P. Brannigian, J.V. Geaga, L.J. Rosenberg, L.S. Schroeder, and K.L. Wolf, Phys. Rev. Lett. 45, 874, 1980.

San 85 M. Sano, M. Guylassy, M. Wakai and Y. Kitazoe, Phys.Lett., in print

Sar 85 S. Sarker and S.K. Chowdhury, Phys. Lett. 153B, 358, 1985.

Sch 25 E. Schrödinger, Ann. Phys. (4) 79, 361 and 489 1925.

Sch 68 W. Scheid, R. Ligensa, and W. Greiner, Phys. Rev. Lett. 21, 1479, 1968.

Sch 74 W. Scheid, H. Müller, and W. Greiner, Phys. Rev. Lett. 32, 741, 1974.

Ser 47 R. Serber, Phys. Rev. 72, 1114, 1947.

Ser 85 B. Serot and J.D. Walecka, Advance in nuclear physics, Plenum 1985

Shu 80 E.V. Shuryak, Phys. Rep. 61C, 71, 1980.

Sie 79 P.J. Siemens and J.I. Kapusta, Phys. Rev. Lett. 43, 1486, 1979.

Sky 59 T.H.R. Skyrme, Nucl. Phys. 9, 615 and 635, 1959.

Sob 75 M.I. Sobel, P.J. Siemens, J.P. Bondorf and H.A. Bethe, Nucl. Phys. A251, 502, 1975.

Sta 71 H.E. Stanley, Introduction to Phase Transitions and Critical Phenomena, Clarendon Press, Oxford 1971.

Sto 80 R. Stock, H.H. Gutbrod, W.G. Meyer, A.M. Poskanzer, A. Sandoval, J. Gosset, C.H. King, G. King, Ch. Lukner, N.V. Sen, G.D. Westfall, and K.L. Wolf, Phys. Rev. Lett. 44, 1243, 1980.

Sto 82 R. Stock, R. Bock, R. Brockman, J.W. Harris, A. Sandoval, H. Stroebele, K.E. Wolf, H.G. Pugh, L.S. Schröder, M. Maier, R.E. Renfordt, A. Dacal, and M.E. Ortiz, Phys. Rev. Lett. 49, 1236, 1982.

Sto 83 R. Stock, R. Bock, R. Brockmann, A. Dacal, J.W. Harris, M. Maier, M.E. Ortiz, H.G. Pugh, R.E. Renfordt, A. Sandoval, L.S. Schröder, H. Stöbele and K.L. Wolf, Physica Scripta T5, 130, 1983.

Stö 77a H. Stöcker, W. Scheid and W. Greiner, Proc. of the Topical Conf. on Heavy Ion Collisions, Fall Creek Falls State Park, Oak Ridge, TN 1977.

Stö 77b H. Stöcker, J. Hofmann, W. Scheid, and W. Greiner, Conf. on Nuclear Collisions, Bled, Yugoslavia, Fizika 9, Supp. 4, 1977a, p. 671.

Stö 78 H. Stöcker, W. Greiner and W. Scheid, Z. Phys. A286, 121, 1978

Stö 79a H. Stöcker, J.A. Maruhn and W. Greiner, Phys. Lett. 81B, 303, 1979.

Stö 79b H. Stöcker, J.A. Maruhn and W. Greiner, Z. Phys. A290, 297, 1979.

Stö 80a H. Stöcker, R.Y. Cusson, J.A. Maruhn and W. Greiner, Z. Phys. A294, 125, 1980.

Stö 80b H. Stöcker, J.A. Maruhn, and W. Greiner, Phys. Rev. Lett. 44, 725, 1980.

Stö 81a H. Stöcker, A.A. Ogloblin and W. Greiner, Z. Phys. A303, 259,1981.

Stö 81b H. Stöcker, R.Y. Cusson, J.A. Maruhn and W. Greiner, Phys. Lett. 101B, 379 (1981).

Stö 81c H. Stöcker, C. Riedel, Y. Yariv, L.P. Csernai, G. Buchwald, G. Graebner, J.A. Maruhn, W. Greiner, K. Frankel, M. Guylassy, B. Schürmann, G. Westfall, J.D. Stevenson, J.R. Nix, and D. Strottmann, Phys. Rev. Lett. 47, 1807, 1981.

Stö 81d H. Stöcker, M. Gyulassy and J. Boguta, Phys. Lett. 103B, 269, 1981.

Stö 82a H. Stöcker, L.P. Csernai, G. Graebner, G. Buchwald, H. Kruse, R.Y. Cusson, J.A. Maruhn, and W. Greiner, Phys. Rev. C25, 1873, 1982.

Stö 82b H. Stöcker, G. Buchwald, L.P. Csernai, G. Graebner, J.A. Maruhn and W. Greiner, Nucl. Phys. A387, 205, 1982.

Stö 83 H. Stöcker, G. Buchwald, G. Gräbner, P. Subramanian, J.A. Maruhn, W. Greiner, B.V. Jacak and G.D. Westfall, Nucl.Phys. A400, 63,1983.

Stö 84 H. Stöcker, J. Phys. Lett 10, 111, 1984.

Sub 81 P.R. Subramanian, L.P. Csernai, H. Stöcker, J.A. Maruhn, W. Greiner and H. Kruse, J. Phys. G7, L241, 1981.

Sub 85 P.R. Subramanian, W. Greiner, D. Hahn, H. Stöcker and U. Heinz, to be published

The 83 J. Theis, G. Graebner, G. Buchwald, J.A. Maruhn, W. Greiner, H. Stöcker, and J. Polonyi, Phys. Rev. D28, 2286, 1983.

Ueh 33 E.A. Uehling and G.E. Uhlenbeck, Phys. Rev. 43, 552, 1933.

Vas 80a D. Vasak, H. Stöcker, B. Müller and W. Greiner, Phys. Lett. 93B 243, 1980.

Vas 80b D. Vasak, B. Müller and W. Greiner, Physica Scripta 22, 25, 1980.

Vas 84 D. Vasak, W. Greiner, B. Müller, Th. Stahl and M. Uhlig, Nucl.Phys. A428, 291c, 1984.

Vau 72 D. Vautherin and D.M. Brink, Phys. Rev. C5, 626, 1972.

Wal 74 J.D. Walecka, Ann. Phys. 83 491, 1974.

Wil 77 L. Wilets, E.M. Henley, M. Kraft and A.D. MacKellar, Nucl. Phys. A282, 341, 1977.

Wil 78 L. Wilets, Y. Yariv and R. Chestnut, Nucl. Phys. A301, 359, 1978.

Won 77 C.Y. Wong, J.A. Maruhn and T.A. Welton, Phys. Lett. 66B, 19, 1977.

Yar 79 Y. Yariv and Z. Fränkel, Phys. Rev. C20, 2227, 1979.

Yar 81 Y. Yariv and Z. Fränkel, Phys. Rev. C24, 488, 1981.

Figure Captions

Fig. I.1 Possible phase diagram of nuclear matter shows the various transformations that have been conjectured. Experimentally, we still know very little about any of these.

Fig. I.2 U (960 MeV/nucleon) + Ag collision in emulsion: we see only the remnants of this central collision. What happened in the 10 fm/c that we do not see?

Fig. I.3 Pion multiplicities versus the temperature for baryon densities two times (solid line) and four times (dashed line) normal nuclear matter density. The curves describe the properties of a hot and dense piece of nuclear matter.

Fig. I.4 Contributions to the pion yields per baryon for a C + C reaction with the quadratic equation of state in the shock model.

Fig. I.5 The freeze out temperature of the pions calculated from the pion multiplicity data per nucleon. For $E_{lab} < 400$ MeV/nucleon, a freeze-out occurs for $\rho_0 < \rho < 3\rho_0$, for higher energies between two and five ρ_0.

Fig. I.6 The liquid gas phase transition in nuclear matter in the pressure density plane.

Fig. II.1 Nb (400 MeV/nucleon) + Nb as a function of time in the Newtonian Force Model: strong collective flow is caused by the short range repulsive nuclear force.

Fig. II.2 Time evolution in configuration and momentum space for C (85 MeV/nucleon) + C at b= 1 fm for TDHF, the Vlasov equation, and the Vlasov-Uehling-Uhlenbeck theory. Transparency occurs in both cases with a mean field only.

Fig. II.3 The nuclear equation of state with K= 200 MeV and K= 380 MeV as used in the VUU theory compared with values extracted from pion yields.

Fig. II.4 The stability of nuclei in the VUU approach versus a corresponding instability in the Cugnon cascade for Nb (0 MeV/nucleon) + Nb.

Fig. II.5 Fraction of Pauli blocked collisions in the VUU theory versus energy for the Nb + Nb system at b = 3 fm.

Fig. II.6 The evolution in momentum space in the VUU theory of Ar (137 MeV/nucleon) + Ca at b = 0 fm. The results from several parallel ensembles are superposed in order to represent the distribution function. The collision term results in substantial equilibration.

Fig. II.7 Initial and final states in configuration and momentum space in the VUU theory for C (85 MeV/nucleon) + C at b = 1 fm. The nucleons which equilibrate are those that collide.

Fig. II.8 Single particle inclusive proton spectra experimentally and theoretically (histograms) in the VUU theory for the Ar + Ca system.

Fig. II.9 The number of uncollided projectile nucleons in the VUU model emitted for C (85 MeV/nucleon) induced reactions is used to extract a mean free path.

Fig. II.10 In the VUU theory, the evolution of Ar (770 MeV/nucleon) + Pb in configuration space at b = 1, 3, and 5 fm.

Fig. II.11 The time development of Ar (770 MeV/nucleon) + Pb in momentum space in the VUU approach at various impact parameters.

Fig. II.12 Collision of Ar (770 MeV/nucleon) + Pb at b = 0 fm in the Nuclear Fluid Dynamic model. Note the remarkable similarity to the VUU theory.

Fig. II.13 The same system only at b = 4 fm in the Nuclear Fluid Dynamic model.

Fig. II.14 Nb (400 MeV/nucleon) + Nb at b = 1, 3, and 5 fm in momentum space as a function of time (VUU).

Fig. II.15 The same system in configuration space in the VUU approach.

Fig. III.1 Experimental slope factors compared to fluid dynamic calculations for a pure Fermi gas and for a classical ideal hadron gas.

Fig. III.2 Pion multiplicities per nucleon versus bombarding energy calculated in a simple shock model with the linear EOS and K_1 = 1200, 1600, and 2000 MeV for the solid, dashed, and dotted lines, respectively.

Fig. III.3 The cross section for photon production in the C + C system calculated within the shock model with the best overall fitting (to the pion data) linear and quadratic EOS's ($K_1 = K_q$ = 250 MeV).

Fig. III.4 Number of π^- versus energy for Ar + KCl in the cascade, VUU, and the experimental data.

Fig. III.5 The total pion multiplicity versus time in the VUU approach for Nb (1050 MeV/nucleon) + Nb at b = 3 fm; note the small but significant effect of re-absorption.

Fig. III.6 Total pion multiplicity versus energy for Nb + Nb at b = 3 fm in the VUU theory.

Fig. III.7 VUU predictions for pion multiplicities versus energy for Au + Au at b = 3 fm.

Fig. III.8 Kinetic energy flow angle distributions for Nb (400 MeV/nucleon) + Nb in the Newtonian Force Model compared to the experimental data.

Fig. III.9 Kinetic energy flow angle distributions for Nb (400 MeV/nucleon) + Nb from NFD, experiment, and the INC.

Fig. III.10 The bound and unbound Cugnon cascade compared to the experimental data for Nb (400 MeV/nucleon) + Nb in various multiplicity bins.

Fig. III.11 The average flow angle for Nb (1050 MeV/nucleon) + Nb at b = 3 fm versus time in the VUU approach.

Fig. III.12 The compression for Nb (1050 MeV/nucleon) + Nb at b = 3 fm in a central region of radius 2 fm versus time (VUU).

Fig. III.13 Maximum density in the center of mass frame for Au + Au collisions at b = 3 fm (VUU).

Fig. III.14 Effect of the compressibility on the flow angle distribution for Nb (400 MeV/nucleon) + Nb at b = 1 fm (VUU).

Fig. III.15 Peak flow angle versus bombarding energy for Nb + Nb at b = 3 fm.

Fig. III.16 Peak flow angle in the VUU model for E = 400 MeV/nucleon at b = 3 fm strongly depends on atomic number due to the increased number of collisions.

Fig. III.17 Peak flow angle versus energy for Au + Au at b = 3 fm (VUU).

Fig. III.18 Flow angle distributions for Ar (770 MeV/nucleon) + Pb for a) the experimental data with high and low multiplicity cuts using the momentum flow tensor; b) corresponding predictions of the VUU theory; and c) a standard kinetic energy flow analysis done in the nucleon-nucleon center of momentum frame using only the projectile momentum hemisphere.

Fig. III.19 VUU predictions for two different methods of detecting collective flow are shown for Ar + Pb : a) the standard kinetic energy flow analysis in the NN center of momentum frame is done on the forward hemisphere for b = 1, 3, and 5 fm and b) the transverse momentum analysis is shown at the same impact parameters.

Fig. III.20 Transverse momentum spectra for Nb + Nb at b = 3 fm as a function of energy (VUU).

Fig. III.21 Transverse momentum at projectile rapidity for Au + Au at b = 3 fm versus energy (VUU).

Fig. III.22 Transverse momentum spectra for Ar (1800 MeV/nucleon) + KCl for the experimental data (a), intranuclear cascade (b), and the VUU approach with hard (c) and soft (d) equations of state.

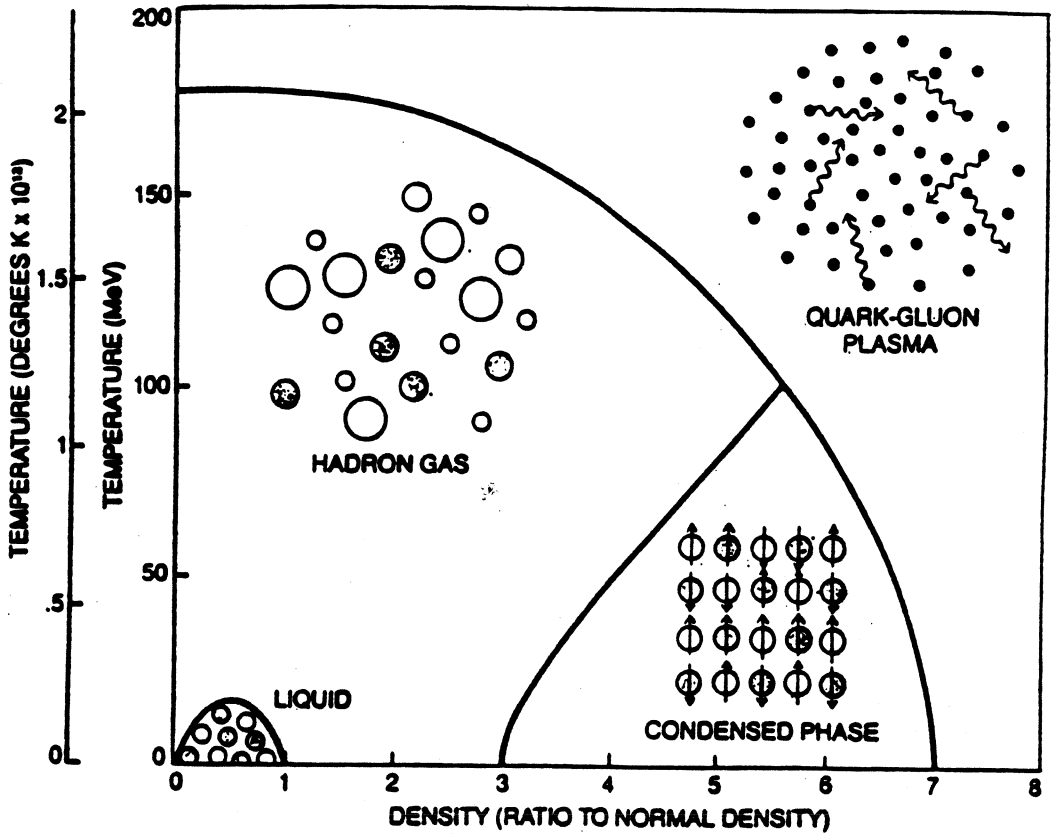

Figure I.1

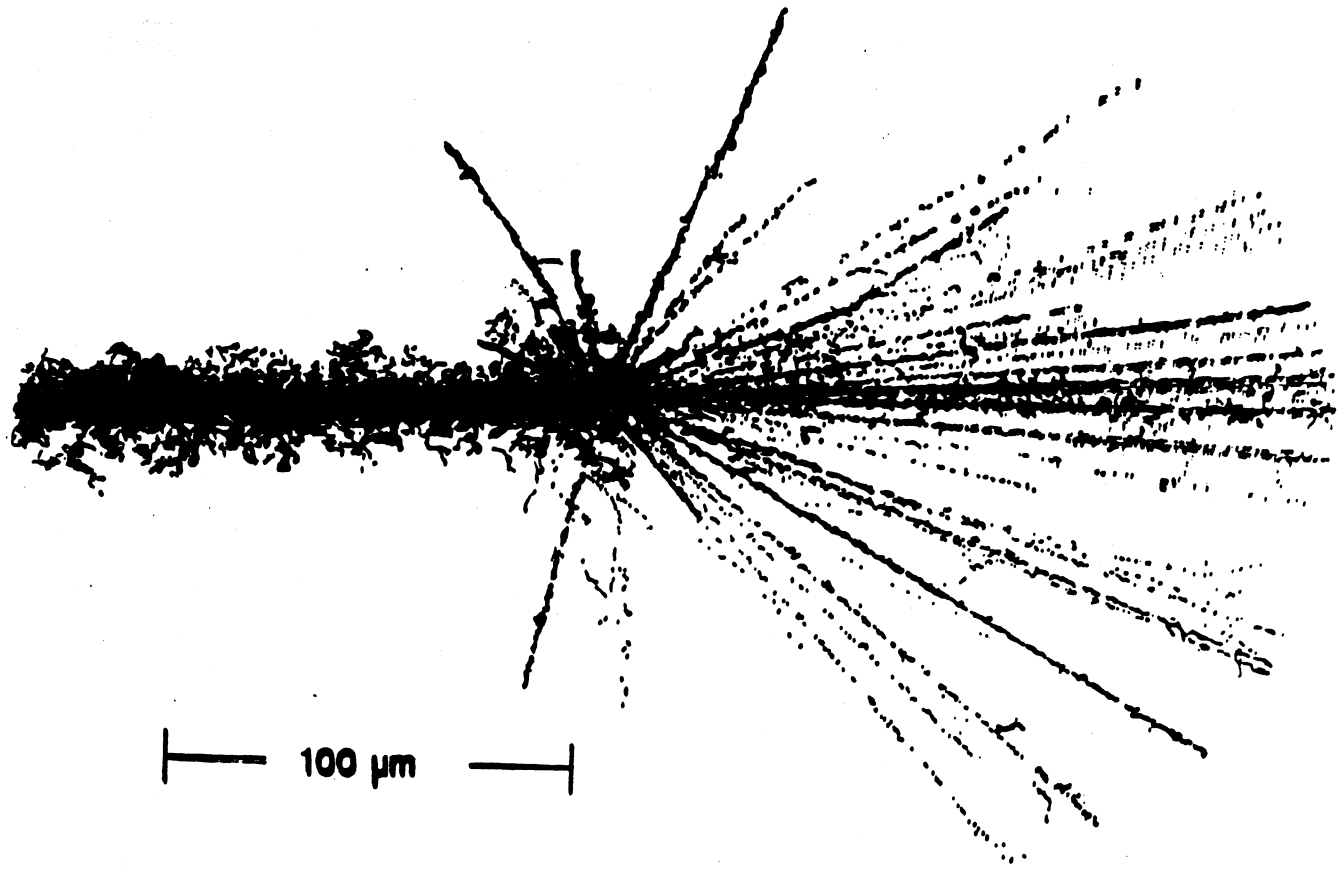

Figure I.2

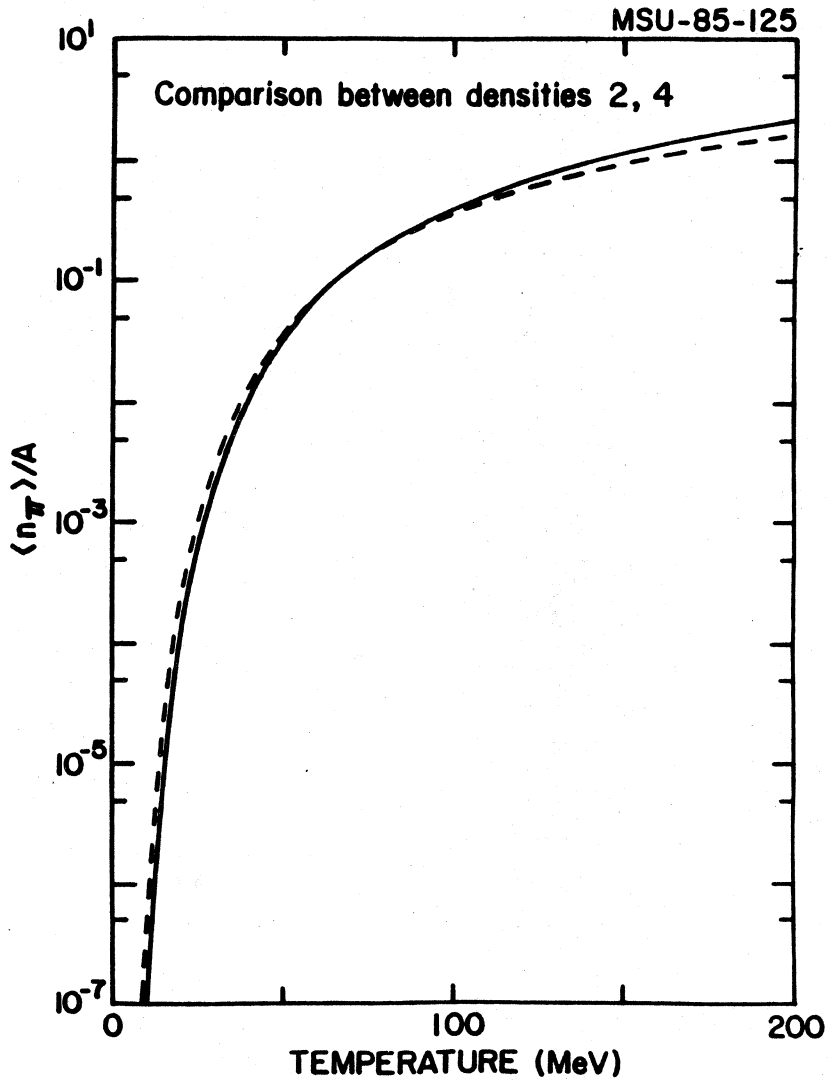

Figure I.3

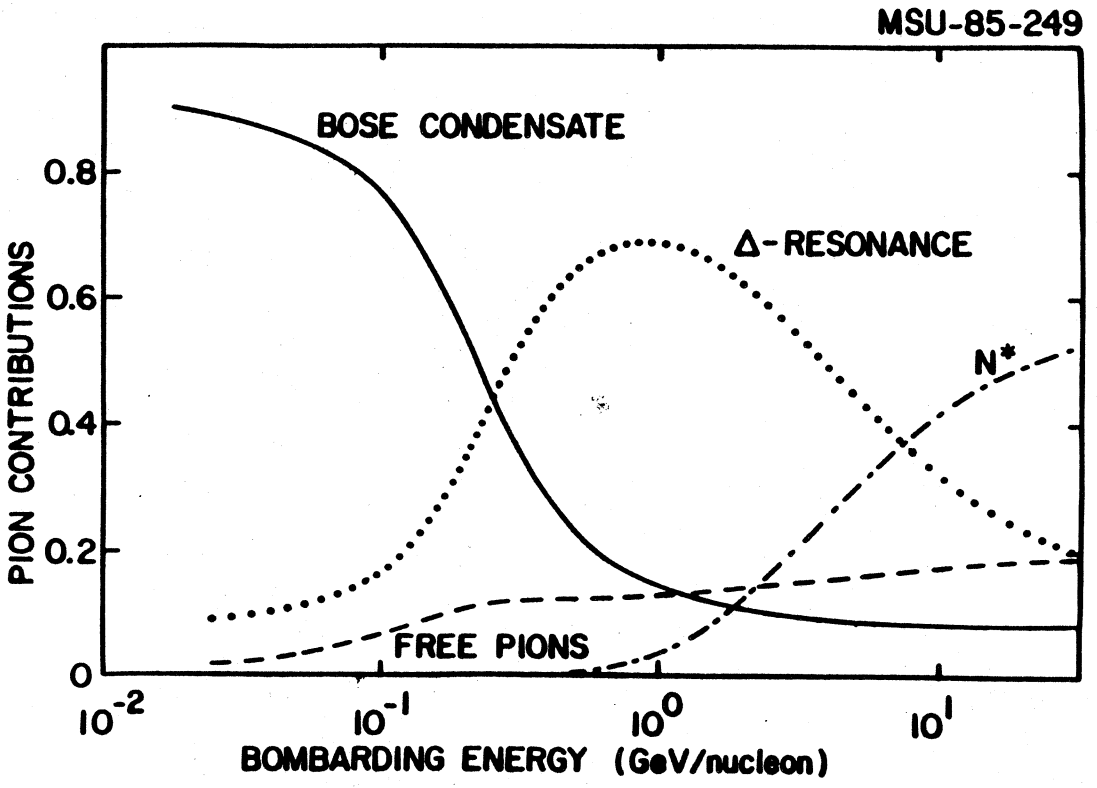

Figure I.4

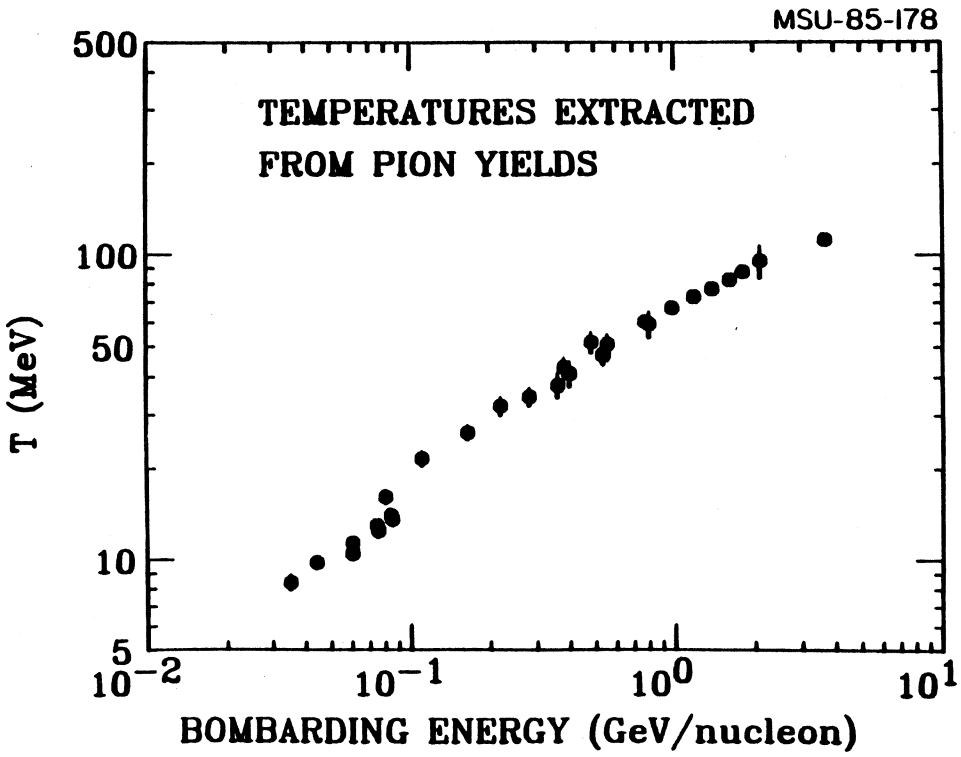

Figure I.5

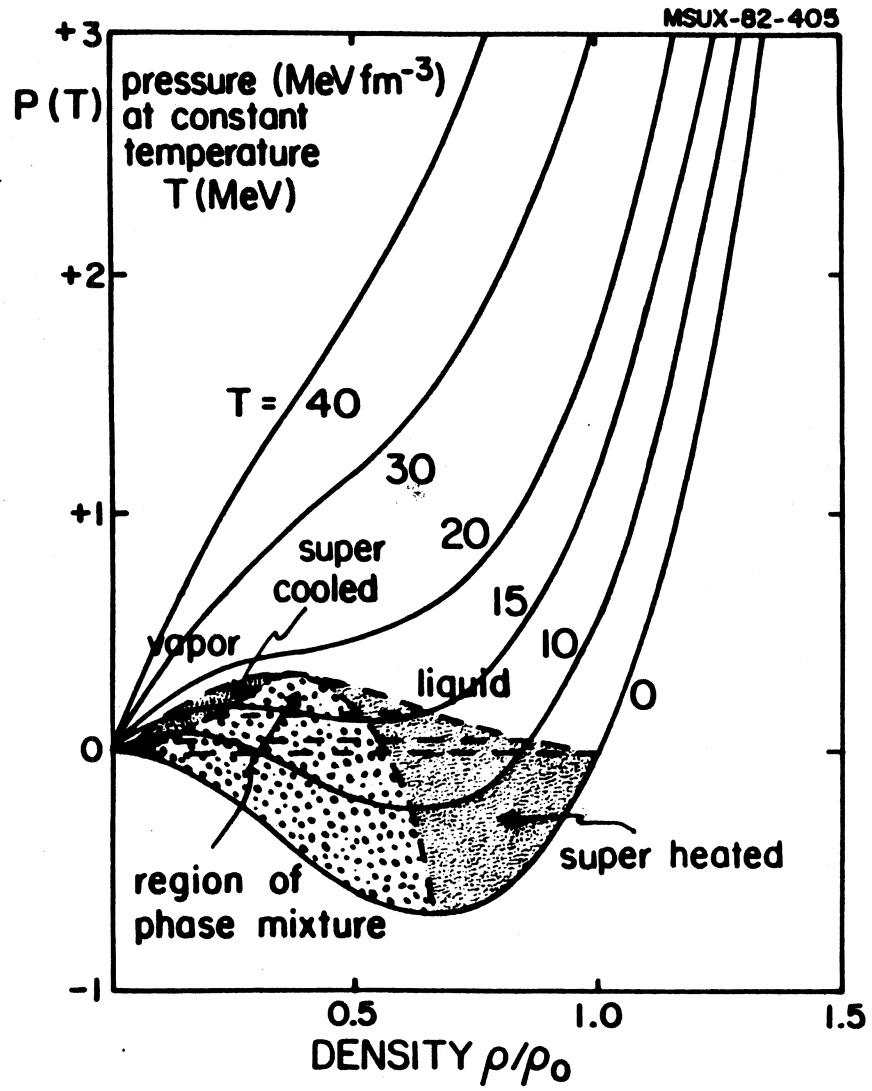

Figure I.6

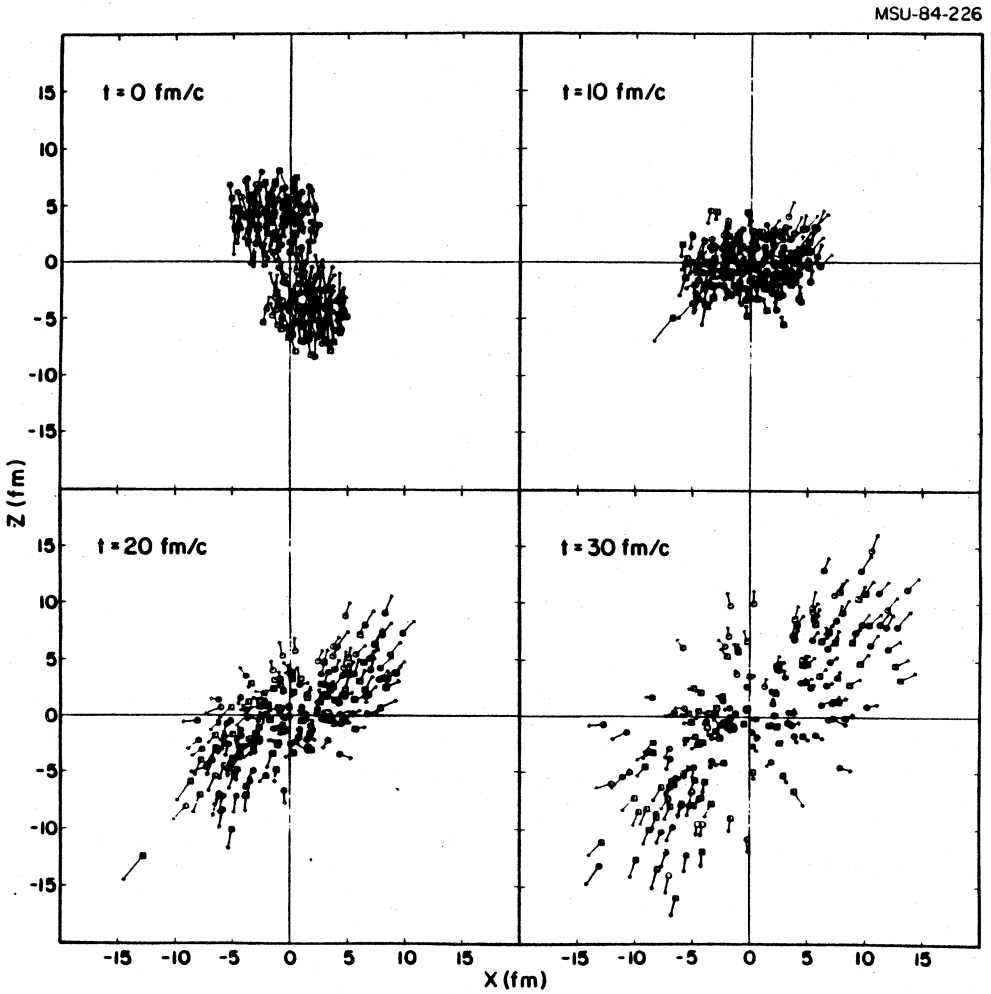

Figure II.1

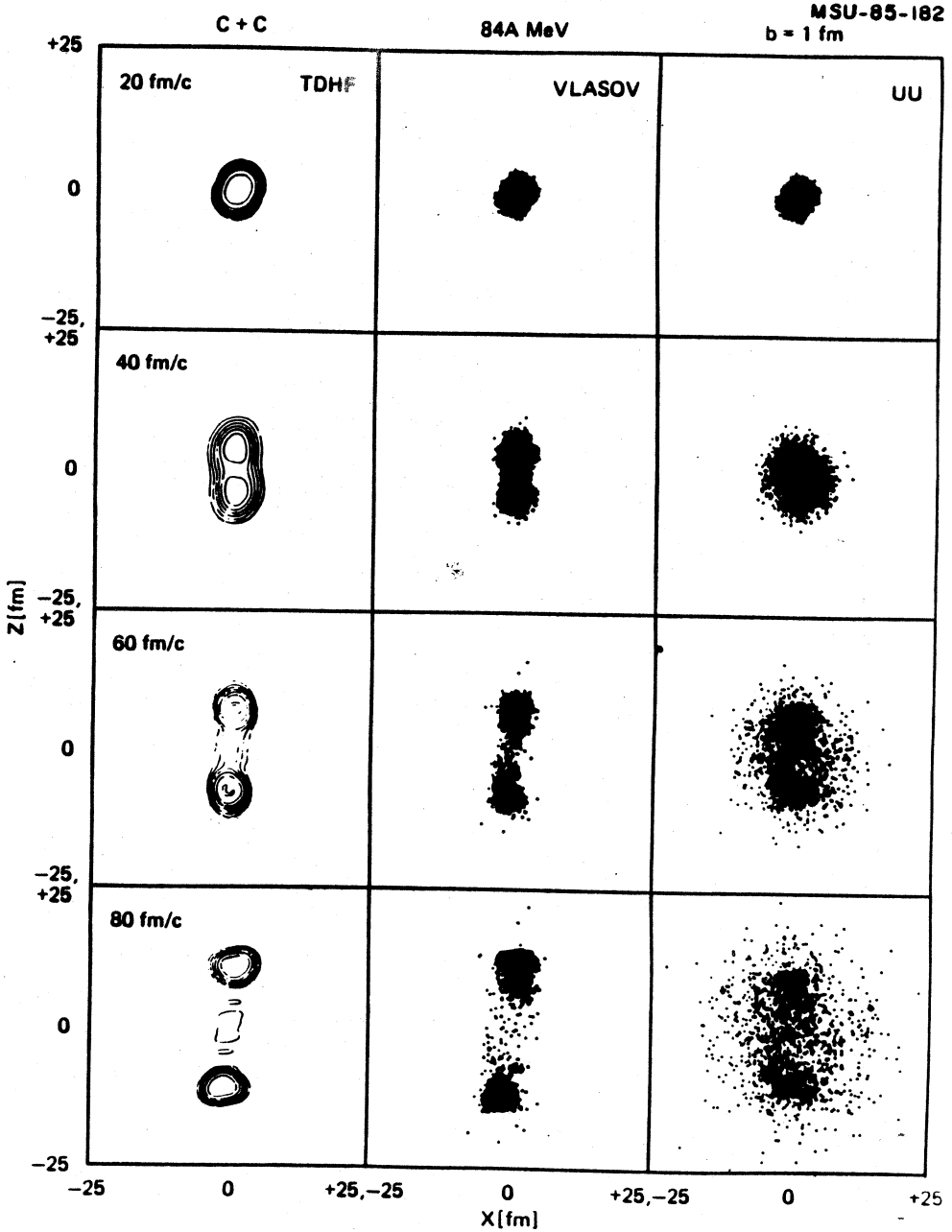

Figure II.2

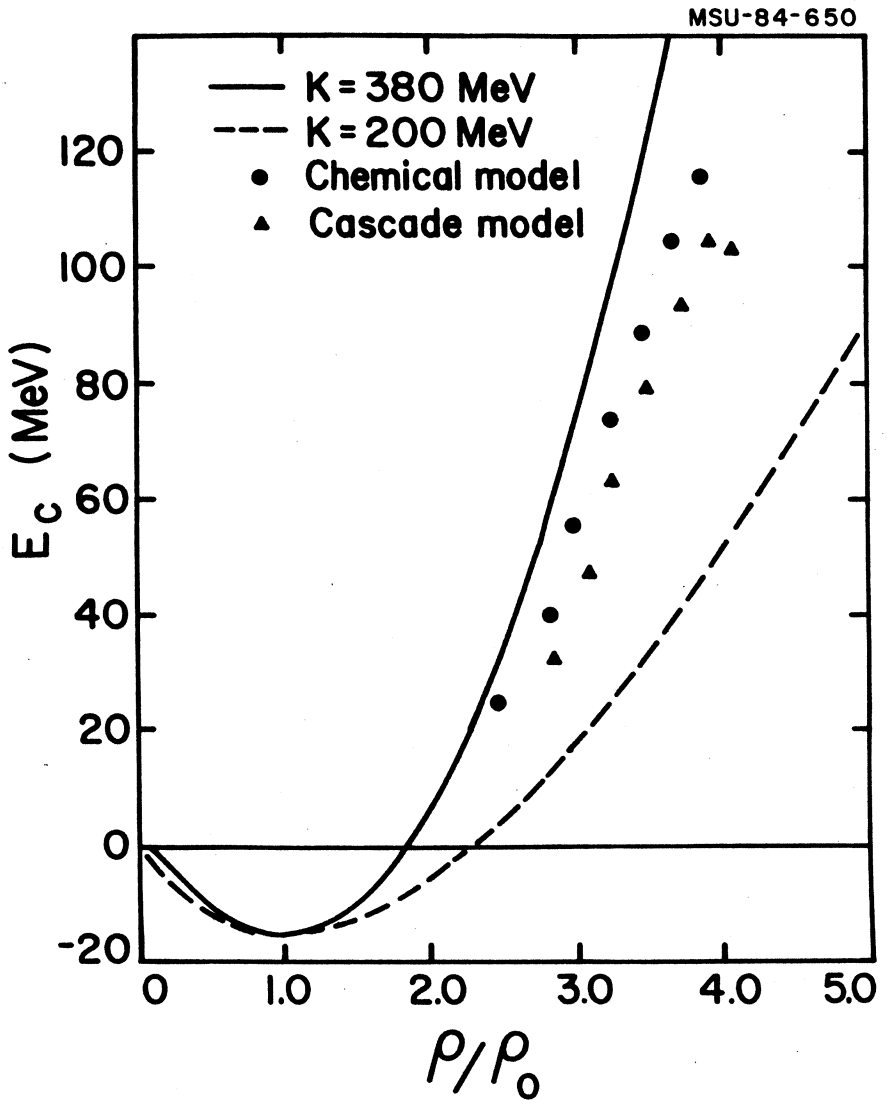

Figure II.3

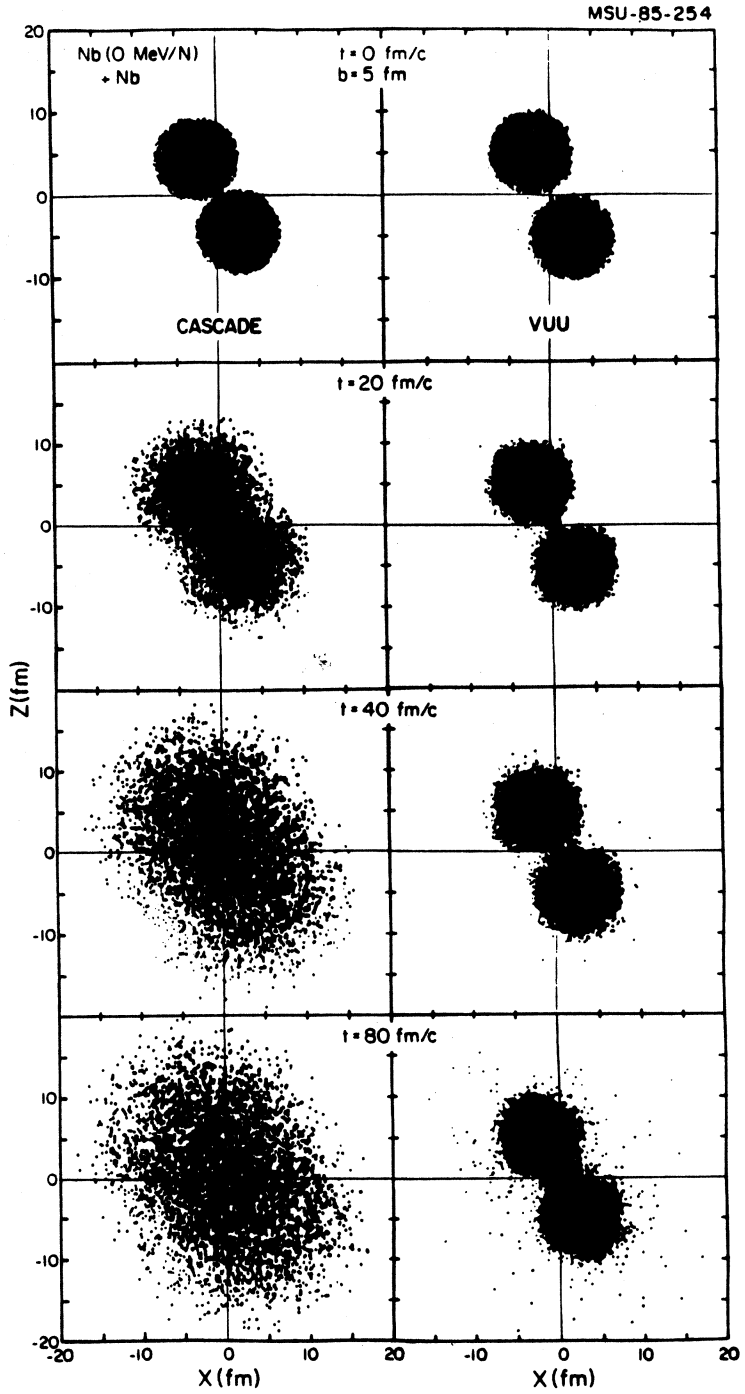

Figure II.4

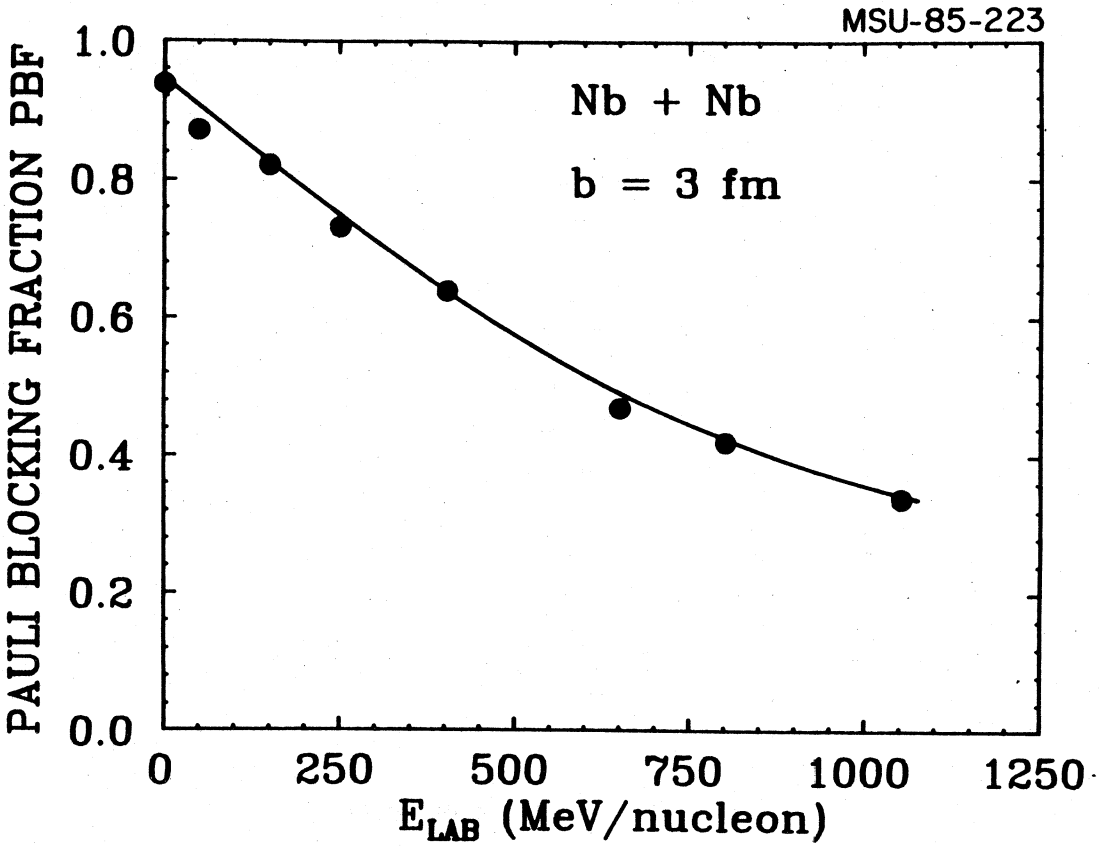

Figure II.5

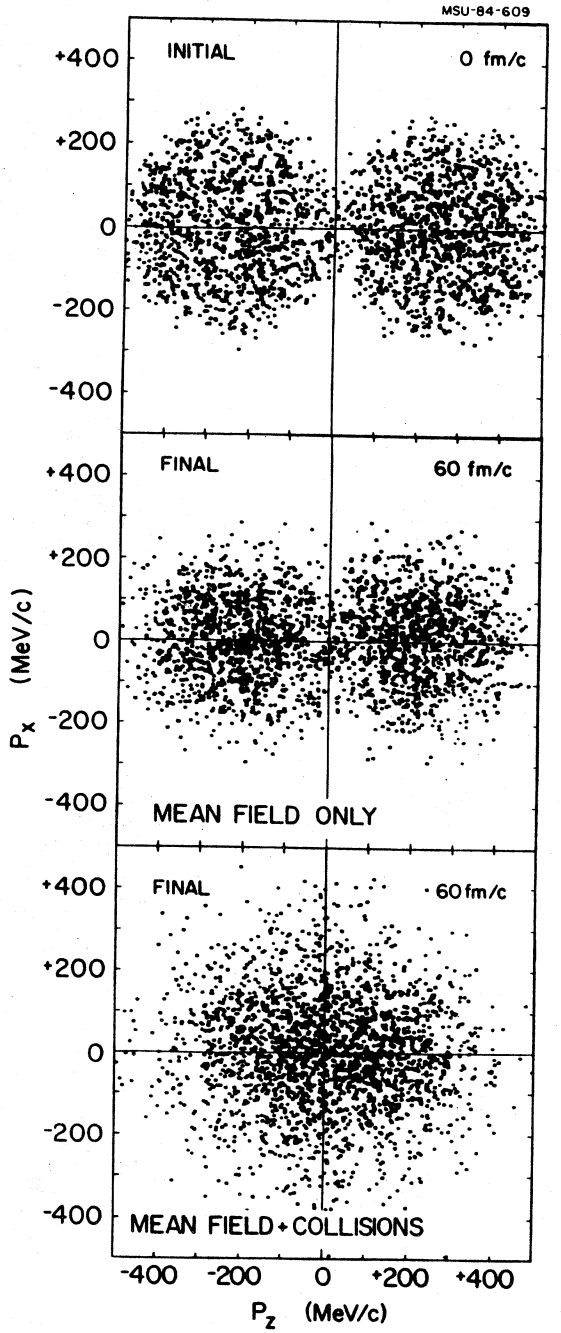

Figure II.6

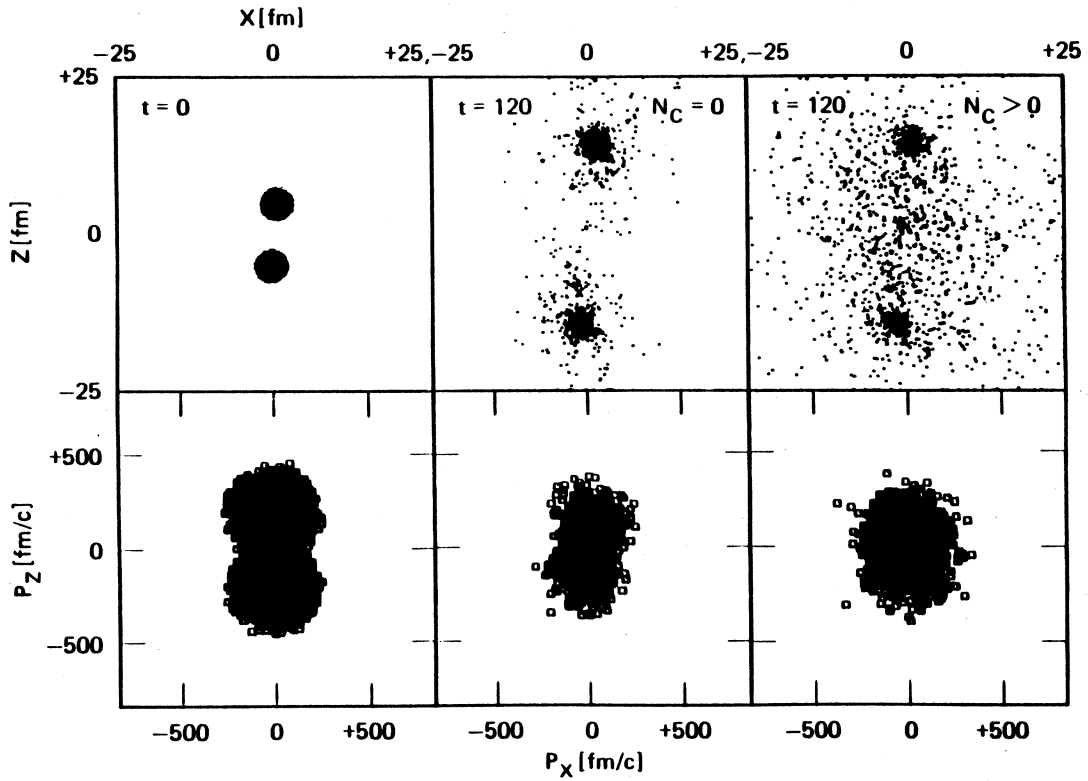

Figure II.7

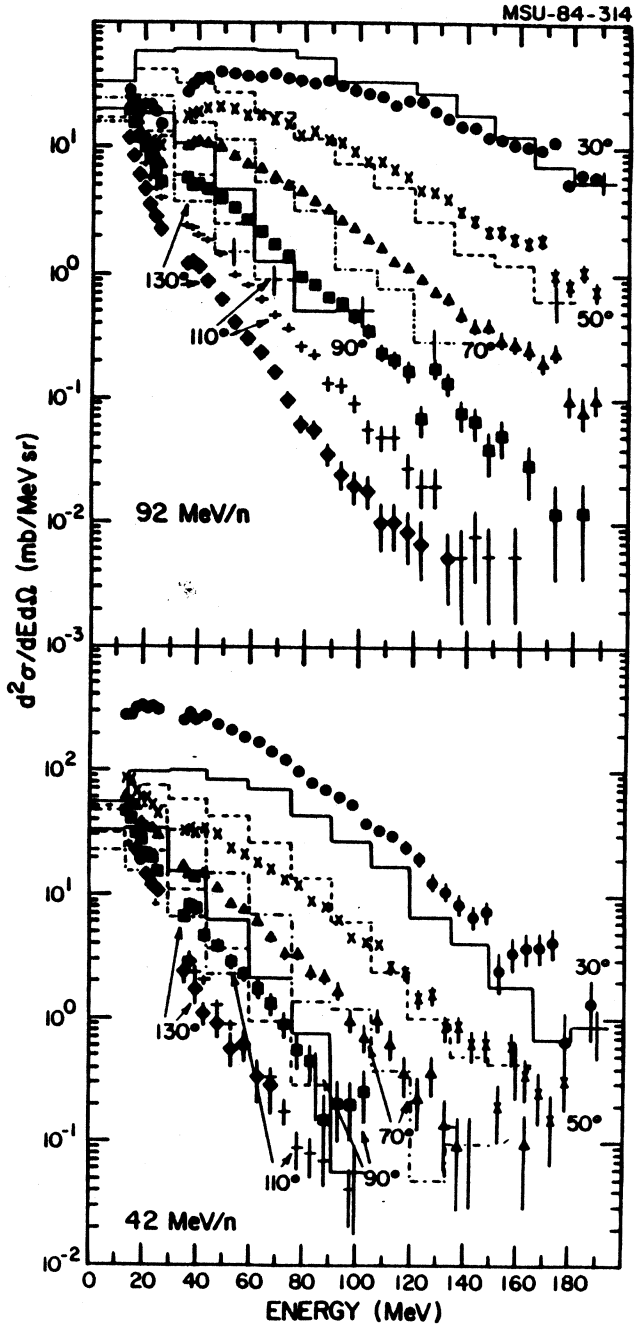

Figure II.8

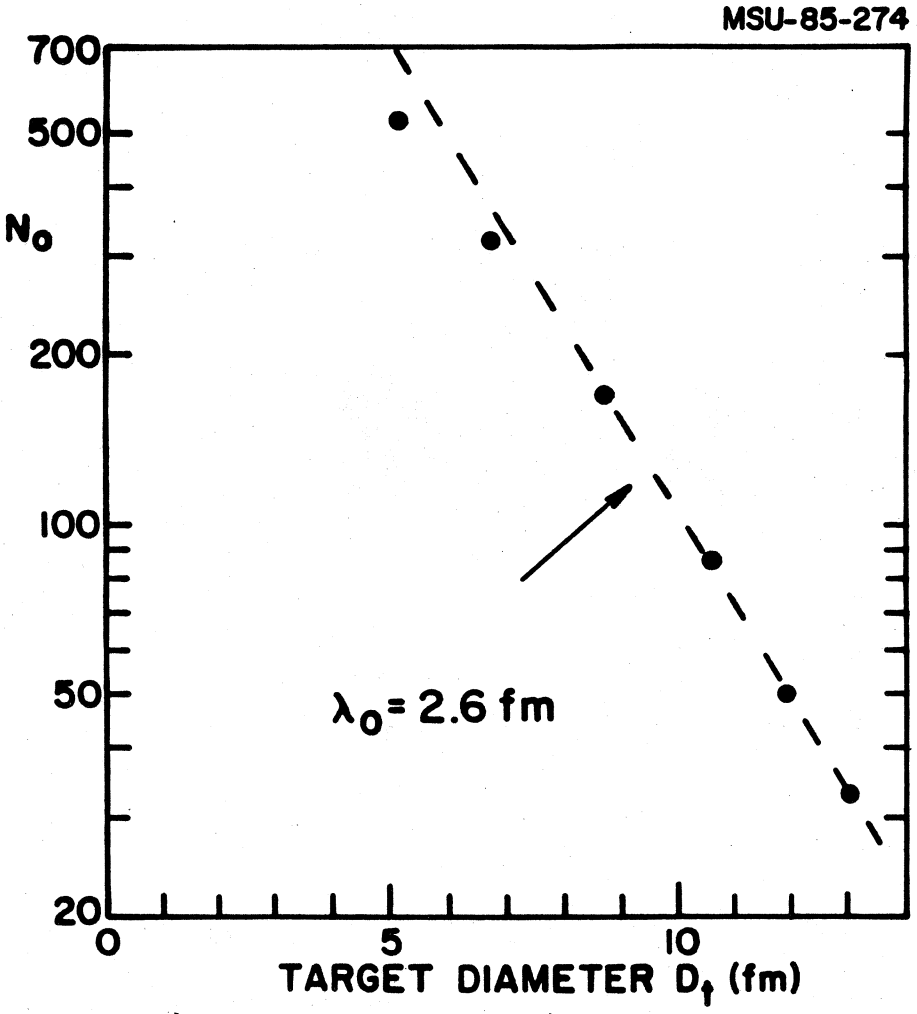

Figure II.9

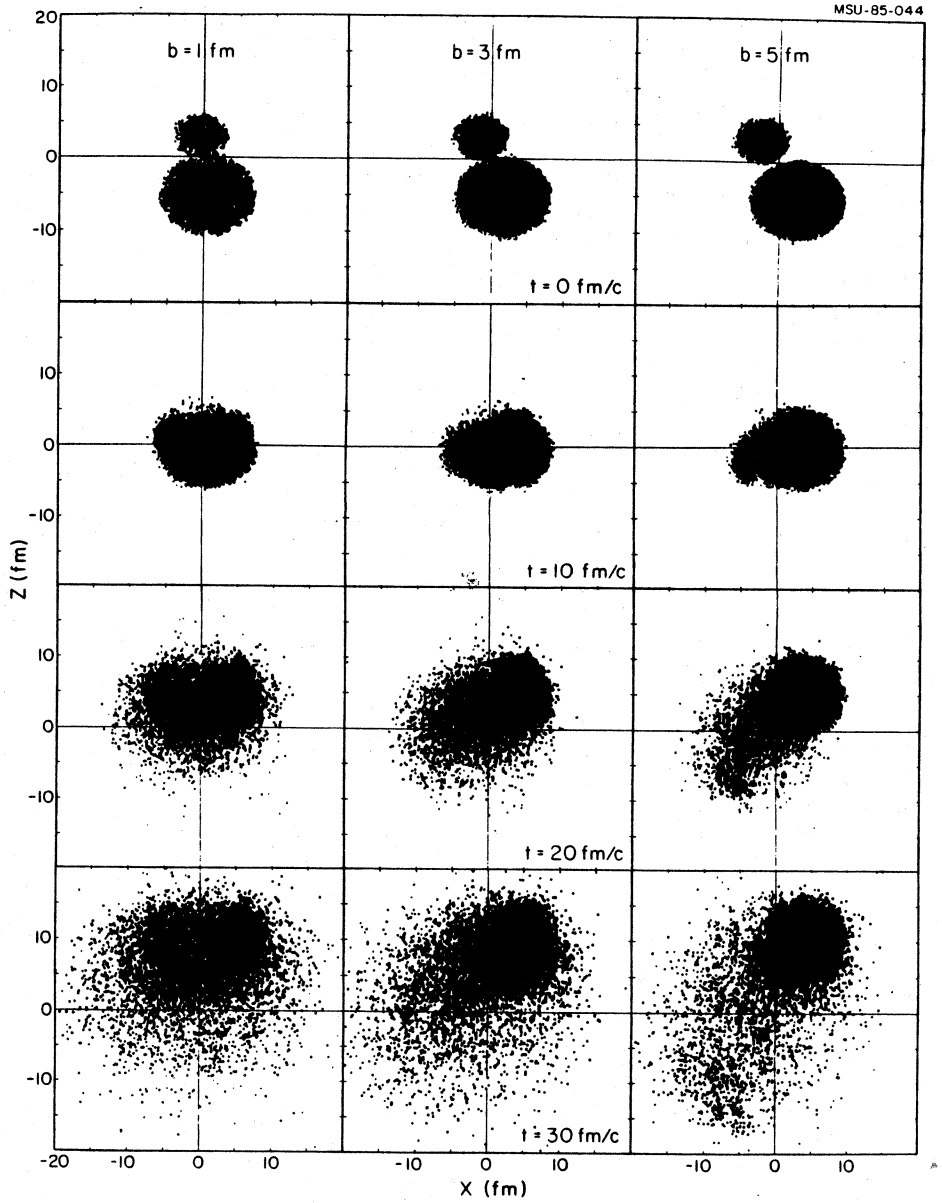

Figure II.10

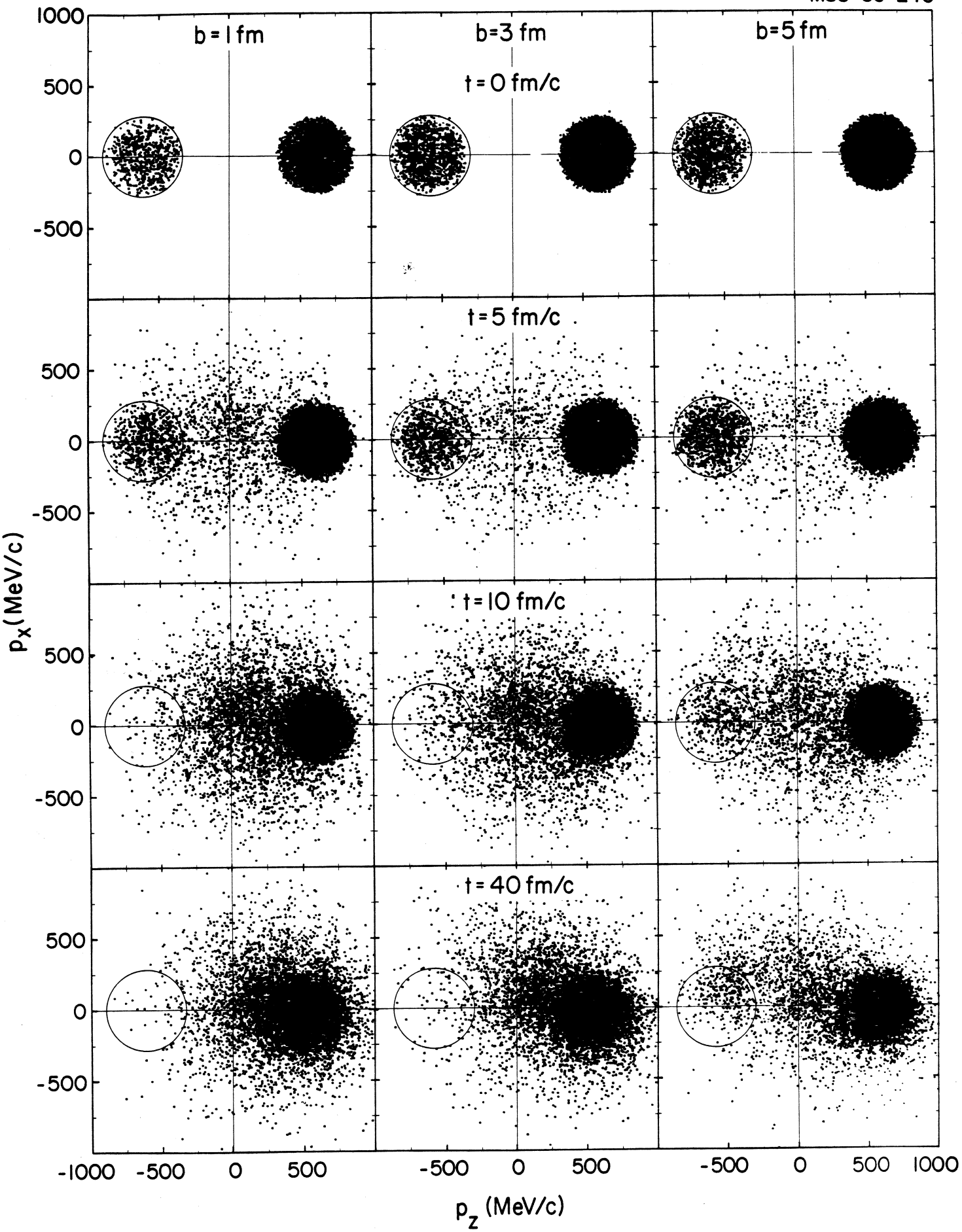
b = 1 fm
b=3 fm
b=5 fm
t = 0 fm/c
t=5 fm/c
t=10 fm/c
t=40 fm/c
1000
500
0
-500
p_x(MeV/c)
-1000 -500 0 500
-500 0 500
-500 0 500 1000
p_z (MeV/c)

Figure II.11

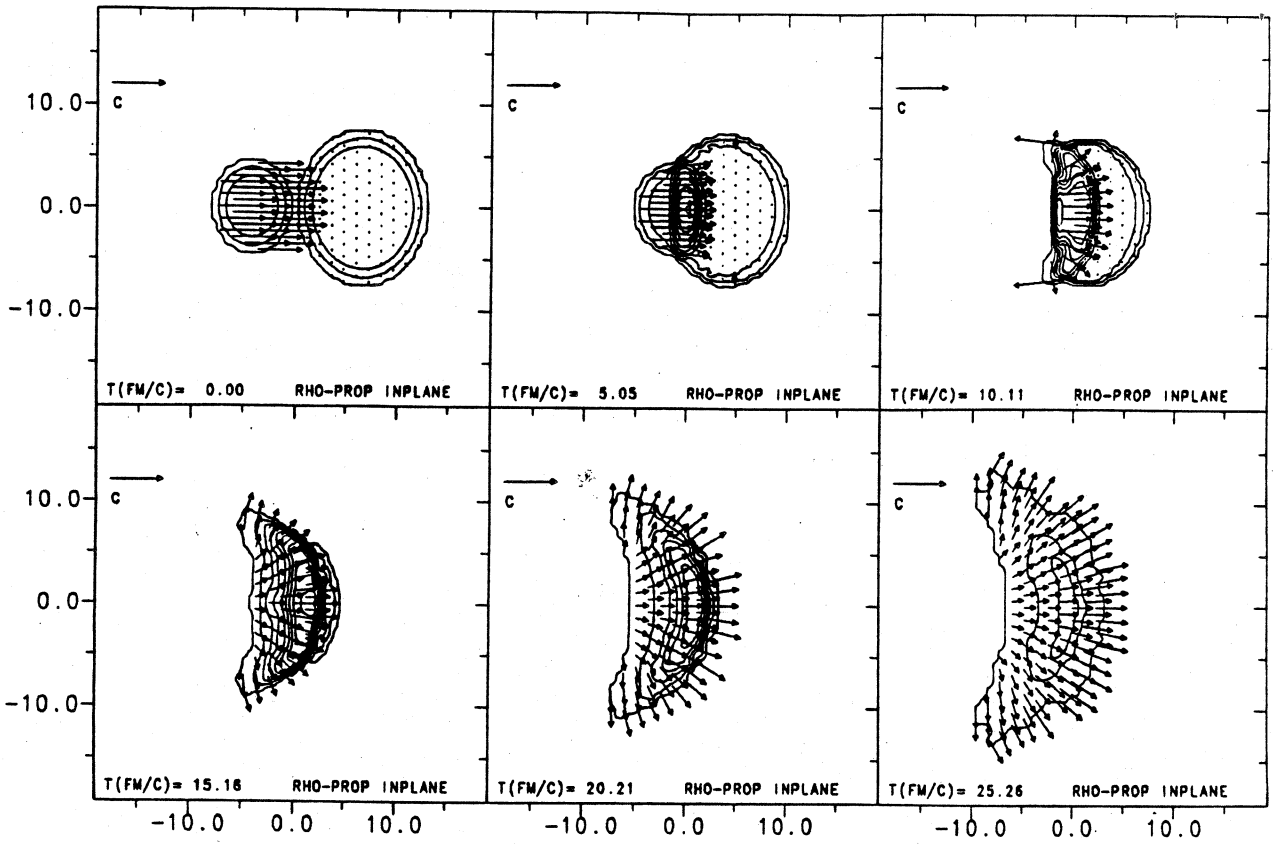

Figure II.12

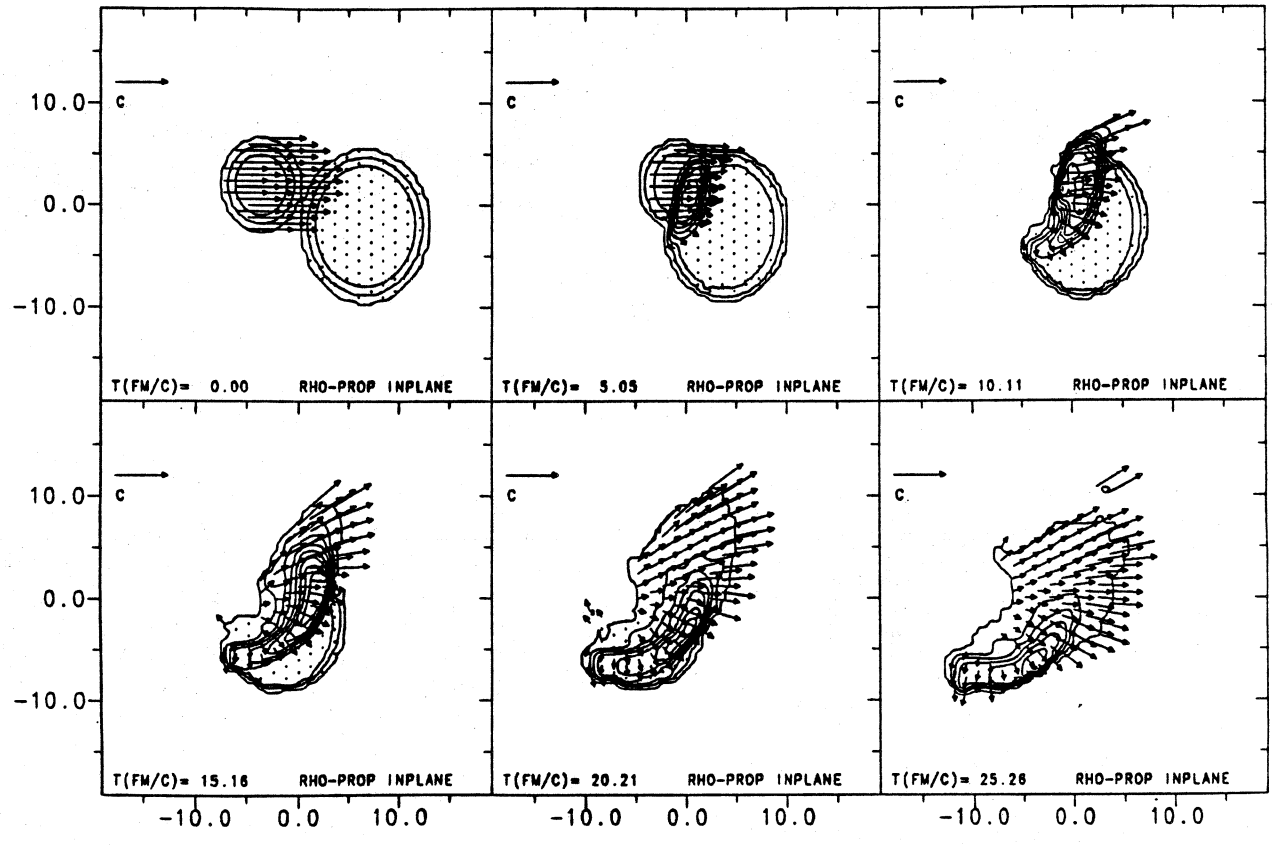

Figure II.13

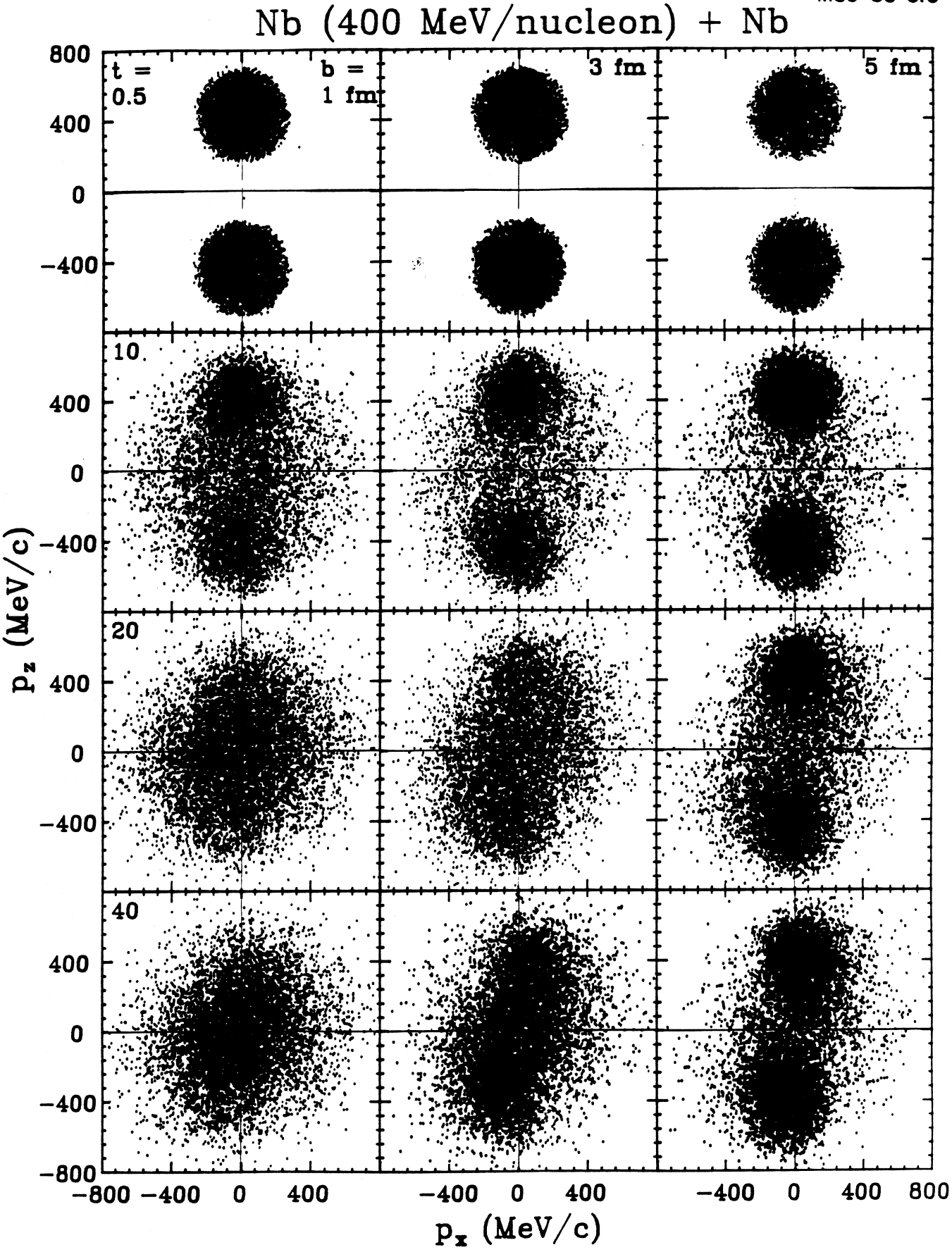
Nb (400 MeV/nucleon) + Nb
t = 0.5
b = 1 fm
3 fm
5 fm
10
20
40
800
400
0
-400
-800
p_z (MeV/c)
p_x (MeV/c)

Figure II.14

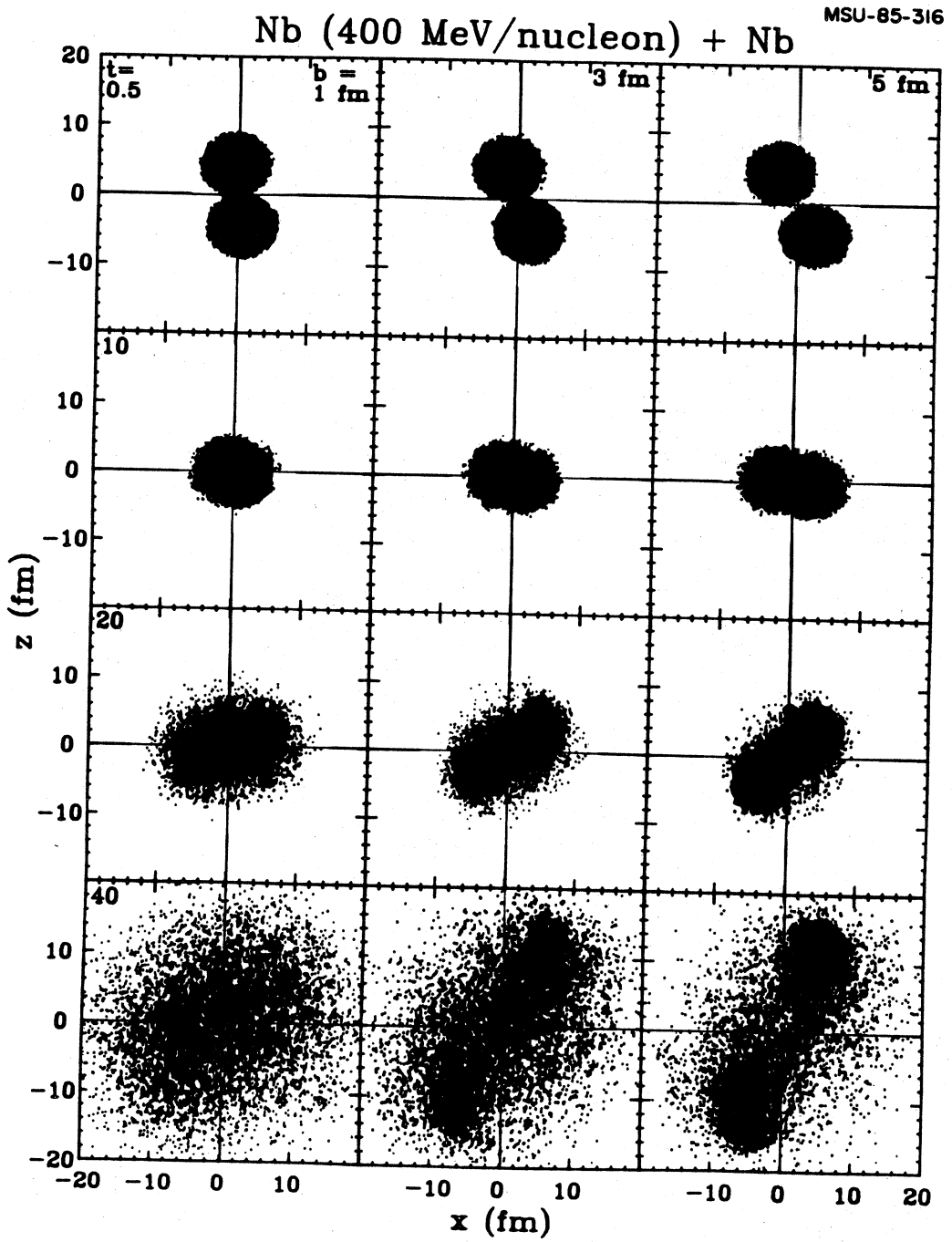

Figure II.15

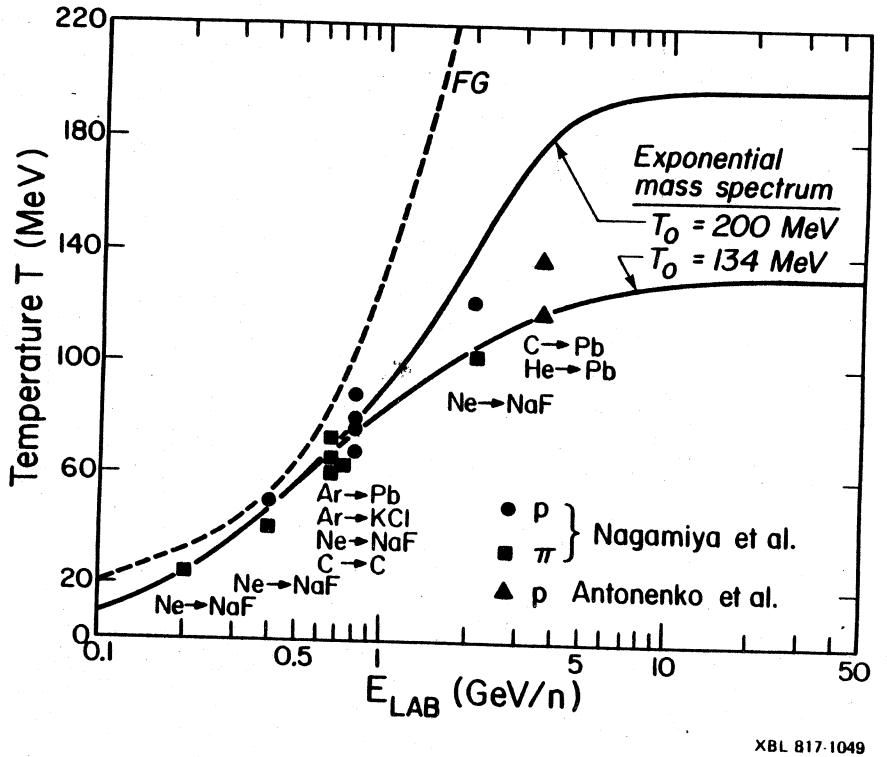

Figure III.1

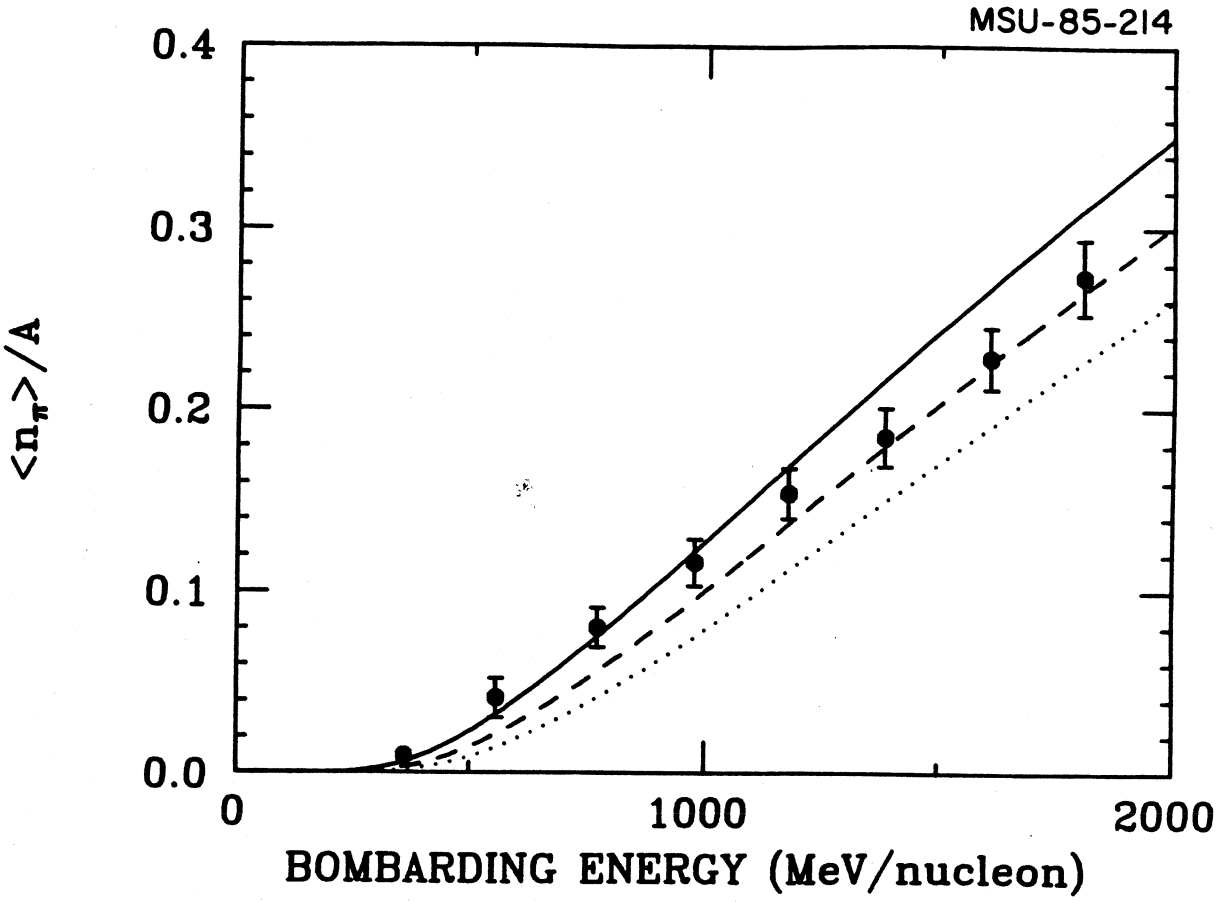

Figure III.2

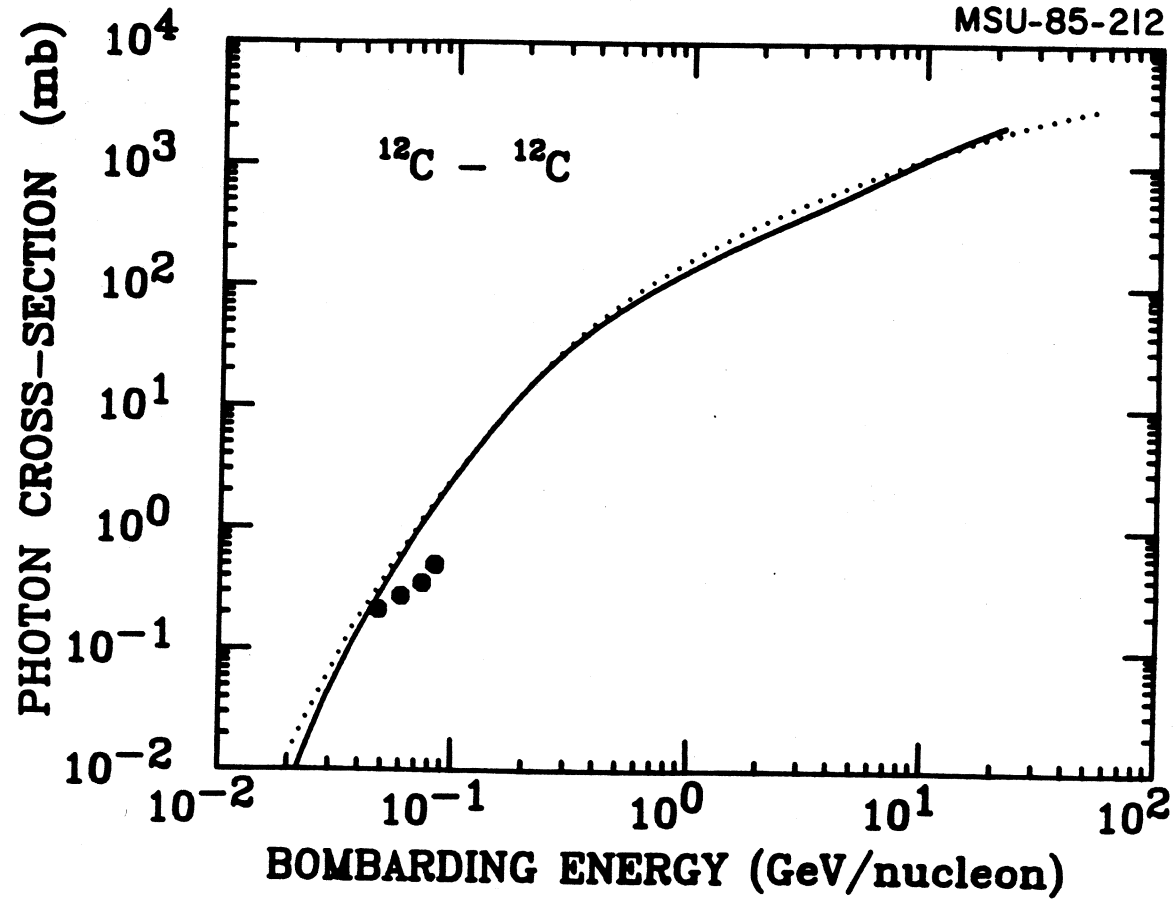

Figure III.3

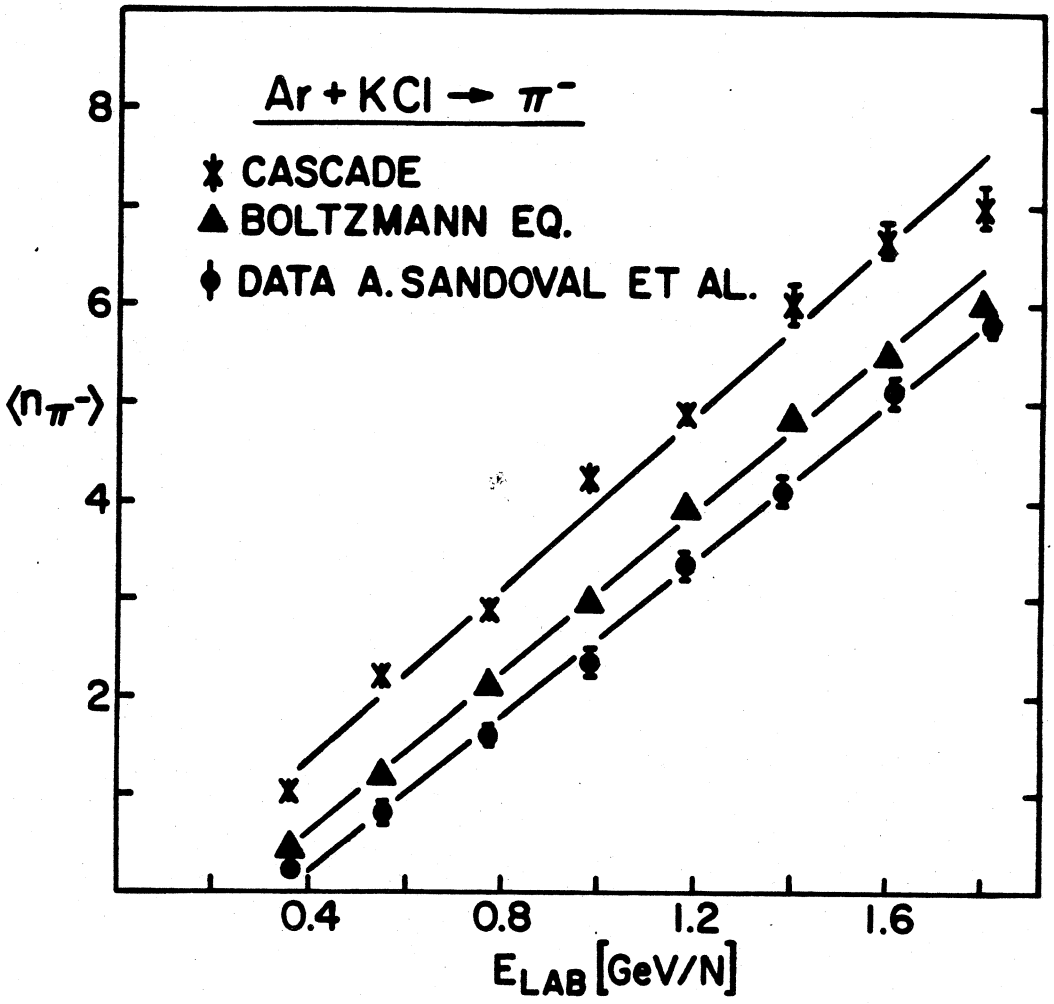

Figure III.4

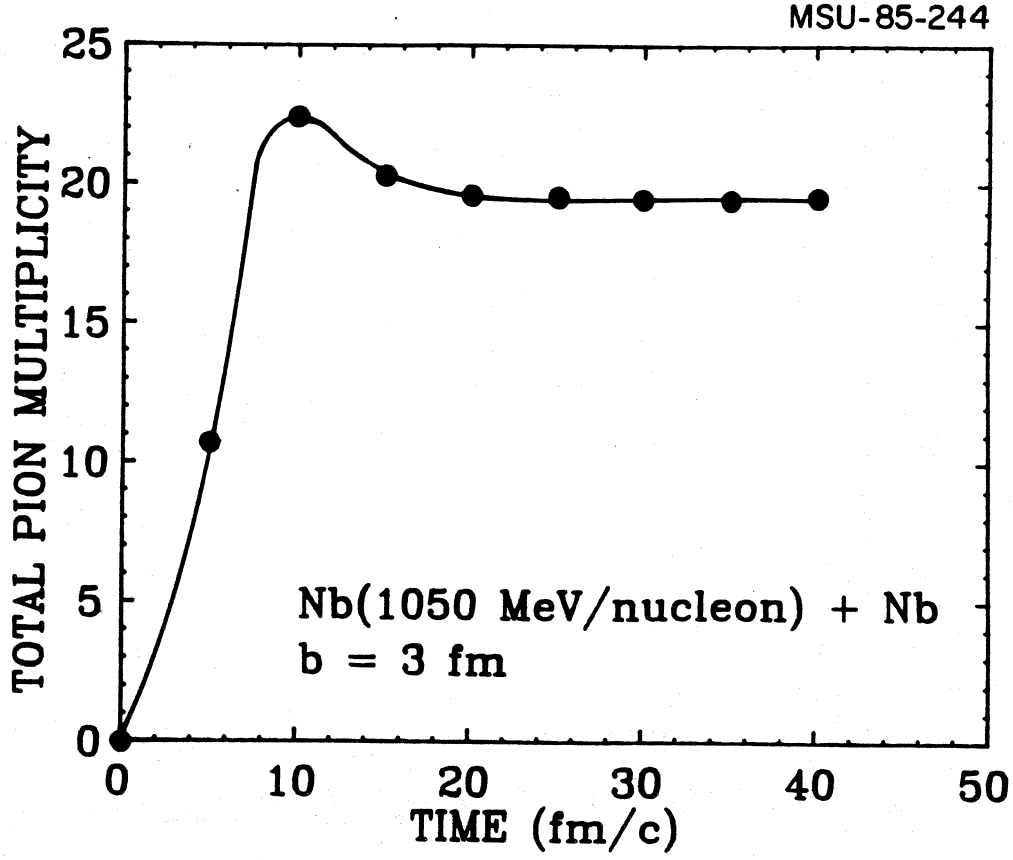

Figure III.5

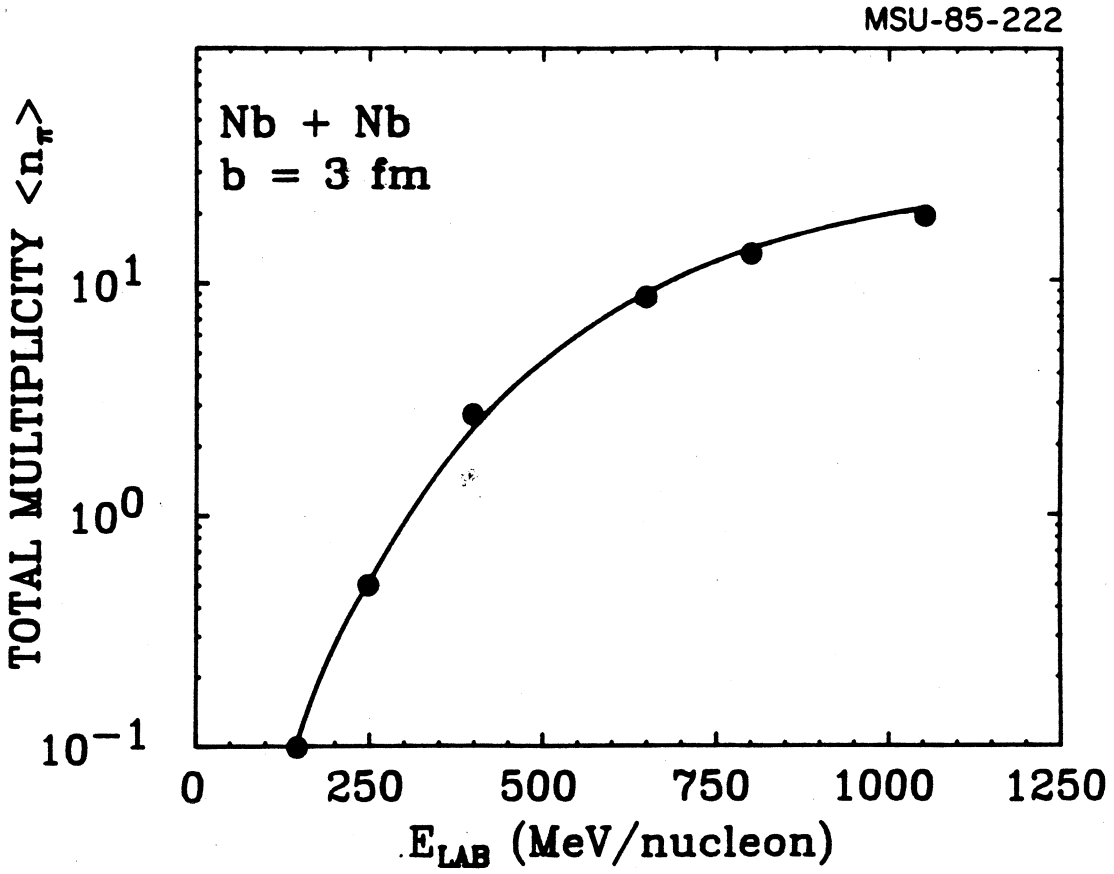

Figure III.6

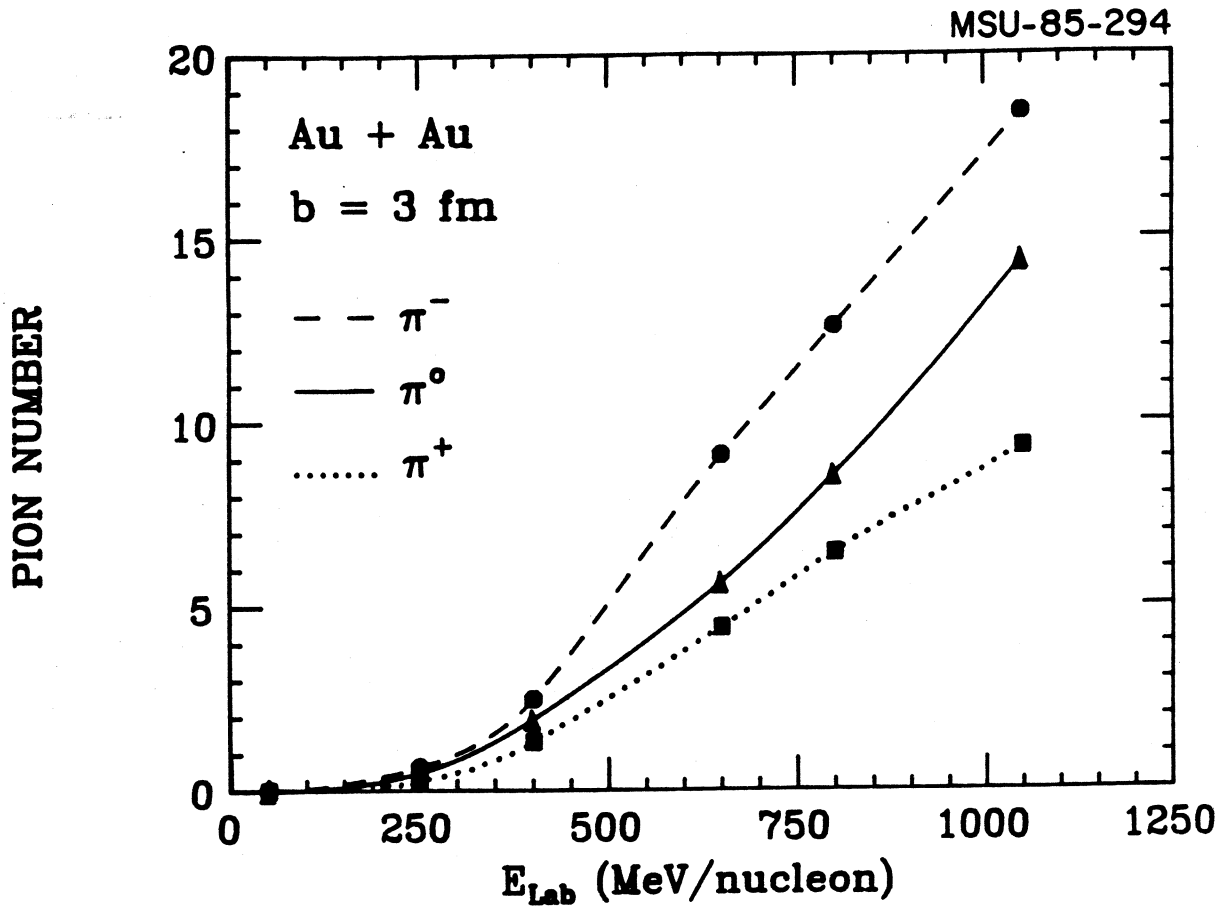

Figure III.7

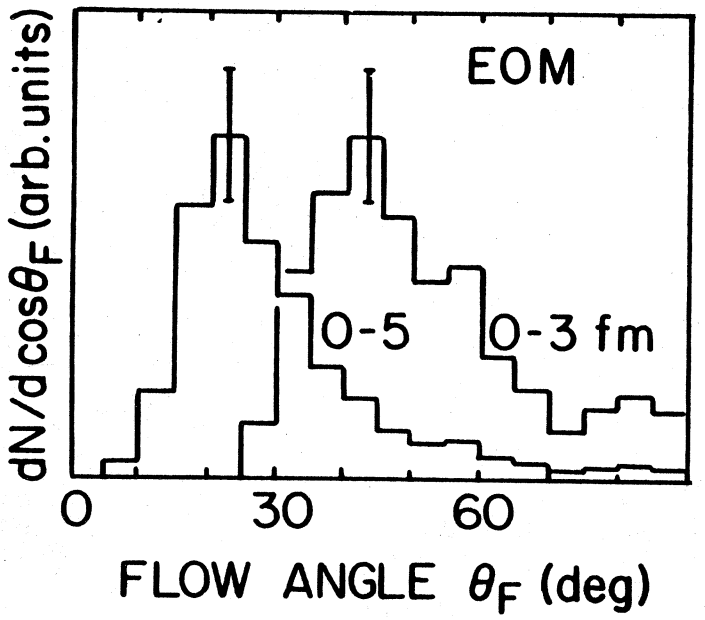

Figure III.8

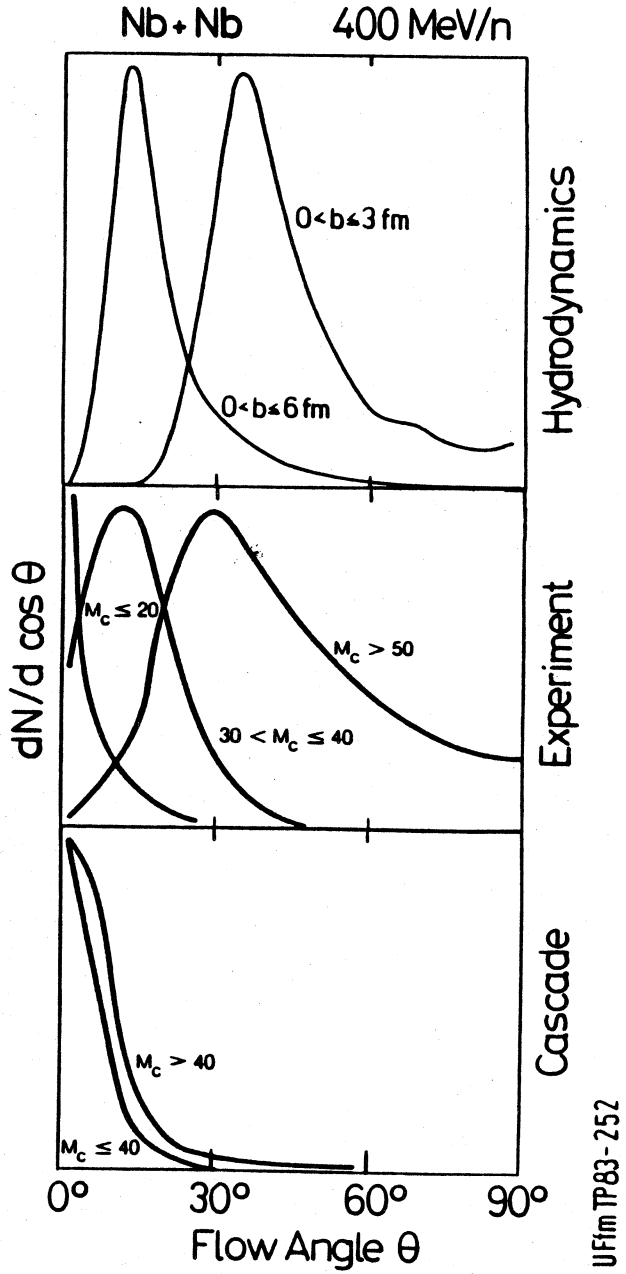

Figure III.9

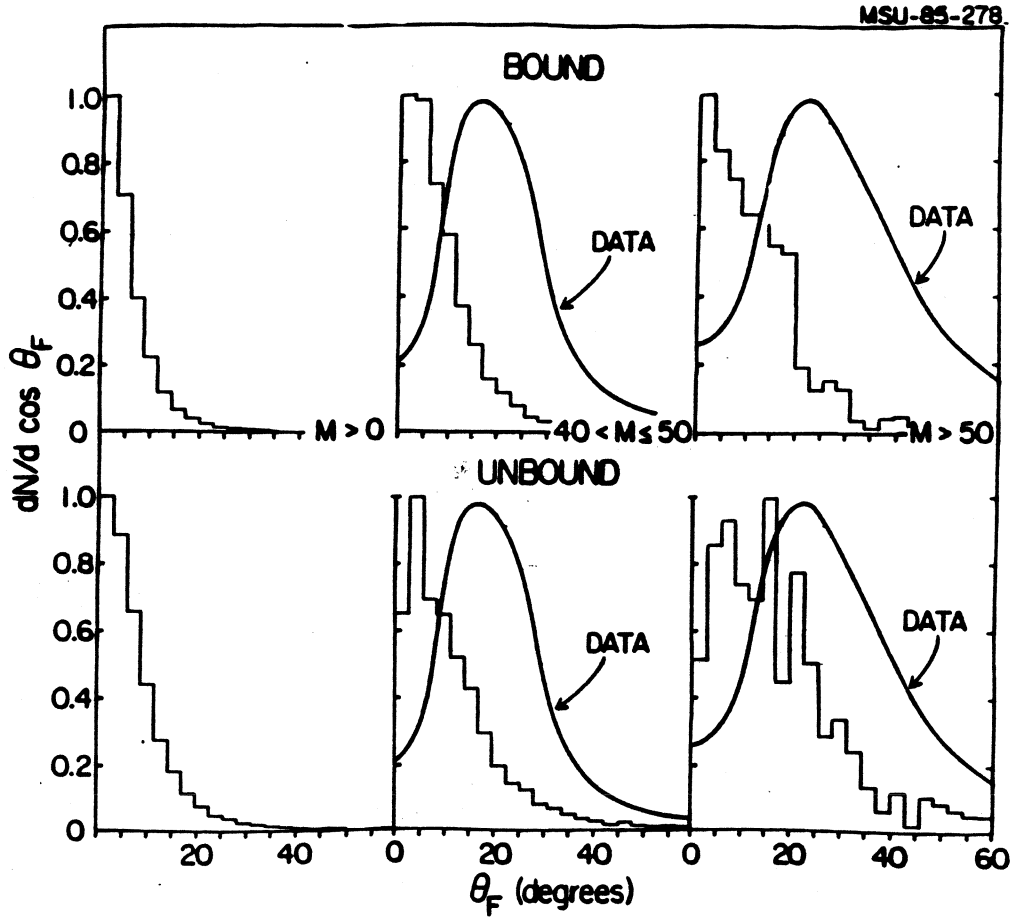

Figure III.10

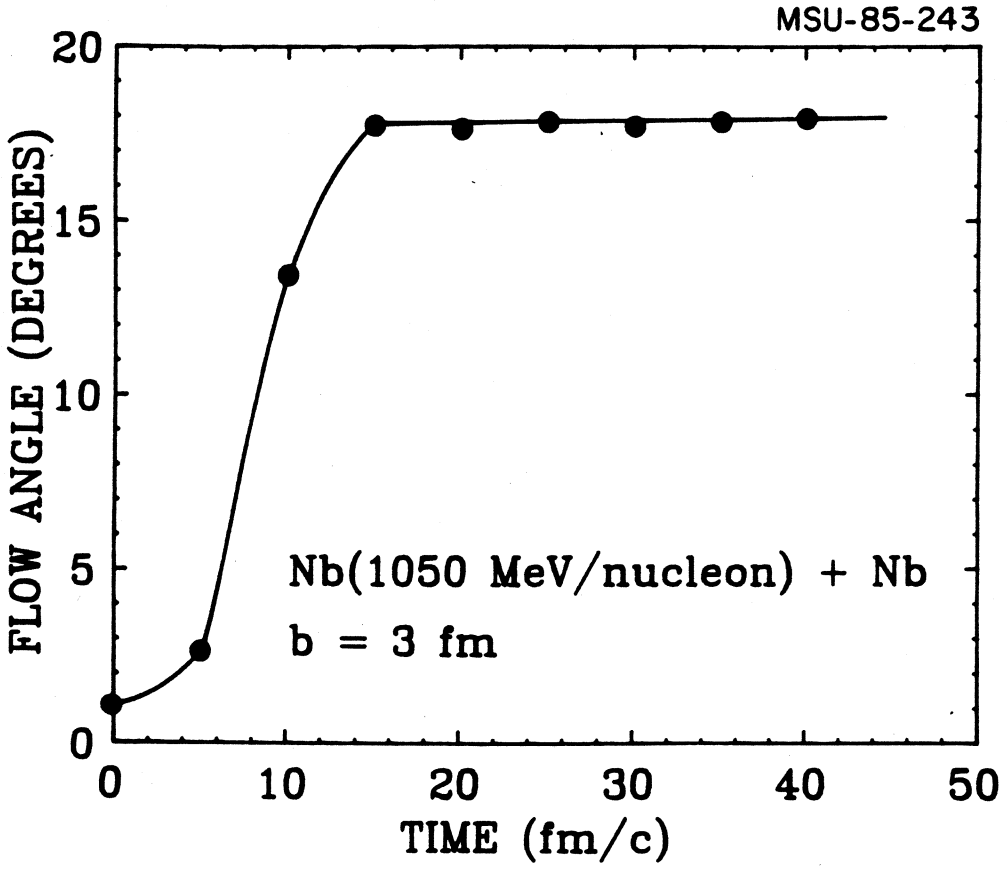

Figure III.11

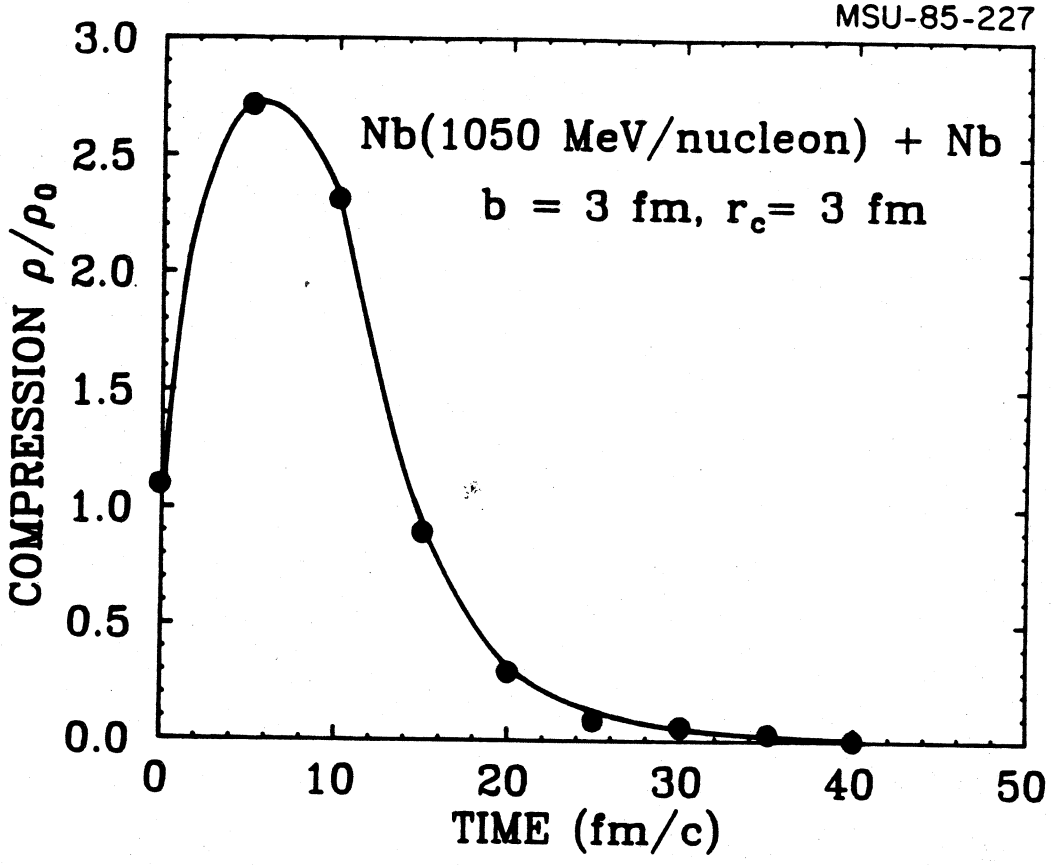

Figure III.12

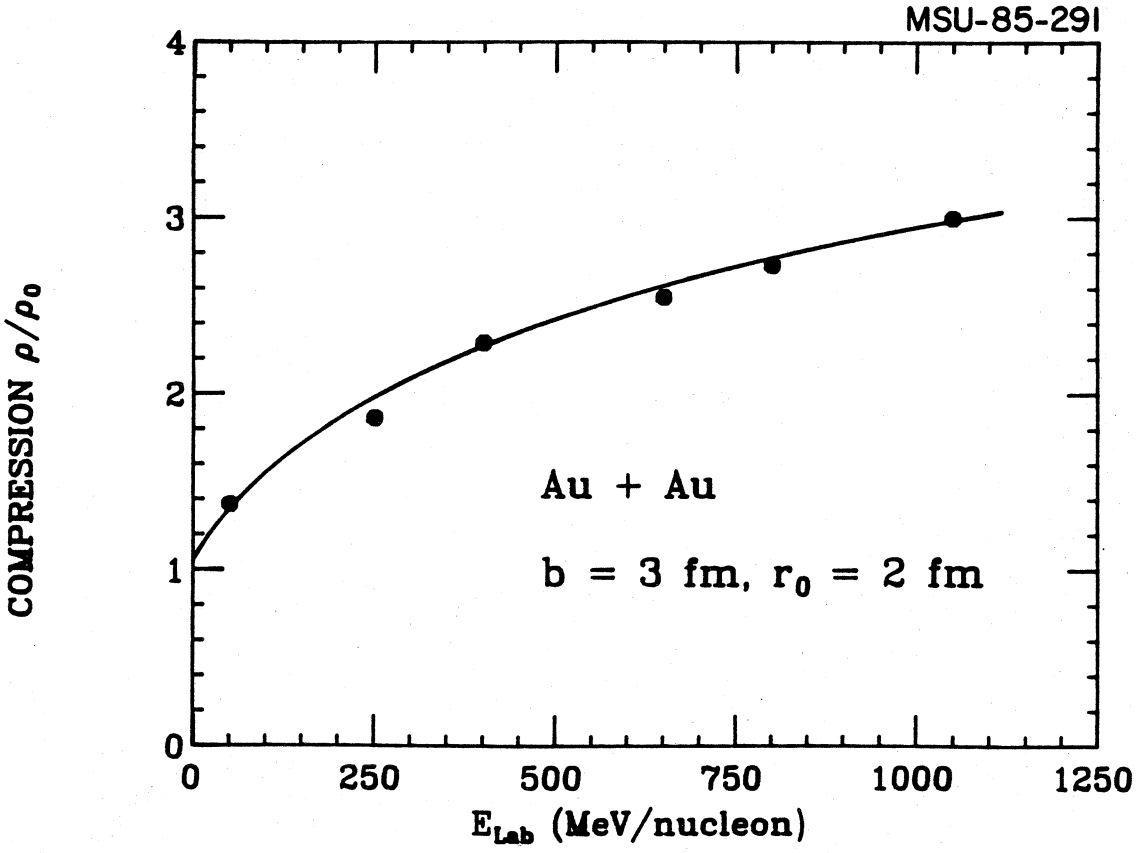

Figure III.13

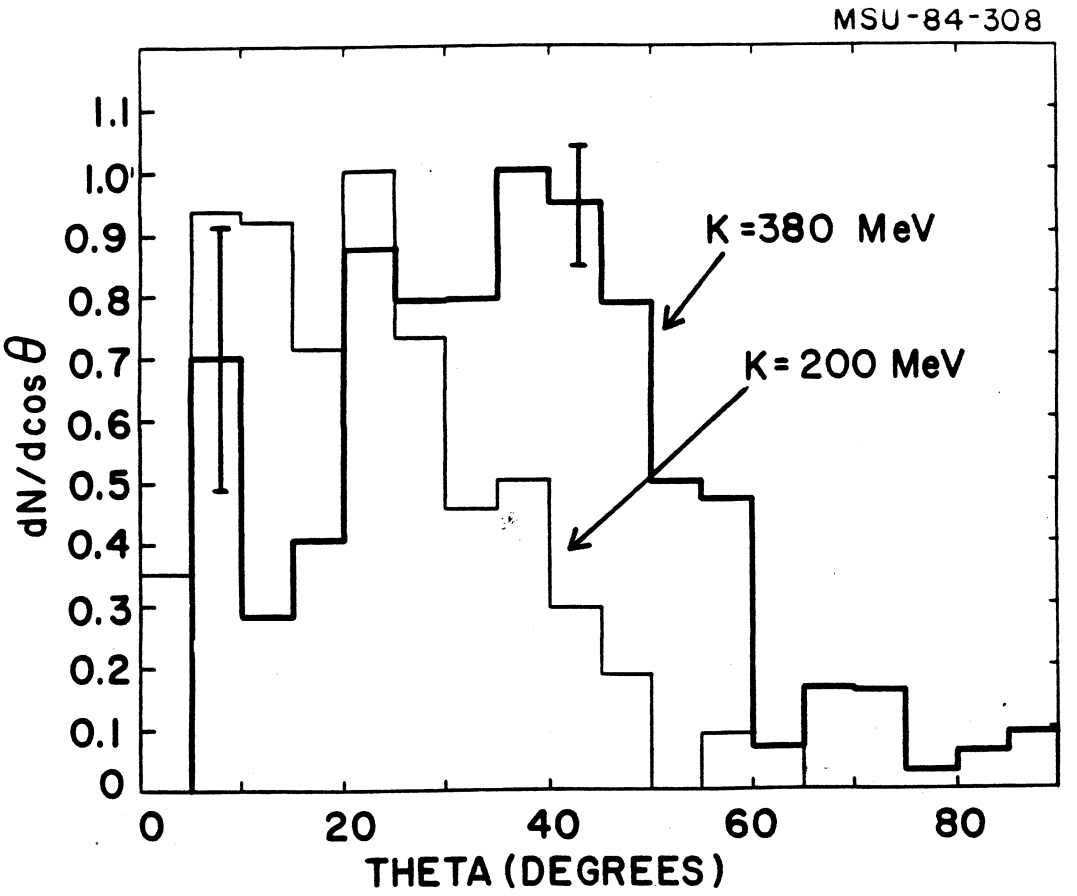

Figure III.14

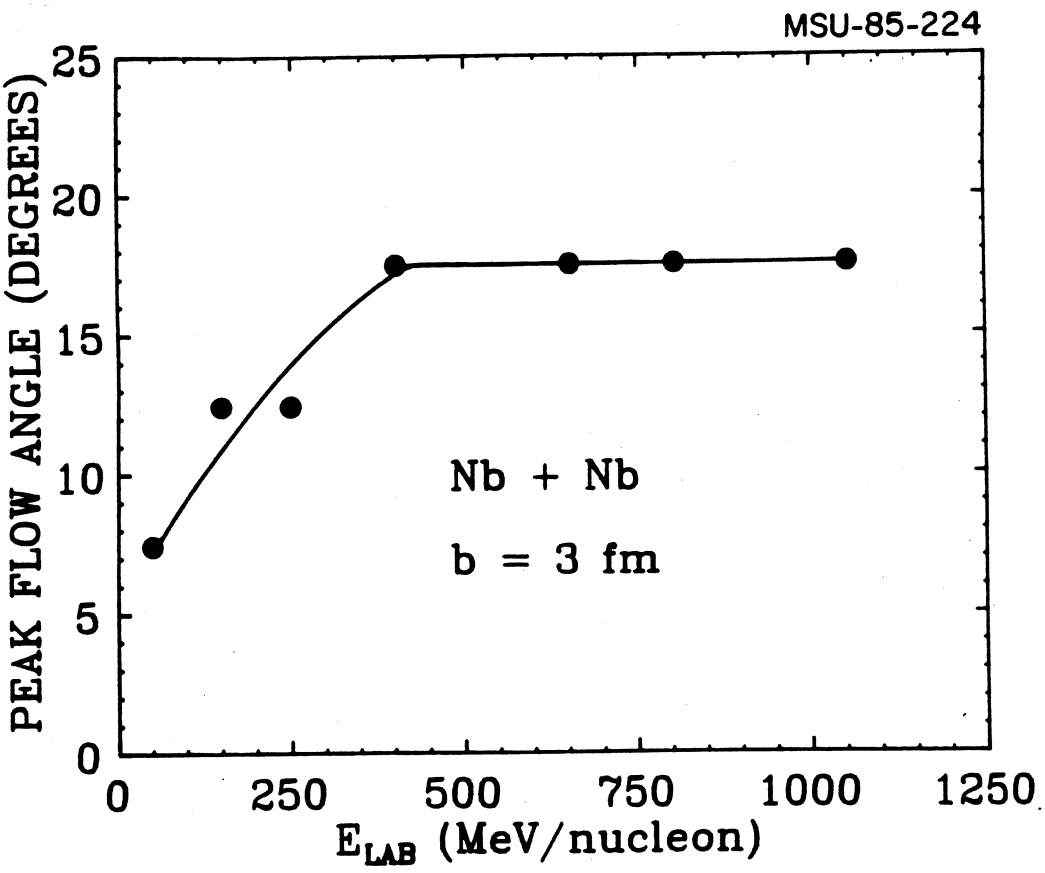

Figure III.15

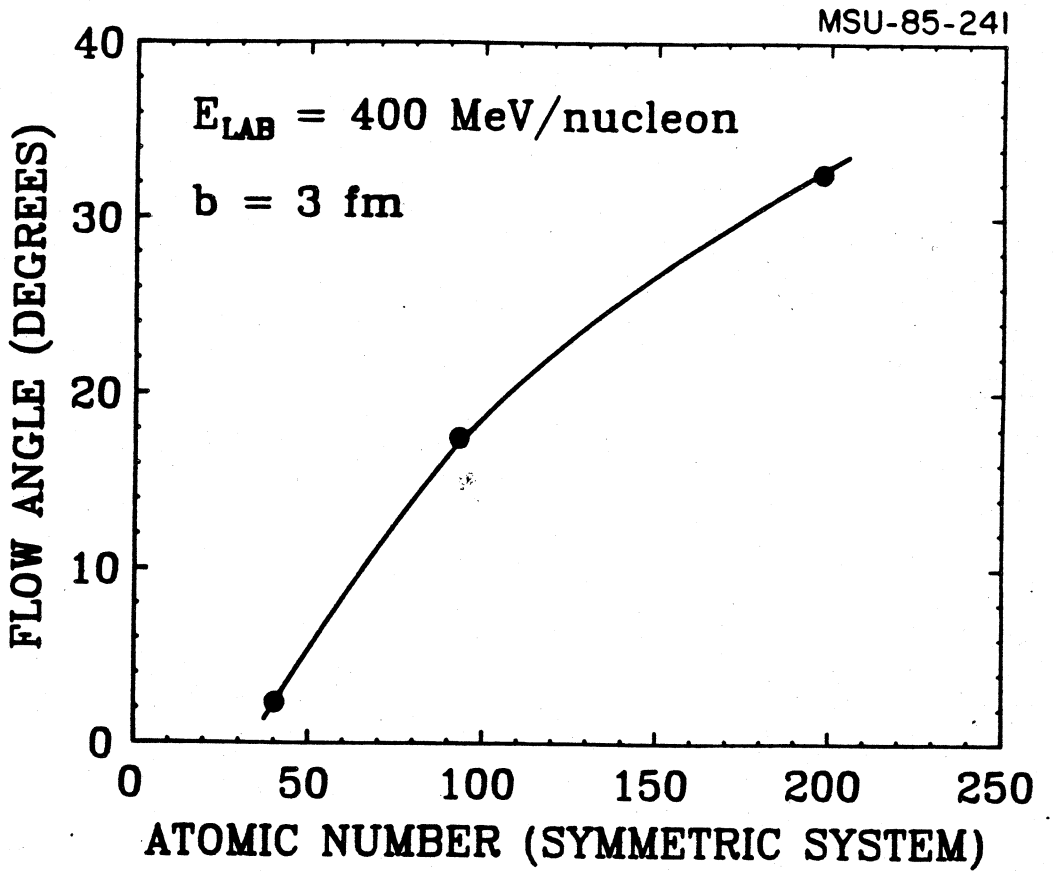

Figure III.16

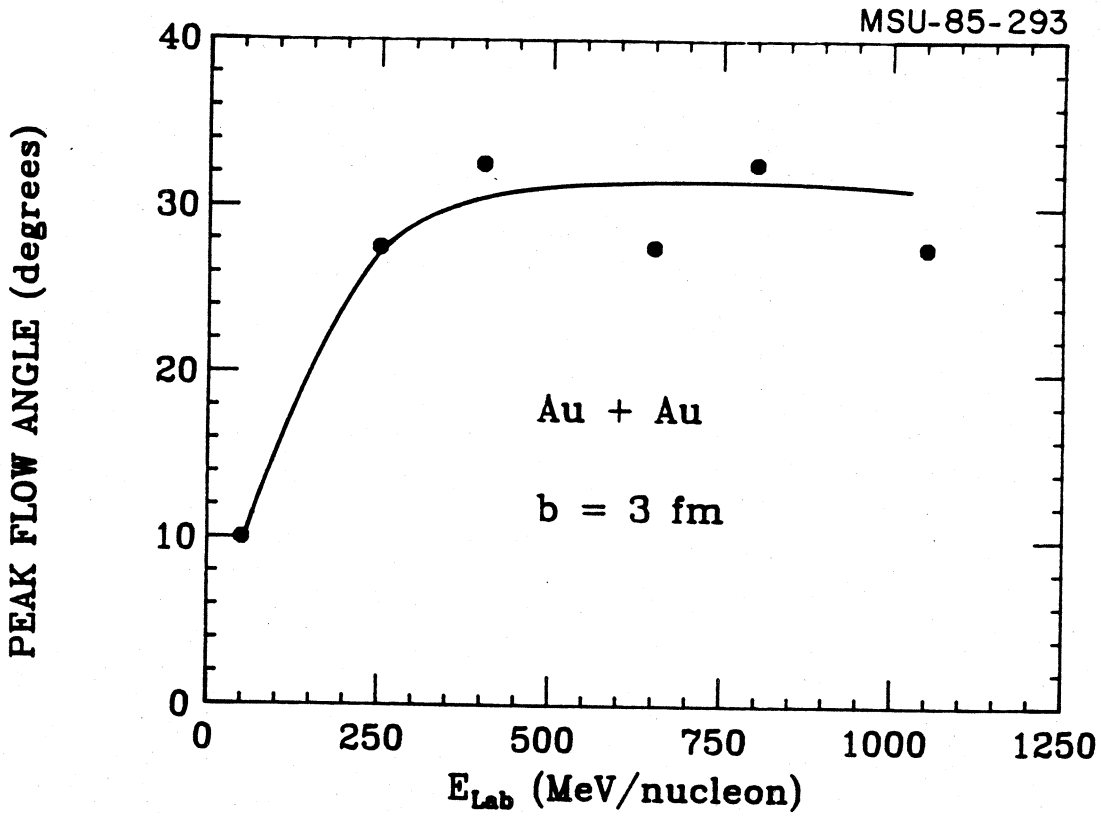

Figure III.17

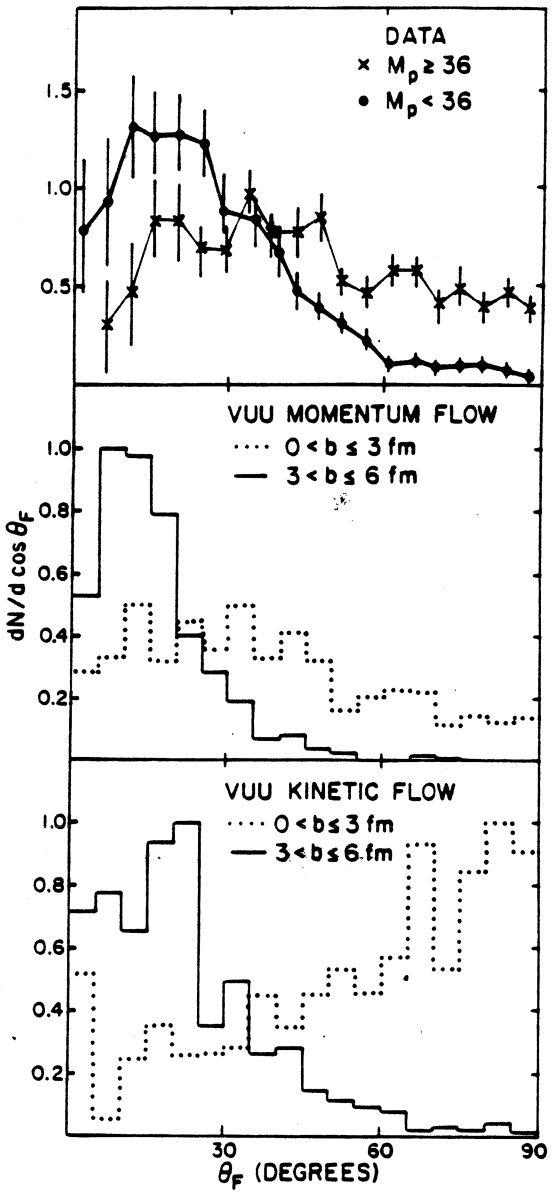

Figure III.18

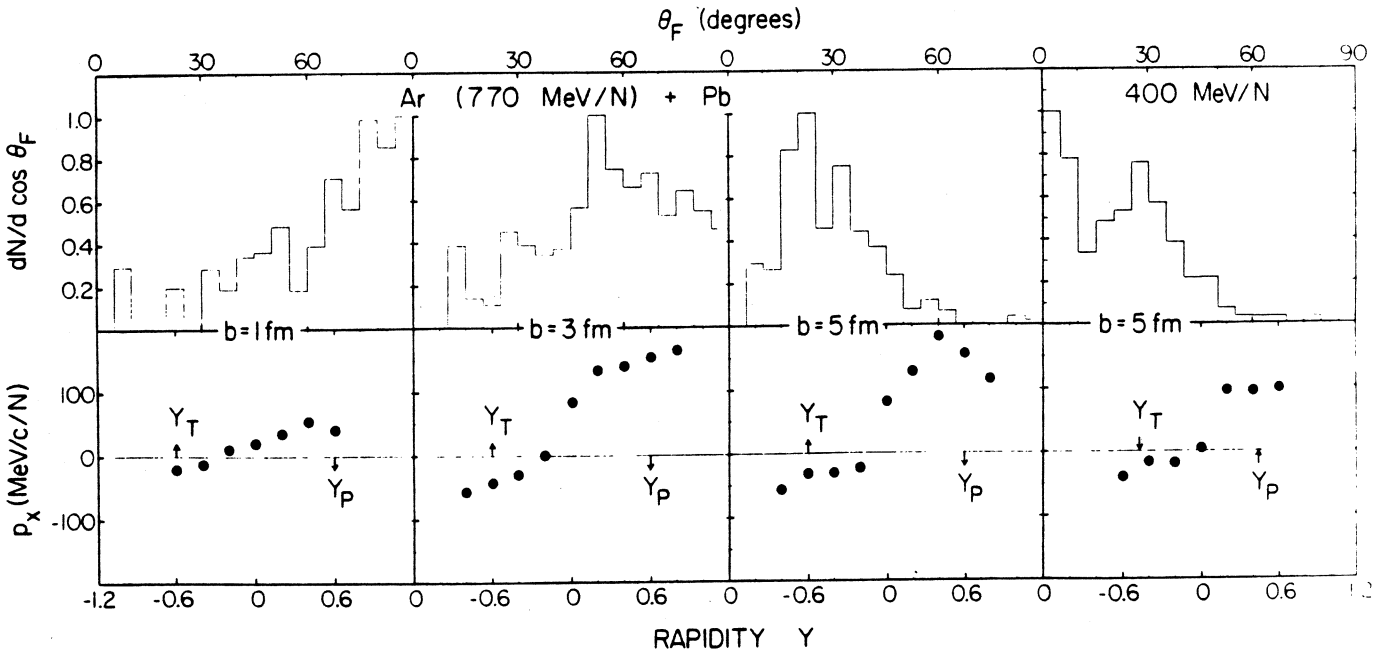

Figure III.19

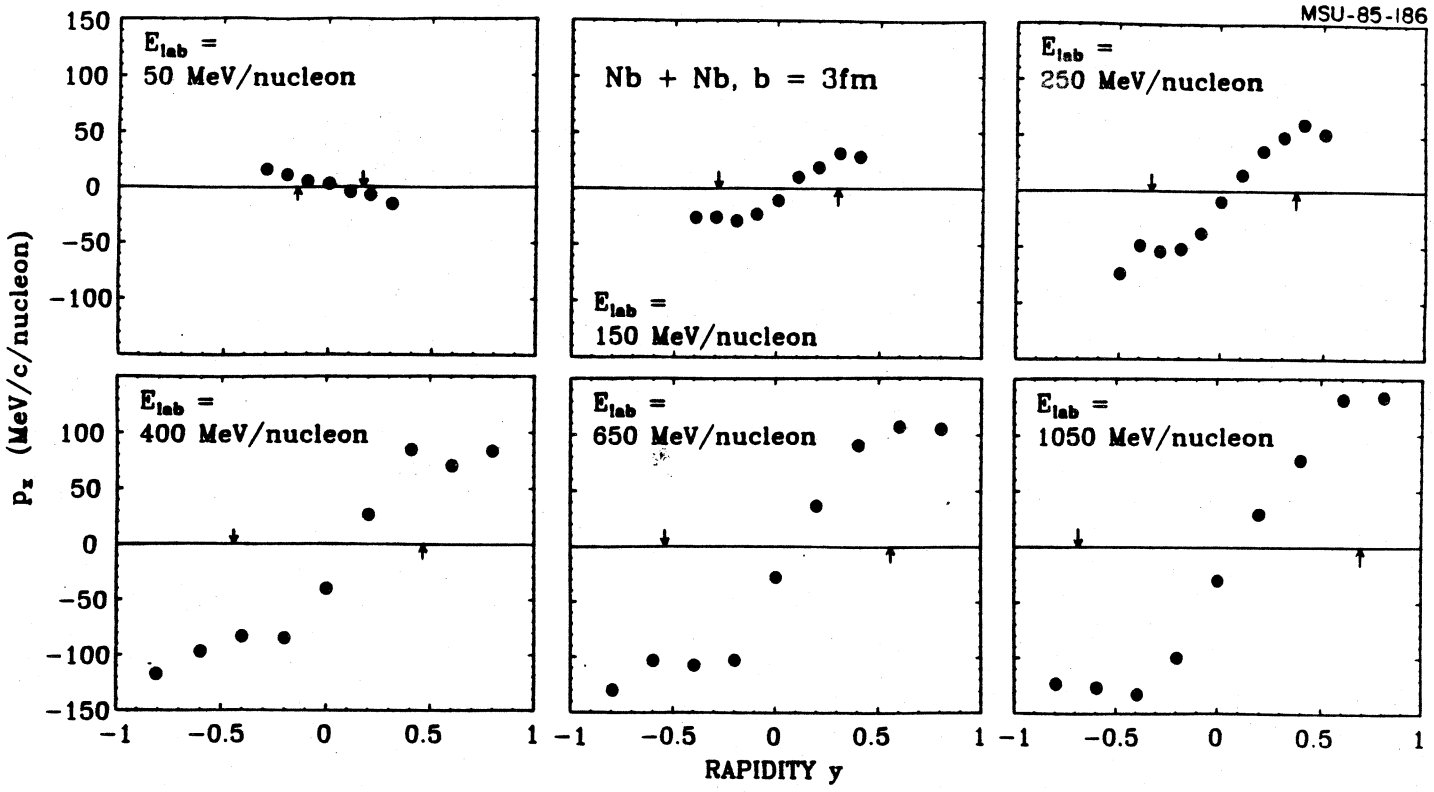

Figure III.20

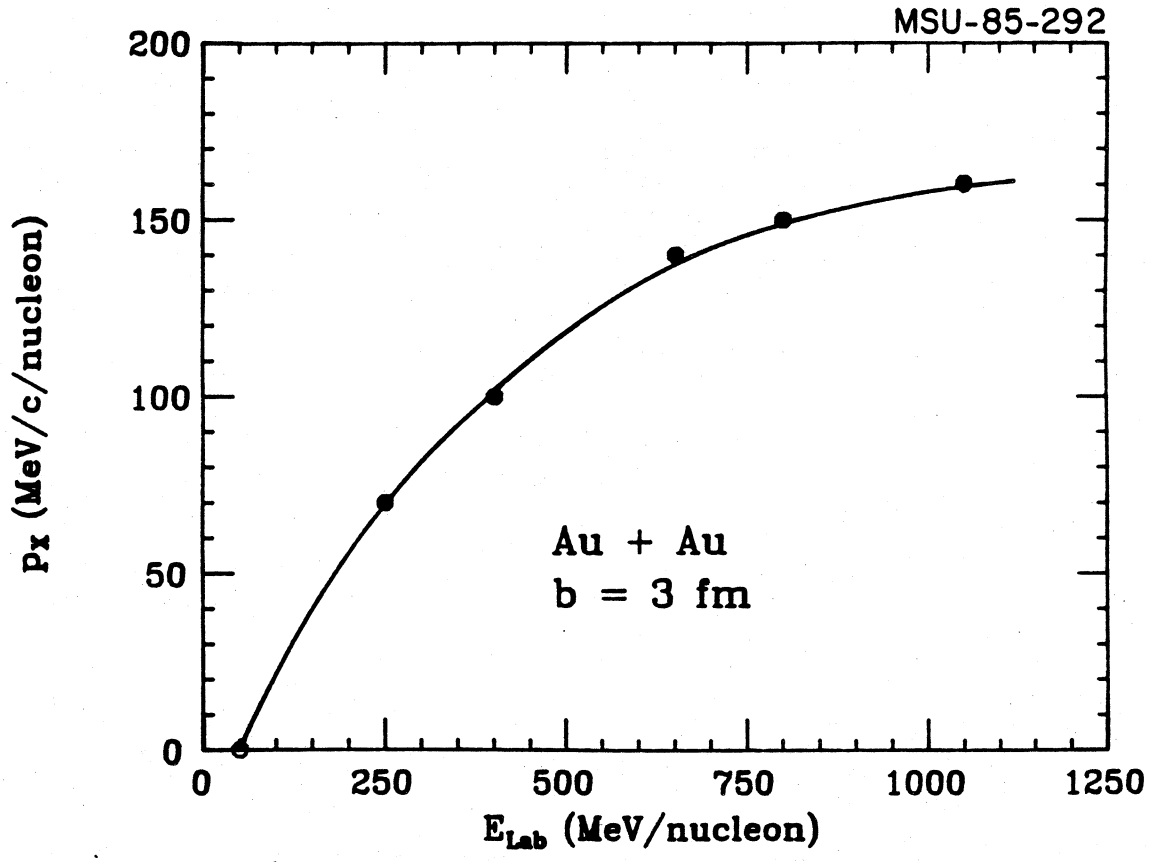

Figure III.21

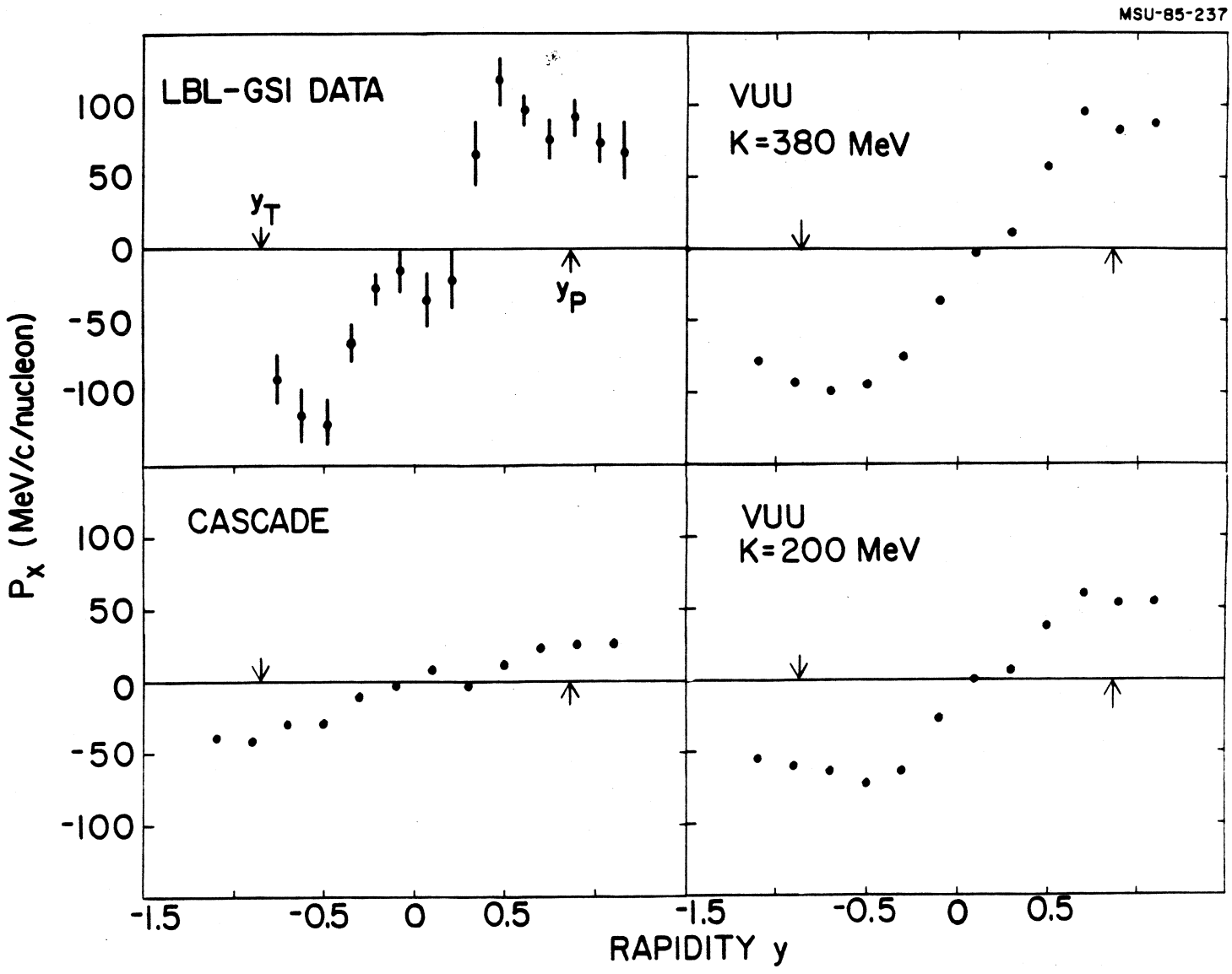

Figure III.22